KATHMANDU UNIVERSITY

SCHOOL OF ENGINEERING

DEPARTMENT OF MECHANICAL ENGINEERING

DISSERTATION ON

"DESIGN AND ANALYSIS OF FRANCIS TURBINE FOR SEDIMENT LOAD"

In Partial Fulfillment of the Requirements for the

Doctorate Degree

in

Mechanical Engineering

Krishna Prasad Shrestha

August 22, 2017

ACKNOWLEDGEMENT

First and foremost, I want to thank my supervisors Prof. Dr. Bhola Thapa and Prof. Ole Gunnar Dahlhaug for the continuous support of my PhD study. It has been the matter of pride to research under such proficient mentors. Their supports and advices on both research as well as on my career have been invaluable. The patience and enthusiasm they showed for this research, even during the hard times in my PhD pursuit, is really commendable and stimulating for me.

The student groups and committee members of Waterpower Laboratory, NTNU (2012 - 2014) have really contributed a lot to bring my research to this successful stage. I would especially like to thank Kristine Gjoaster and Mette Eltvik for their continual support and encouragement throughout the research. Their insightful comments and suggestions on MATLAB usage, Khoj software really inspired me to broaden my research from various viewpoints.

Dozens of individuals who were always there by my sides suggesting and influencing me at various stages of the research, a profound gratitude to them. JB Paulsen, your suggestions and comments in designing using Pro/E and FSI simulation really made my task easier. The discussion regarding computational domain in Pro/E with Einar Agnalt and Amod Panthi were really supportive and handful in guiding me to strive towards my goal. Peters aid in turbine design and refurbishing it using La Higuera software and Bjorns CFD post processing assistance deserve special mention.

In regards to the use of super computer, I thank Kristoffer Vegdal for his guidance in uploading definition file from workstation to super computer and post processing stages. While carrying out CFD simulation in ANSYS CFX, the tips and tricks given by Martin Aasved Holst of EDR MEDESO, Oslo, Norway helped me a lot. His willingness and explanatory comments aid me to troubleshoot the vortex formation between the runner blades with an ease. I am also hugely appreciative to those helping hands of several individuals during the twilight days in my dissertation. I would like to share the acknowledgement to Lars Froyd for his time, interest, and helpful

comments during the thesis work. Also, special appreciation goes to Shailendra K. Jha, Sailesh Chitrakar, Hari Dura, Dadi Ram Dahal and Pradeep Parajuli for helping in desktop service and thoroughly reviewing the final manuscript. And thank you to Saurav Gautam and Amit Shrestha for helping me in converting the MS Word file to Latex. I would also like to thank Mr. Kapil Pudasaini for allowing me to visit NHE, Nepal during Francis turbine repairing process and providing pictures of Francis turbines.

I would like to thank the Department of Mechanical Engineering, Kathmandu University for allowing me to conduct this research in pursuit of PhD degree. My special thanks go to the then departmental head, Prof. Dr. Bim Prasad Shrestha and current one, Dr. Hari Prasad Neopane for their continual support and guidance to bring my research to this stage. Prof. Dr. Bhupendra Bimal Chhetri and Prof. Dr. Ramesh Kumar Maskey owe me lots for streamlining the research theme during the proposal defense phase. All the staffs of Turbine Testing Laboratory, Kathmandu University deserve special praise too. My grateful acknowledgement goes to the funding sources that made my PhD study possible. I was funded by NORAD through ENPE PhD program, supported by KU and NTNU and am very much thankful to them.

Lastly, I would like to express my indebted acknowledges to my beloved parents, wife Babi, and daughter Riju for their continuous support, incessant inspiration and understanding, during all testing moments.

Table of Contents

List of Figures

List of Tables

ABSTRACT

Hydraulic turbines of several hydropower projects have been facing severe problem due to sediment erosion. In fact, the problem is much worst in case of run-off-the river hydropower plants as the sediment particles dont get enough settling time in contrast to reservoir hydropower plants. The particles eventually find their way towards the turbine and causes the subsequent change in flow pattern inducing several operational and maintenance problems in such plants. Several erosions inducing factors like particle velocity, sediment shape, size, concentration, operating conditions, impingement angle, hardness of substrate etc. are responsible for the loss of efficiency and working capability of hydraulic turbines operating in sand laden conditions.

In order to overcome these challenges, several approaches were put forward. Among them, usage of coated materials and expansion of settling basin have drawn the interest of some of the researchers. The application of the coating has been practiced in few hydropower plants in Nepal, but the results were not found economically favorable. In addition, maintaining uniformity in coating thickness at all surfaces in case of Francis turbine runner blade is quite difficult task. Due to the countrys geographical condition, it is always not possible to construct large settling basin. In such circumstances, hydraulic design changes may be only available last resort for this case.

This research was carried out to address these issues and assist in hydro sectors to achieve the high performance Francis turbine with less prone to sand erosion. First of all computational tools were implemented in order to study the effects of erosion inducing factors at different operating conditions. Further, encompassing the previously conducted experiments, the nature of effects due to different combinations of input factors like shape, size, concentration, and impingement angles on the turbine material were analyzed. The analysis includes digital image processing to extract shape and size of sediment particles from the erosion sensitive power plants and its experimental studies carried out at Kathmandu University (KU) using two different

methods High velocity impact and Rotating Disc Apparatus (RDA).

In this PhD study, Computational Fluid Dynamics (CFD), Finite Element Method (FEM) and Fluid Structure Interaction (FSI) were employed in order to minimize the sediment effects on turbine material. The application of CFD, FEM and FSI at different design stages innovated new way for Francis turbine design with less erosion impact as compared to reference design. Comparative study was carried out among the five different shapes of runner varying the guide vane and stay vane angles. The effect of erosion was studied in terms of average erosion density rate on optimized runner design with Lagrangian particle tracking method in CFD and comparison was done using two turbulence models. The simulation analysis results are compared with the measurements carried out in the real turbine. The results showed that runner material is more susceptible to erosion at part load conditions rather than at best efficiency point (BEP), however erosion in guide vanes is dominant at full load conditions. The comparison of five different shapes demonstrated that Shape 5 provides an optimum performance with high efficiency and lesser erosion on the studied operating conditions. To conform structural integrity, multidisciplinary optimization was performed on shape 5 in which energy extractions occur with high and low energy distribution from inlet to mid span in first half and then from mid span to the outlet of the runner in the latter half.

Although the problems of sediment cant be eliminated completely from its root, the findings of this research will definitely assist in minimizing its consequences. Further, the outcomes are believed to aid to lessen the erosion problem of turbine components and increase the life time.

BIOGRAPHICAL SKETCH

Krishna Prasad Shrestha, has received master degree in Mechanical Engineering from the Kathmandu University (KU). Currently, he is a PhD candidate at Department of Mechanical Engineering founded by NORAD through ENPE program supported by KU and NTNU. He served as research associate for design and development of Pico Propeller turbine testing laboratory, KU and he has shown his expertise as a Mechanical specialist for preparing technical manuals on vertical and horizontal drilling for the drinking water purpose. He has got training on computational fluid dynamics from American Society of Mechanical Engineers (ASME), and Norplan, Spain. His current research is based on Design and Analysis of Francis Turbine for Sediment Load. He was also an active member of Turbine Testing Lab, KU, Nepal.

Corresponding address: kp@ku.edu.np

LIST OF ABBREVIATIONS

APDL	ANSYS Parametric Design Language
BEP	Best Efficient Point
BPC	Butwal Power Company
CAD	Computer Aided Design
CFD	Computational Fluid Dynamics
FEM	Finite Element Method
FSI	Fluid structure Interaction
gm	gram
GV	Guide Vane
HVOF	High Velocity Oxy-Fuel
IEC	International Electro-technical Commission
JHC	Jhimruk Hydroelectric Center
KU	Kathmandu University
kW	kilowatt
m	meter
mm	millimeter
MPa	Mega Pascal
MW	Megawatt
NTNU	Norwegian University of Science and Technology
R&D	Research and Development
RANS	Reynolds Averaged Navier-Stokes
RDA	Rotating Disc Apparatus
ROR	Run of the River
SOE	School of Engineering
SST	Shear Stress Transport
SV	Stay Vane
TA	Turbine Abrasion
TTL	Turbine Testing Laboratory
V	Volt

LIST OF SYMBOLS

A	Constant factor	[-]
A_F	Effective particle cross section	[m^2]
B_1	Inlet height	[m]
c	Mean sand concentration	
C_D	Drag coefficient	[-]
D_1	Inlet diameter	[m]
D_2	Outlet diameter	[m]
F_B	Buoyancy force	[N]
F_D	Drag force	[N]
F_P	Pressure gradient force	[N]
F_R	Rotational force	[N]
F_{VM}	Virtual or added mass force	[N]
H	Head	[m]
H_S	Submergence required	
i	Imaginary number	[-]
k	Normal component of particle impact velocity	
k_1	Coefficient for shape	[-]
k_2	Coefficient for hardness	[-]
k_3	Coefficient for abrasive resistance	[-]
K	Impeller shape factor	
M	Total mass of impacting particles	[kg]
N	Rotational Speed	[rev/s]
N_ed	Speed factor	[-]
p	constant	[-]
P	Power	[kW]
P_1	Radial velocity	[m/s]
P_2	Tangential velocity	[m/s]
P_3	Head	[m]

P_4	Shaft power	[kW]
P_5	Total efficiency	[%]
P_6	Flow rate(For the optimization process, P6=Q)	[m^3/s]
P_7	RPS	[l/s]
P_9	Erosion rate density	[kg/m^2s]
P_a	Density of liquid	[kg/m^3]
P_f	Abrasive power	[kW]
P_s	Density of particle	[kg/m^3]
q	Quartz constant	[-]
Q	Discharge flow rate	[m^3/s]
Q_{ed}	Flow factor ‘	
Q^n	Concentration of solid in mixture	
R_p	Radius of curvature	[m]
S_1	Coefficient of silt concentration	[-]
S_2	Coefficient of silt hardness	[-]
S_3	Coefficient of silt particle size	[-]
S_4	Coefficient of silt particle shape	[-]
T	Torque	[Nm]
V	Volume of particle	[m^3]
v_f	Flow velocity	[m/s]
W_s	Coefficient of abrasive wear	[-]
X	Coefficient of abrasiveness of solids	
z	Exponent for relative velocity	
θ	Impact angle	[-]
α	Correction factor	
ϵ	Deformation factor	[-]
δ	Abrasive rate	
γ	Constant	[-]
ϕ	Constant	[-]
β	Constant	[-]
η	Efficiency	[-]

η_m	Turbine peak efficiency with sediment-laden flow	[-]
η_w	Turbine peak efficiency with clean water	[-]
μ	Coefficient of friction	[-]
Ω	Speed number	[-]

Chapter 1: INTRODUCTION

1.1 Background to the research

Nepal has an enormous hydropower potential. Several researchers has noted that the economically feasible hydropower potential of Nepal is more than 43,000 MW [1, 2, 3] . Despite having a tremendous potential, Nepal is still lagging behind in power generation and blackouts are common all around the year. Slow technological transfer from the developed countries and lack of the state of the art of maintenance for the installed hydropower plants are the major causes for the current situation. In the past studies, it has been revealed that the new exploration of hydropower project is not the only solution, but there are forthcoming problems during the operation and maintenance after the installation. The rivers in Nepal have a higher concentration of sediment due to the young mountains and late man-madedevelopment activities around the Hilly areas/ regions. During the monsoon period, Nepalese river and river bullets carry a higher concentration of sediment. These sediments passes through the wet hydro-turbine components and are more prone to sediment erosion than during the other seasons. Identifying the problems due to sand erosion and the appropriate measures for its minimization is crucial for the sustainable development of hydropower plants in Nepal.According to Constitution Assembly election in Nepal (dated Nov 19, 2013), promises were madein major parties manifesto to develop 5000 MW of generating capacity 5 years, 10,000 MW in 10 years; 25000 MW by 20 years; and 45000 MW by 40 years [4].

Apart from different socio-economic and political hindrances that limit the new hydropower development, sediment erosion has evolved as one of the major obstacle in run-off-river plants. About 60% -80% particles present in sediments of the rivers have hardness number above 6 in Mohs scale [5, 6, 7]. The presence of hard particle in sprouting velocity causes the wet turbine parts to erode rapidly than the normal erosion due to pressure gradient. This eventually reduces the efficiency and life of the turbine. Furthermore it fosters on break down maintenance of eroded parts each year causing huge economic losses.

Figure 1.1 shows the effects of sediment erosion in Francis turbine operating in Himalayan basins.

Figure 1.1: Effect of sediment erosion in Francis turbine

Not only the run-off-river power plants, the hydro turbine running in the Himalayas and Andes Mountain of the South America are facing the same challenges [8, 9, 10]. In context of Nepal, Jhimruk power plant can be considered as one of the hydropower running with high head Francis turbine and severely prone to turbine erosion. Basnyat 98 presents the size of particle and mineralogical distribution in Table 1.1.

Table 1.1: Particle size and mineralogical distribution, from gravel trap site in Jhimruk river [11].

Size of Sieve(mm)	Particle size range (mm)	% retained (weight wise)	% of mineral (volume wise)		
			Quartz	Feldspar	Mica group
0.5	>0.5	0	-	-	-
0.2	(0.5-0.2)	0.15	15	<2	77
0.09	(0.2-0.09)	16.85	57	<2	41
<0.09	<0.09	83.0	85	<1	14

The Himalayan basins potential sediment erosion can be imagined and personalized by experimenting the effect of river sand flowing with water on hydro turbine blade material. The erosion measurement test at KU is carried out on turbine material after taking the different sample of sediment from several locations of Nepalese rivers of the different Himalayan basin [8]. Quartz content and their shapes in different rivers are identified through mineralogical analysis of the samples. Turbine material 16Cr5Ni Martensitic Stainless steel along with 1 kg sand samples were taken for the erosion tests. Operating condition was adjusted same for each of the testing while sand samples are taken between 425-300, 300-212 and less than 212 μm in size. The erosion rate obtained from each of the testing are averaged and plotted in graph along with corresponding quartz contents as below [12].

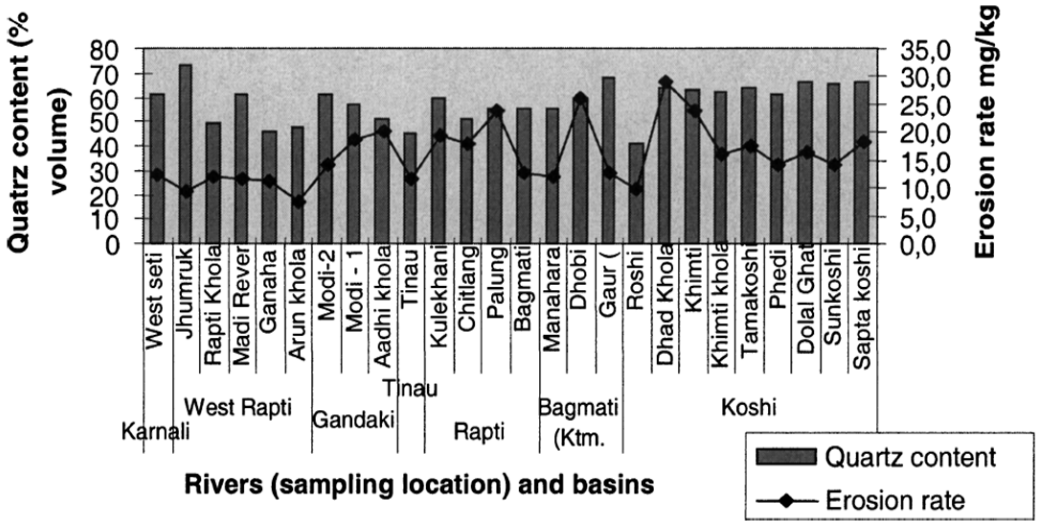

Figure 1.2: Quartz content from mineralogical analysis and erosion rate from laboratory erosion test [12]

Various attempts were made to neutralize the sediment erosion problems using different ways of coating which effectiveness of tackling problem depended upon the spray parameters and powder properties [6, 13]. The coating done at Marsyangdi hydropower project and HVOF coating done at Kaligandaki 'A' reduced the erosion rate [13, 14], while the consequence was not the same in case of Jhimruk hydropower project as the coating did not even last for one season [14].

1.2 Objectives of the research

The main aim of this research is to develop and analyze a Francis Turbine that can handle sediment load. The specific objectives are as follows:

- To analyze the impact of sand erosion on Francis turbine.
- To determine the effective area and its impact on erosion on Francis turbine runner blade and investigate the possible solution for the minimizing effect of erosion on the turbine.
- To innovate optimization technology with utilizing meta-models 0n Francis Turbine runner design for sediment load.

1.3 Motivation for research

The concept of development of new hydropower plants is facing several technical and socio economic challenges. The performance of the hydro-turbines is being limited by the sediment erosion problem as it is one of the burning issue in Himalayan basin. The presence of young mountains and man-made activities are adding fuel to the fire by contributing more to flourish the problem rather than minimizing it. This sort of hindrance has been considered as one of the major technological challenges in context of Nepal for developing new hydropower plants. Most of the economically feasible hydro-power plant in Nepal which has to be harnessed onwards fall within the working envelop of Francis turbine [15]. The present scenario regarding the problem minimization is considered as mostly specific and local problem for Himalayan region and Andes Mountain of South America [7, 10]. This local problem with huge hydro-electricity potential is basically addressed locally. Hence, the globalization of the problem is must without any delay. There is a strong need to have an ultra-review on sediment erosion pattern and suggest appropriate mitigation measures that targets to minimize its effect on the turbine components.

The sediment erosion problem can be addressed through the development of new materials and expansion of settling basin; however, both remedial approaches are un-

favorable in context of Nepal due to the unavailability of sophisticated technologies, presence of young mountains and its geographical condition[6, 16]. It goes without saying that many industrialist and academic intellectuals are keen to contribute to minimize this problem as it can neither be controlled nor be avoided. Kathmandu University has started research on hydro turbines since 2003, this can be considered as a preliminary date for the advancement. This kind of problem has lured higher academic interest which could foster new technology in design, manufacturing and operating strategy.

1.4 Scope of the research

The scope of the research is to develop a tool or methodology that can be used in conceptual design of Francis turbine runner design for the sediment laden conditions. In order to avoid critical sediment erosion for developing phase new hydro power this research final outcomes may play the vital role for reducing sediment erosion than the traditional design. The study uses numerical techniques to study the effect of sediments on runner blades and guide vanes. The design process adopted in this thesis is based on parametric design, redesign, selection design and configuration design. The numerical results are compared with the site measurements. Erosion in other components of the turbines are not considered in this study. CFD is carried out by using commercial code, ANSYS CFX and the simulations are done in one guide vane and one runner blade passage.

The design and analysis of Francis turbine for sediment load research aim to contribute the knowledge for:

1. Conceptual design of high head Francis turbine for sediment load conditions.
2. The effect of sand erosion on 10 different guide vane angles and its strategic development for operations.
3. Application of optimization procedure for Francis turbine design for the sand laden condition.

Chapter 2: LITERATURE REVIEW

This chapter contains exhaustive literature survey regarding the abrasive wear and effects of several parameters like hardness, direction on the turbine material. Additionally, coating effects, particle trajectory and information on testing performed to visualize the erosion are also presented.

2.1 Abrasive wear in hydraulic machinery wear theory

Based on wear test results, several authors [17, 18, 19, 20, 21, 22, 23, 24] state that wear rate depends upon the function of velocity, material hardness, grain size and concentration of solid i.e.

$$\text{wear} \propto (\text{velocity})^n \tag{2.1}$$

Where, the index 'n' varies according to the material and other factors involved and its common value is 3 [18, 19, 22, 23, 24].
In 1971, Bovet states the abrasive power 'P_f', depends upon velocity of the particle and several other parameters given by equation (2.2) [24, 25]

$$P_f = \frac{\mu V (P_s - P_a) C^3}{R_p} \tag{2.2}$$

Where, μ is coefficient of friction between particle and surface, V is volume of particle, P_s is density of particle, P_a is density of liquid, C is velocity of particle and R_p is radius of curvature of surface.

2.1.1 Effect on hydraulic performance and working life

Bezinge et. al. [24, 26] study on worn labyrinth seal clearances and present the impact on the performance of turbines. In addition, Ferry et. al. [27] claim the role of increased clearances of Francis turbine and worn out runners in reducing the turbine efficiency.

For the prediction of hydraulic turbine working life, Bak and Bergeron states that [19, 28, 29]:

$$\text{life} \propto \frac{1}{(\text{total head})^{3/2}} \quad \text{i.e.} \propto \frac{1}{\text{wear rate}} \tag{2.3}$$

Additionally, Bak formulated the following equation to show other factors that affect wear and tear.

$$T(life \in h.) = A\frac{KQ^n}{H^{3/2}W_sX} \tag{2.4}$$

Where, A is constant factor, Q^n is Concentration of solid in mixture (%), K is Impeller shape factor (1.0 for multi-bladed impellers, 1.4 for channel impeller), H is total head/stage, W_s is coefficient of abrasive wear for impeller material and X is Coefficient of abrasiveness of solids.

2.1.2 Effect of hardness

Several test results showed that hardness of substrate materialshould be increased to resist the abrasive wear [17, 18, 24, 29, 30]. While Antunes and Youlden [23] admitted the linear relationship between hardness and resistance of metals, Stauffer [18] didnt find any relation between them. In support of latter one, Bergeron [28] stated that hardness is not the factor that determines the wear in a material. However, in case of hydro turbine, erosive wear is found to be more with increase in hardness of the erodent [6, 7]. Based on the experimental experiences, the hydro-abrasive wear was commonly quantified by means of wear rate, W and generally expressed as [31].

$$W = f \text{ (Properties of eroding particles; properties of base material and operating conditions)} \tag{2.5}$$

Kjolle [31, 32] made detailed study on the hydro turbines and proposed that cavitation, sediment, fatigue etc. are the main causes for the failing of hydro turbines,

mainly the runners of the Francis turbine. These effects can be minimized by altering the design aspects of the component at the design phase.

Neilson and Gilchrist [31, 33] assumed that the total wear is contributed by only deformation wear which gives a deformation factor ($\in$) as below:

$$\in = \frac{W_d}{\frac{1}{2}M(Vsin\theta - k)^2} \tag{2.6}$$

Where,W_d is deformation wear at normal impact condition, M is the total mass of impacting particles, V is velocity of particle, θ is impact angle and k is the normal component of particle impact velocity that initiates the erosion.

Bain et al. [34, 35] developed a correlation to assume erosion rate which is expressed as,

$$W = KV^{\beta}d^{\gamma}c^{\phi} \tag{2.7}$$

Where, W is erosion rate, V is velocity of particle, d is particle size, C is solid concentration and, K, β, γ and ϕ are constants that depend on the properties of the erodent as well as the target material.

Based on the hydraulic performance tests on a Francis turbine model with sediment laden flow conducted in Japan, Okamura and Sato [36] reported the turbines efficiency is correlated to solid concentration by the following expression:

$$\eta_m = (1 - 0.085C_w)\eta_w \tag{2.8}$$

Where, η_m is turbine peak efficiency with sediment-laden flow, η_w is turbine peak efficiency with clean water and C_w is fraction of solid by weight.

According to Krause and Grein [31, 37], the abrasion rate on conventional steel Pelton runner made of X5CrNi 13/4 is given by equation 2.9,

$$\delta = pqcv^3.4f(d_{p50}) \tag{2.9}$$

Where, δ is abrasion rate (μm/h), p is a constant, q is quartz content, c is mean sand concentration,v is relative jet velocity and f(d_{p50}) is function defining particle size.

As the above equation is applicable to turbine components of particular material only, Naidu [38] suggested the expression equation 2.10 for predicting the silt erosion rate:

$$W = S_1 S_2 S_3 S_4 M_r v^x \tag{2.10}$$

Where, S_1 is coefficient of silt concentration, S_2 is coefficient of silt hardness, S_3 is coefficient of silt particle size, S_4 is coefficient of silt particle shape, M_r is coefficient of wear resistance of base material and v is relative velocity of water. The exponent has value 3 for Francis runner, 2.5 for guide vanes and pivot ring liner.

Asthana [31, 39] expressed the turbine abrasion as:

$$TA = f(PE, v^z) \tag{2.11}$$

Where, PE is modified suspended sediment content, v is relative velocity between flowing water and turbine parts where abrasion is severe and z is exponent for relative velocity

Further, the modified sediment content (PE) is obtained by the equation 2.12:

$$PE = P^\alpha a^\beta k_1 k_2 k_3 \tag{2.12}$$

Where, P is the average annual suspended sediment content in gm/l, α is exponent of 'P' representing correction factor for suspended sediment concentration. It has value 1 for concentration up to 5 g/l. a is average grain size coefficient of suspended sediment with a base of 0.05 mm. β is exponent of 'a' representing correction factor for average particle size, which was taken as 1 for particle up to 0.6 mm and curved flow; k_1, k_2, k_3, represent the coefficient to account for shape, hardness and abrasion resistance of base metal, respectively. k_1 is taken as 0.75, 1.0 and 1.25 depending on irregularities ranging from few to severe, k_2 was taken as 1 for hardness greater than

3 (on Moh's scale) and 0.5 for less than 3, k_3 was taken as 1 for 13Cr4Ni steel.

Schneider and Kachele [31, 40] stated that wear rate, W is the function of sand concentration, hard particle contents, median particle size and flow velocity.

$$W \simeq cqf(d_{50})v_f^n \tag{2.13}$$

Where, c (kg/m^3) is sand concentration, q (kg/kg) is hard particle contents, d_{50} (m) is median particle size and v_f (m/s) is flow velocity.

2.1.3 Effect of direction (impact angle)

While studying the hydraulic turbines impact angle of abrasive wear, considering tangential velocity only, Bovet [24, 25] found decrease of wear on increasing impact angle. But effect of wear in hydro machineries are more complex. When considering cutting and deformation cases, Bitters expression [41] showed wear depends on both normal and tangential velocity component of striking velocity.

2.1.4 Effect of medium on impingement angle

Levy et. al. [42, 43, 44] studied on the trajectory of particles that strike a cylindrical body and found that viscosity has great influence on the erosion of material. He stated that less number of particles strike the body in high viscous media as compared to low one due to change in the impingement angle of the striking particle which results in lesser wear of the material.It is visible from the Figure 2.1 that higher viscous medium shifts the particle trajectory towards the periphery of the cylinder which alters the location and form of wear.

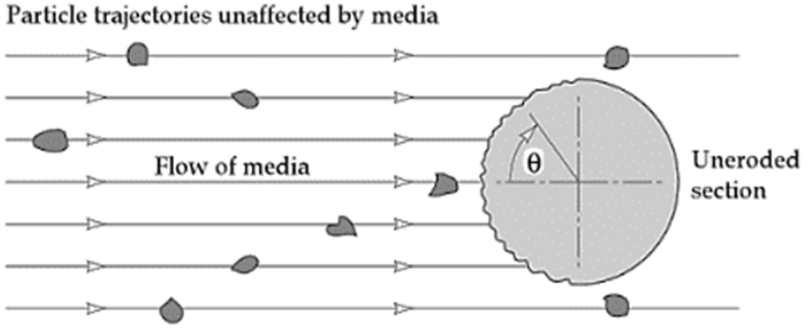

(a) Low viscosity media

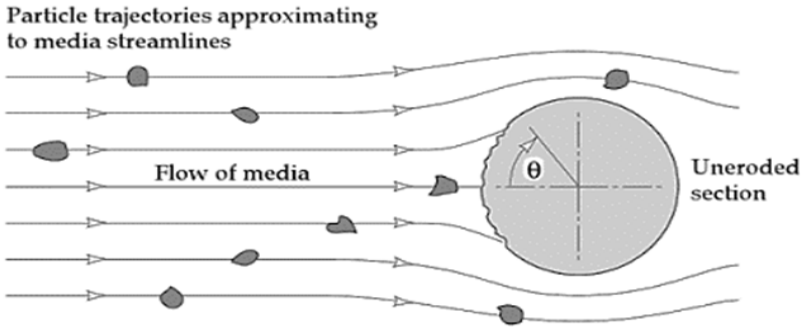

(b) High viscosity media

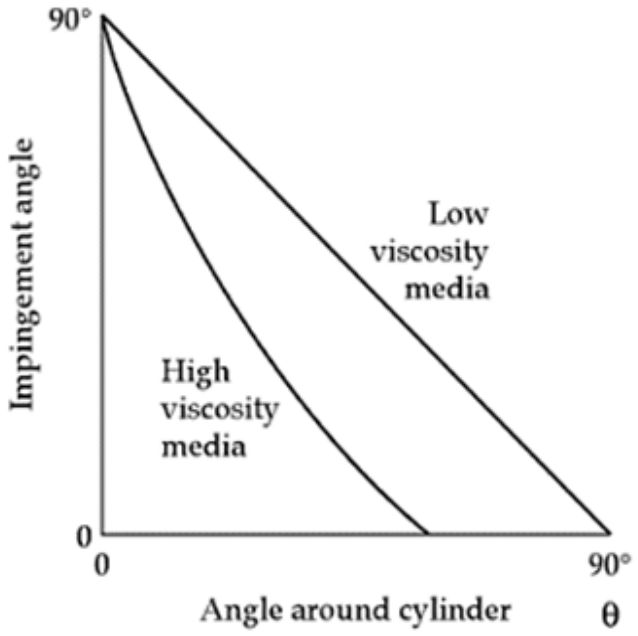

(c) Combined low and high viscosity media

Figure 2.1: Effect of medium on impingement angle by erosive particles [45].

2.2 Status and current researches

In 1984, Professor Brekke postulated erosive wear in hydro turbines. According to his PhD lecture note, sand erosion basically occur in the inlet valve system, spiral casing, the pressure relieve system, the guide vane system, runner and runner steel and the draft tube. Brekke insisted that the major problem in case of hydro turbine-sand erosion is inevitable but can be reduced because it is not possible to sediment silt with grain size less than 0.1 mm or 0.06 mm can cause substantial damage [46].

Padhyet. al. [31] performed review on silt erosion and found that hydro turbine functions with highest effectiveness in the initial days of its installation; however, its performance declines after few years of operation. The major reason behind this is erosive wear of the turbines due to the high content of abrasive material during monsoon that can make prime impact in the plants of run-off river schemes and those situated in hilly regions. Further, it leads to increase in vibration, fatigue damage, inefficient operation, and eventually system failure which demand the change in blade profile [31].

Numerous computational and experimental studies have been carried out to inspect the process of erosion in hydro turbines and the effect of solid particles in coated and uncoated turbine blade material surface. The roughness extents measured earlier and after the erosion test indicates the variation in surface roughness in turbine blade material resulted by erosion. The different computational studies were carried out on low pressure turbine. After simulation, the vane and blade surface erosion patterns were assumed combining the data with experimental one [47]. Individual awareness on particle trajectories and blade surface degradation and coating has subsequently increased due to the seriousness of erosion results on turbine life and effectiveness.

Not only the blade surface degradation and coating, extensive research has been conducted to visualize the erosive nature in hydro turbine steels. The experimental task conducted by Chauhan et. al. [48] presented the comparative nature of erosion in

martensitic and nitronic steels and stated the latter one to be high erosion resistance. The test pieces for this experiment were machined for metallographic tests, tensile tests, impact tests and erosion tests.

The metallographic analysis is generalized for example cast steels were ground and polished and the microscopic observation on them determined microstructure about their erosion behavior. In the test, nitrogen strengthened austenitic stainless steel having low Ni and higher concentration of carbon was used. The slopes obtained from erosion tests were almost constant except for nitronic steel at 90^0 impingement angle [48]. This variation in the slope is resulted due to the changes in mechanism of erosion damages during the erosion test. However, the constant nature of slope at both 30^0 and 90^0 impingement angles in case of martensitic steel is due to the characteristics of steel to undergo strain hardening less likely. Whereas, belonging to an austenitic matrix, nitronic steel is more likely to undergo strain hardening resulting in material loss due to embrittlement. The other significant difference on two samples is that the martensitic stainless steel are found less hard and ductile as compared to nitronic steels. In addition to this, the higher nature of erosion resistance in nitronic steel is also due to its tensile toughness which is greater in amount comparing to martensitic steel.

2.3 Shape and size characterization and experimental set-up

To analyze shape and size characterization, samples were taken from rivers like Roshi, Sunkoshi, Indrawati and Modi which lies in middle and western part of Nepal. These were collected from each river different sections considering upstream, human interference zone, tributaries joining points and downstream. Mostly fluvial sediments were collected from the middle section of the rivers using bucket.

Sieve analysis was done to characterize sediment size as it is the one that has great influence in eroding turbine material. Six layered sieve analyzer was used and vi-

brated for 10 minutes to separate each sample by size in its respective sieve plate. Roshi, Sunkoshi, Indrawati and Modi rivers sediments from five different sections were sampled and sieved to respective sizes category as shown by table 2.1.

Table 2.1: Sieve size.

Sieve No.	1	2	3	4	5	6
Size (μm)	$>$500	425-500	300-425	212-300	90-212	$<$90

Among these sieved categories only three different sieve sizes were considered under study that ranges from 90 to 300 micron sediment sizes. Particles larger than this get filtered and are restricted to enter the turbine, so only the smaller sizes sediments were considered for experiment.

2.4 Shape characterization

Shape is another factor that determines the extent to which turbine materials are damaged. Few researches have been conducted showing the effects of sediment shape on turbine material. This study is an attempt of characterizing the sediment particles and its effect using digital image processing which can process the sediment image and trace out the different shapes of sediments. Shape morphology of sediments was extracted and defined using image processing. Fourier Transform was utilized to derive different descriptors that clearly depicted twenty one different shapes of sediments. Primarily impact by size was studied and later on setting these 21 different shapes, its impact was studied and compared.

Complex Fourier function was firstly used to define the sediment image and then its transformation was obtained to define the descriptors of shape, so that all the image analysis which defines shape was done in Fourier domain. Firstly a sediment particle was studied by taking coordinate values as a function within a defined boundary using image processing. Then, different derivatives were obtained from the image giving real and imaginary parts. It is mathematically governed by the Complex Fourier

function defined by equation (2.14) as:

$$x_m + iy_m = \sum_{-\frac{N}{2}+1}^{+N/2} (a_n + ib_n) \left[cos\left(\frac{2\pi nm}{M}\right) + isin\left(\frac{2\pi nm}{M}\right)\right] \tag{2.14}$$

Where, x, y are coordinates describing the particle; N is the total number of descriptors; n is the descriptor number; M is the total number of points describing the particle; m is the index number of a point on the particle; a, b are coefficients for each descriptor; i denotes an imaginary number.

Matlab platform and Matrox Imaging library tools were utilized for image processing. Image of sand particles were taken and its inherent coordinate were utilized to process and analyze. Sand particles shape perimeter and its different neighbors were accounted which was equally assessed and broken into 128 equal new coordinates. Fast Fourier Transform was carried out after the division of shape to describe and understand the descriptor of shapes. An image taken first, also known as parent image, gives the original profile and it is done by image analysis which is shown by figure (2.2). It is the original image being processed and its edges has been fairly traced to give its exact perimeter.

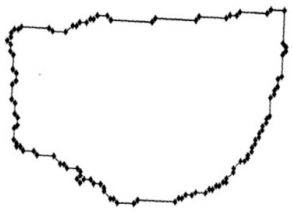

Figure 2.2: Digitized Outline of Particle [49].

The original image was suppressed using higher order of descriptors. The highest order of the particle descriptors is of +/-64. The main aim is to have a refined morphology of sediment particle which output is shown by figure 2.3(a). Furthermore the image was reconstructed applying fast Fourier Transform which are shown by figures 2.3(b), 2.3(c), 2.3(d) and 2.3(e) respectively.

(a))+/- 64 Fourier Descriptors (b) +/- 24 Fourier Descriptors (c) +/- 8 Fourier Descriptors

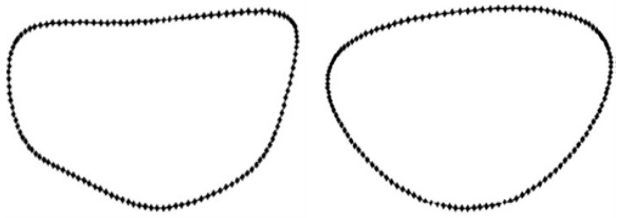

(d) +/- 5 Fourier Descriptors (e) +/- 3 Fourier Descriptors

Figure 2.3: Fourier Descriptors [49].

The particle image was reconstructed defining the Fourier descriptors in their respective orders. It is found that the image are suppressed but have retained their original morphology. Its equivalent data were statistically observed and analyzed using digital image processing. 21 different sediment shapes obtained from four different rivers were given by their own specific name in this research. These were quantitatively analyzed in Machine Vision laboratory at Kathmandu University and defined by following shape no index and shape morphology terminology given in table 2.2.

Table 2.2: Shape no. and morphology of 21 different sand [49].

Shape No Index	Sediment Shape Morphology
1	Well rounded with high sphericity
2	Well rounded with low sphericity
3	Rounded with high sphericity
4	Rounded with low sphericity
5	Sub rounded with high sphericity
6	Sub rounded with low sphericity
7	Rounded angular with high sphericity

Shape No Index	Sediment Shape Morphology
8	Rounded angular with low sphericity
9	Low angular with high sphericity
10	Low angular with low sphericity
11	High angular with high sphericity
12	High angular with low sphericity
13	Slight Elongation (E)
14	Moderate Elongation (E)
15	High Elongation (E)
16	Slight Square (S)
17	Moderate Square (S)
18	High Square (S)
19	Slight Triangular (Irregular) (T)
20	Moderate Triangular (Irregular) (T)
21	High Triangular (Irregular) (T)

2.4.1 Characterization of Sediment Particles

An image processing program has been developed on MATLAB platform to extract the exact shape of sand particles collected. Sand particles were collected from the erosion sensitive power plants and its digital images had been acquired.

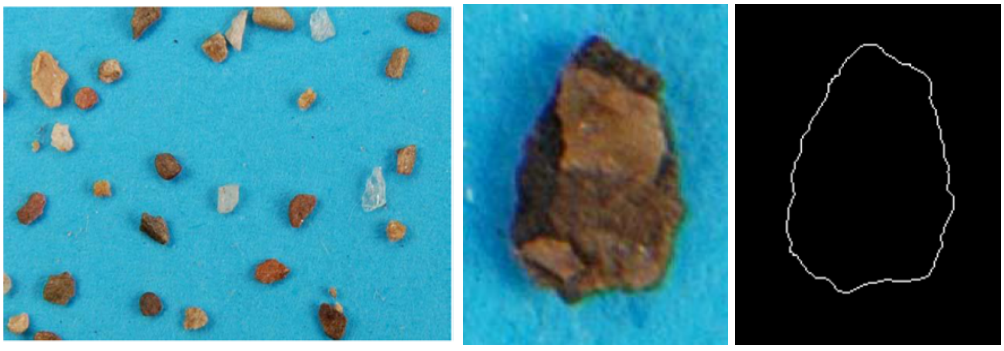

(a) Raw image of sand particles (b) Cropped image of single sand (c) Edge boundary of single sand

Figure 2.4: Different images of single sand particles [49].

These shapes have further been analyzed by artificial neural network. This network has been first trained for the known input and known output. After that it is trained for unknown input and known output. Finally these networks could recognize any shape given to it and gives the shape which is nearest to the seven predefined shape [50]. Figure (2.4) shows the image processing steps used to characterize the sediment particles.

2.5 Hard coating

The study about design of hard coating architecture for the optimization of erosion resistance discusses about TiN coating response to impact, effect of coating thickness and youngs modules effect of impact velocity. It further includes particle size effect of substrate material and hardness and super hard erosion resistance coating systems. The identification about the hard coating architecture which is personalized to make distinguished about propagation suppressed and it allows to predict and minimize the erosion rate. The study has obtained the new perspective of FE model incorporated mechanical properties of the hard coatings such as hardness and hydro turbine fracture toughness and the probable prediction of the area of probable crack propagation in the hard coating optimization under particle impact [51]. While examining the experimental result with stress reduction on surface, multi-layer configuration of hard coating was found to be best in terms of high performing erosion resistant coatings.

At Kathmandu University, different strategies like rotating disc apparatus (RDA), high velocity impact jet are developed to study the effect of sand erosion and minimize the failure of hydro turbines. The objective of this test was to compare the performance of HVOF coatings with that of stainless steel. A disc, made up of Stainless Steel SS316, was taken and half of it was coated with tungsten carbide (86% Co 10% Cr 4%). Based on the area and pattern of erosion, analysis of the erosion damage in stainless steel and HVOF coatings was done through comparison [8, 13]. Figure 2.5 shows the erosion test of stainless steel and HVOF coating and Figure 2.6 shows the erosion pattern generated by combined effects of sediment erosion and cavitation.

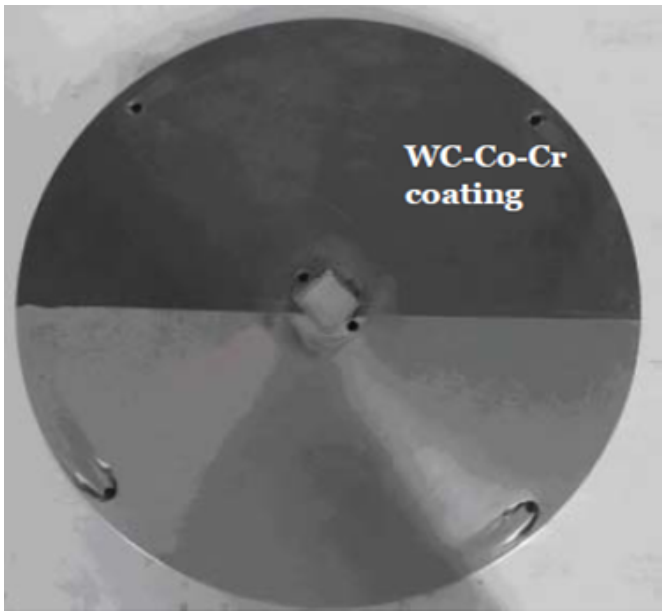

Figure 2.5: Erosion test of stainless steel and HVOF coating [52].

Figure 2.6: Erosion pattern generated by sand erosion [52].

2.6 Accelerated testing for erosion resistance

Two different test rigs, High Velocity Jet Rotating Test Rig and Rotating Disc Apparatus (RDA), at Kathmandu University were used for this purpose.

2.6.1 Erosion test rig

Figure 2.7 below shows the basic construction of a hydraulic circuit with high velocity jet that was used to investigate the accelerated erosion effect on turbine material and surface coating. It consists of 5.5 kW mono-block centrifugal pump having head 45 m and discharge 6l/sec along with valves -to control the flow of water and sand particles and bypass circuit -to control the water flowing through the nozzle. The sand is weighed and filled into the 1 m height hopper ahead of nozzle. As the pump is started and valve of sand hopper is slowly opened, disturbances is created inside the hopper by the water and then sands fall down in the horizontal pipe due to gravity. The water accelerates the sand which then strikes the specimen 100 mm away from nozzle exit. The test goes on till all sand pass through the nozzle. This duration depends on several parameters like size of sand particles, velocity of water and opening of the valve [52].

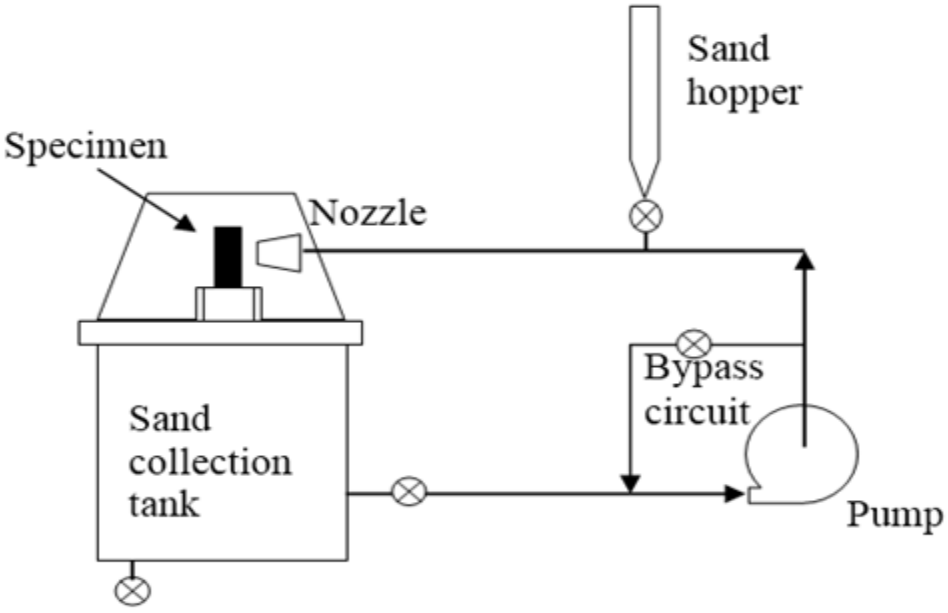

Figure 2.7: High Velocity Jet Erosion Test Rig at KU [52].

The test is carried out on a T-shaped specimen coated with HVOF ceramic coating in all surfaces including edges with focus mainly on three areas of the specimen. Each area is tested for different purposes; Area 1–to focus on the loss of coating and to check if the coating can withstand a large sediment load; Area 2–to study

damage on corners and Area 3–to study if the coating on sharp corner is weaker than other places. Two specimens are attached to study the effect in the joints as shown in figure 2.8(c) which resembles the joint of blades to the runner hub as shown in Figure 2.8(d).

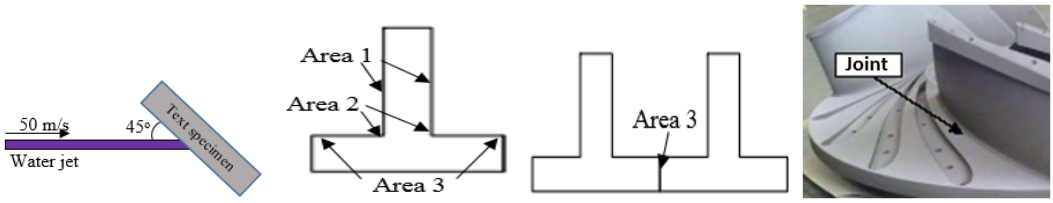

(a) Erosion Test Criteria (b) Test Area in Coated Specimen (c) Test in Joints (d) Detachable coated blades

Figure 2.8: Test condition and materials during erosion testing [52].

The quantification of loss of coating material obtained from this test was not convincing although the symptom of damage coating was visible. The weakest area for the DynaVec Francis runner is expected to be Area 3 at edges and joints but realistic effects of erosion cannot be generated in the test specimen due to interference of jet with splashing water. As this study didnt produce acceptable results for further analysis new specimens were designed to carry out erosion test for the joint similar to Figure 2.8(c) in Rotating Disc Apparatus.

2.6.2 Rotating Disc Apparatus (RDA) Experimental setup

Rotating Disc Apparatus (RDA) was developed at Kathmandu University to overcome the flaws of the previous test and to study the sand erosion, cavitation and its synergic effects [52, 53]. It comprises of a rotating disc driven by a 7.5 kW motor at 2880 rpm in the sand and water slurry chamber. Four specimens can be installed in the disc and rotated along with the disc with velocity up to 39 m/s. The interaction of sand particle with the coated specimen is at low impingement angle and this condition is very much similar to flow in Francis turbines.

Test specimens having 5 different shapes at the edge of joint, both with and without nitrogen carbide based coating were tested with RDA. Four specimens with two sets

of each test samples for validating test data were fitted into the rotating disc at a time. Each test was conducted at 10000 ppm of sediment concentration with particles size of less than 200 microns. Test cycles were increased from 10 minutes to 60 minutes with progressive test cycle. On average 12 cycles of tests were conducted for each sample and scanned image of the specimens together with measurement of weight loss were recorded after each test cycle.

Figure 2.9(a) shows the setup of RDA used for testing erosion on different shapes of joint edges. Figure 2.9(b) shows the rotating disc with slots for holding 4 test specimens at a time. Figure 2.9(c) & figure 2.9(d) shows scanned image of a test specimen's joint before and after the test with RDA at the sediment concentration of 10000 ppm for 550 minutes.

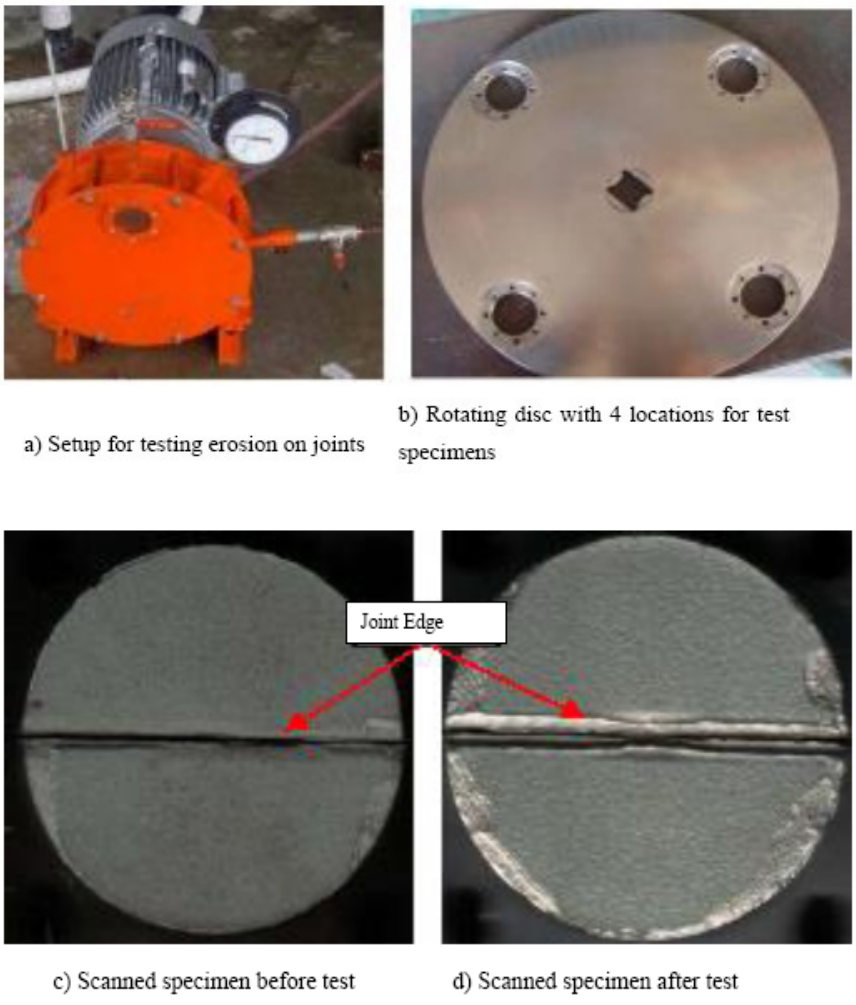

Figure 2.9: Setup, rotating disc and scanned specimen [52].

The experimental study done at Turbine Testing Lab, Kathmandu University was ensued by computational analysis that has been carried out to analyze the effect of shape and size of sand particles in turbine materials of the hydropower plant [49]. Findings from the study suggested that shape and size of such particles along with their velocity directly affect the rate of erosion in turbine components [49].

In 2002, Karlen et.al. [54] predicted the patterns of hydro-erosion to examine the hydro turbines on the basis of metallic lusters, fine-scaly erosion, scaly erosion, large sized scaly erosion, in-depthscaly erosion and depth erosion. These patterns are ultimately assigned to the turbines as a result of different kind of erosion during the operation of power plants. Brekke et.al, 2002 [55] , then, classified the phenomenon of erosion into three different group, namely Turbulence erosion, Acceleration erosion, and Secondary flow.

Neopane[56] revealed that the reduction of erosion takes place when the turbine is operated only at best efficiency point (BEP) and the rate gradually increases when operation occurs in part and full load condition[6, 56]. This increment in erosion rate is the result of increase in turbulence and relative velocity at the outlet.

The traditional designs were made such that most of hydraulic energy conversion takes place at the beginning half of the blade [57, 58]. Several studies showed that the erosion rate can be greatly reduced by changing the hydraulic design procedure[10, 55, 56, 57, 59, 60, 61, 62].

Figure 2.10: Francis runner of Jhimruk Hydropower Plant (Courtesy BPC).

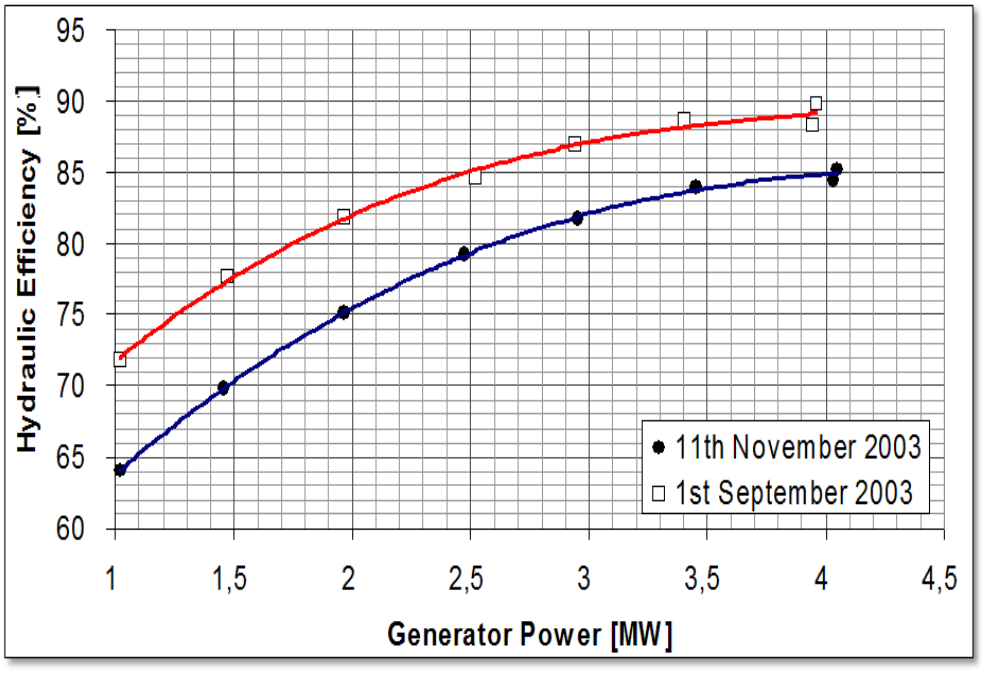

Figure 2.11: Drop in Efficiency at best efficiency point (BEP) [16].

The dawn of commercial CFD and FSI code provides the new horizons to the turbine designer in order to predict pressure velocity and strength of different parts without any experimental testing [63]. These CFD and FSI analysis have played significant value in improving machine design and its performance thereby minimizing the turbine design time and cost [64].

Jhimruk Hydropower plant, a run-off type power plant and severely suffered site due to sediment problem is located in Pyuthan district of Nepal[7, 14]. The plant consists of three Francis Units each of 4.2 MW. Figure 2.10 shows Francis turbine runner damaged by sediment erosion. In 2003, Ole and his team measured the thermodynamic efficiency and found about 4% drop in efficiency at BEP, within the period of 1 September 37, 2003, and 11 November 2003, as presented in the figure 2.11.

Several studies revealed that the sediment effect mainly depends upon flow parameter, sand particle characteristics and properties of material [6, 31, 55, 56, 57, 59]. A study conducted by Pradhan et al., 2004 at Jhimruk Hydropower, Table 2.3, showed that the efficiency is reduced by 4% at BEP condition and by 8% at 25% load condition when 6900 tons sediment is passed through the system. Man et al., 2004 tried to overcome this difficulty by introducing different coating processes like ceramic coating, plasma nitriding, and high-velocity oxy-fuel spray. Besides this, the modification of design of turbine material has been particular field of research and as a result several optimized designs are made to counter the effects of sediments [65, 66].

Table 2.3: Primary Data of Jhimruk Hydropower.

S.N.	Parameter	Unit	Value
1.	Net Head (H)	m	201.5
2.	Discharge (Q)	m^3/s	7.05
4.	Efficiency (η)	%	96

Figure 2.12 showed the reduction in erosion up to 60 % which is resulted through the CFD analysis on the optimized design as compared to the reference design.

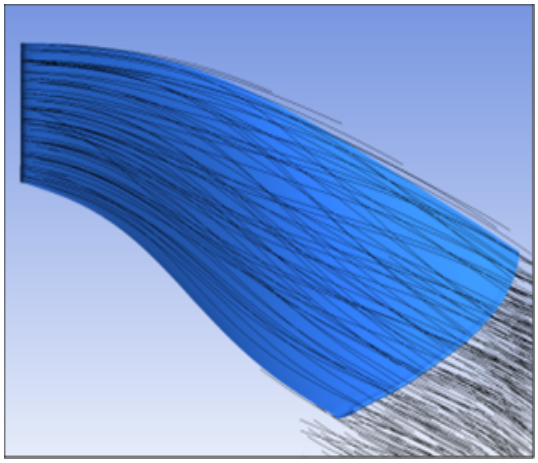

(a) Streamlines on pressure side of reference design

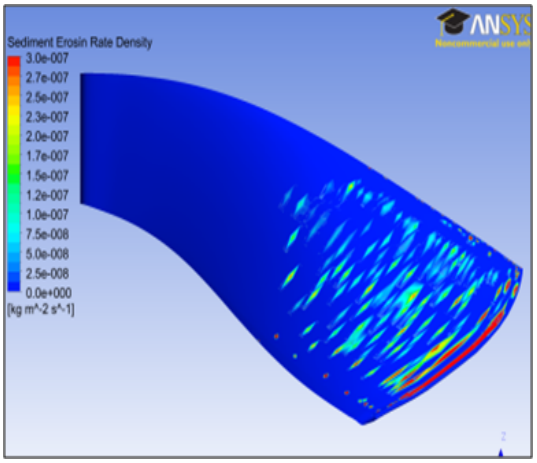

(b) Sediment erosion on reference design

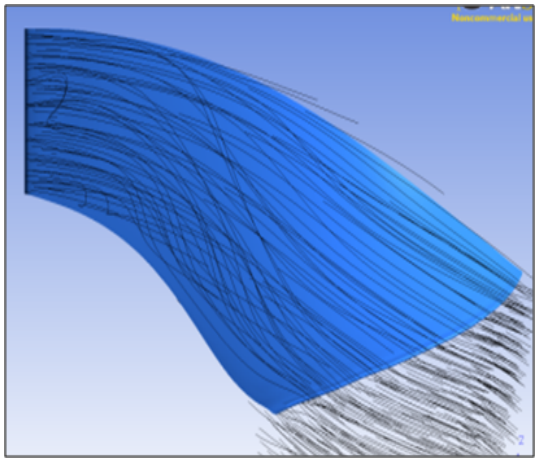

(c) Streamlines on pressure side of optimized design

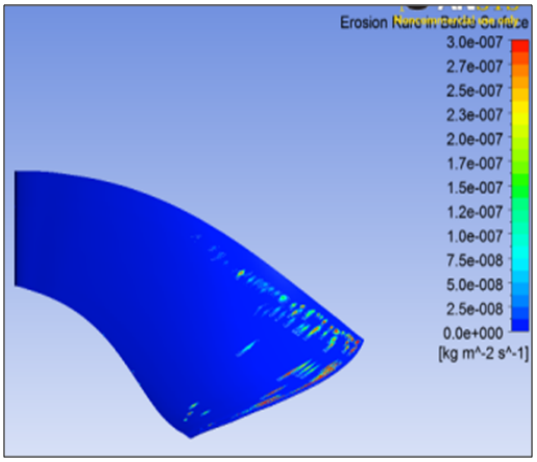

(d) Sediment erosion on optimized design

Figure 2.12: Streamlines and sediment erosion on reference and optimized design [64, 65].

The erosion rate is particularly greater during the monsoon period due to higher concentration in sediment content which causes the turbine components of the power plants to suffer severe damage resulting in efficiency drop. This damage piled up gradually and ultimately cause to shut down the plant for repair or for replacement of the damaged components [6, 7, 14, 56, 57, 67] after a certain period of operation. This has encouraged several research activities in order to quantify the erosion and

minimize its effects in hydraulic turbines [31, 68, 69].

Sand particle analysis of Roshi, Sunkoshi, Indrawati and Modi river basin and its image processing indicated that particles can be categorized in terms of shape factor and its combine effect of all the shapes was quantified by using RDA experiments. But this type of experiment can only conclude the loss in weight during the total operation hours whereas determination of effected spot is almost difficult due to environment of hydraulic nature and its conditions.

During RDA test, 10 different specimens comprising of 5 dissimilar shapes of edge at joint, each with coated and uncoated were tested. The test results showed that the coated samples eroded to lesser extent as compared to uncoated one. Similarly, the erosion rate could be reduced by introducing uniformly curved fillets in the joints with sharp edges or chamfered edges. Such rate varies with variation in fillet radius at joints [52].

Figure 2.13 shows the trend of weight loss from test specimens for different shape of edge joint. It also shows that the weight loss increases significantly for uncoated samples for the same shapes of the edge. Figure 2.14. indicates the average erosion rate on different shape of edge for coated samples. It also shows that keeping all other parameters same, shape of edge joint determines the erosion rate for test specimen. The test specimen S-04 has erosion rates 9 milligram per kg of sediment per hour of operation lower than that of test specimen S-08 [52]. This difference can create substantial difference in material removal in case of a turbine with longer operation time under higher sediment load, and hence significant reduction in performance and expected life of the turbine.

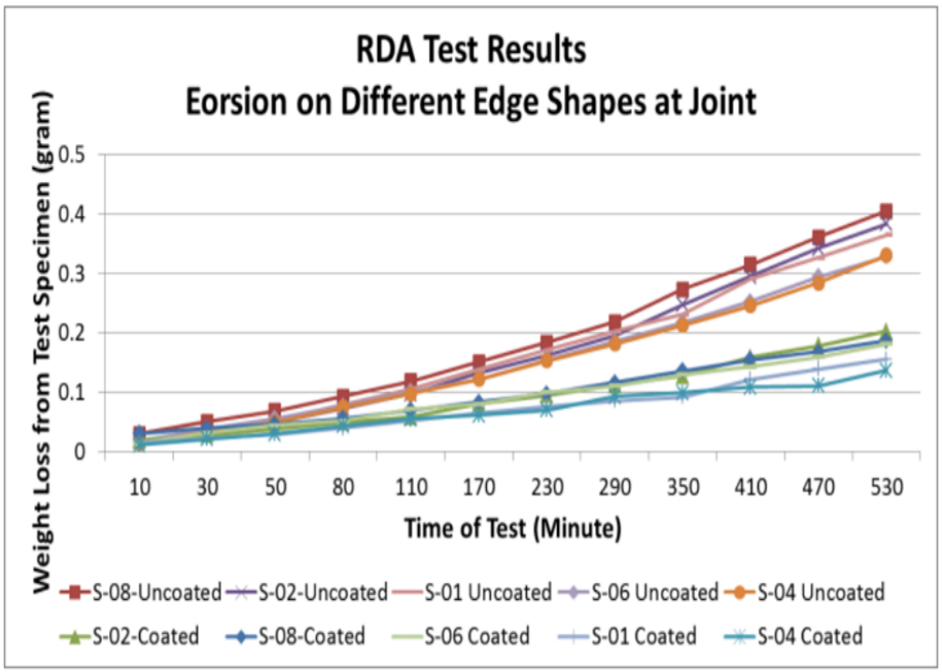

Figure 2.13: Erosion trends for different edge joints [52].

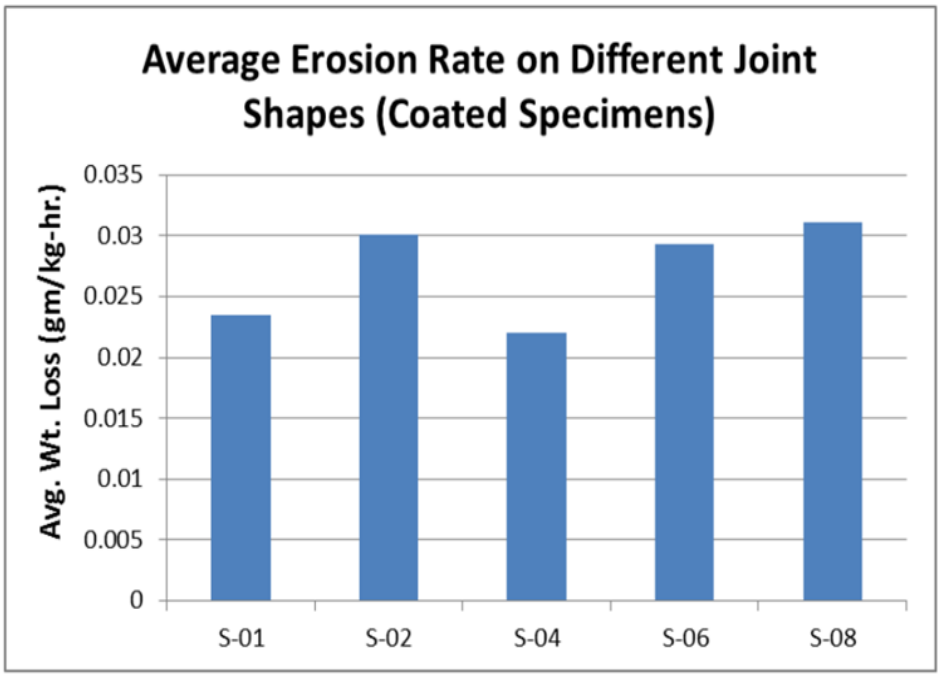

Figure 2.14: Erosion trends for different edge joints [52].

These results were used as the input parameters for design optimization in developing phase 2 runner by DynaVec for the Cahua Power Plant in Peru [52]. from figure

(2.14) The weak spots in pilot runner like edge of runner hub at inlet, edge at joint between runner blade and hub, and edge at labyrinth seals were optimized in shape so that they were less prone to erosion. The phase 2 runner was installed in the power plant and then after passing 159000 tons of sediment, it was inspected on January 2011. The conclusion was significant reduction in erosion on weak spots of phase 2 runner than that of the pilot runner in the same power plant earlier.

Figure 2.15(left) shows pilot runner developed and installed by DynaVec at Cahua power plant after operation under 130,000 tons of sediment load [52]. The leading edge at hub of the runner inlet and joint between runner blade and hub was observed to be eroded significantly. These disturbed the inlet flow pattern causing the efficiency of runner to be dropped further. Figure 2.15(right) shows the phase 2 runner, with design optimization in weak spots, after operation under 159,000 tons of sediment load in the same power plant. It can be observed that the erosion at the inlet edge has been reduced significantly after the optimization. Figure 2.16(left) shows the joint between runner blade and hub for the phase 2 runner after the same period of operation. Figure 2.16(right) shows the edge of labyrinth seals of the same runner after same period of operation. The erosion rate on both the edge at the joint and at the labyrinth seal was reduced considerably which validated the optimization of shapes of the edge in the pilot runner. This was accurately assumed by the acceleration testing on RDA at Kathmandu University.

Figure 2.15: Pilot runner after 130,000 tons of sediment load (left) and Phase 2 runner after 159,000 tons of sediment load (right) [52].

Figure 2.16: Joint between runner blade and hub after 159,000 tons of sediment load (left) and Edge of labyrinth seals after 159,000 tons of sediment load (right) [52].

Sediment samples collected from four different rivers Roshi, Indrawati, Sunkoshi and Modi were categorized according to size and shape and its impact on turbine material was studied separately [49]. Firstly, sediment test rig set at Kathmandu University was used to study the impact of size on turbine material.

2.6.2.1 Impact of sediment size

The average impacts of the sediment collected from four different rivers are presented by figure 2.17–2.19. All the sediments collected were 90 to 425 micron in size and a graph is drawn by depicting the impact of size on turbine materials [49]. Figure 2.17 shows the chart of sediment impact on turbine material on the basis of size. Similar test conditions were used for testing of each sediments in test rig.

Roshiriver originates from hilly region and joins into Sunkoshi river and has peculiar characteristics. The sediment samples were collected from 20 different locations were first sieved to respected four categories and its impact on turbine material was performed. These sediment samples were categorized into four size range as shown in the graph of figure 2.17. The figure depicted that larger the sediment size, larger will be its impact on turbine materials. The impact of sediment size smaller than 90 micron has 0.002995 gram while as 90-212 micron and 212-300 micron size has impact or weight loss of turbine material is 0.00555gram and 0.00695 respectively [49]. The impact of sediment size 90-212 and 212-300 have somewhat in small difference while as comparing it to smaller than 90 micron they have twice more effect on turbine material. It is also clear that the impact due to size range 300-425

micron size has 5 times more effect than the sediment size smaller than 90 and about 2 times more than the effect of 90-212 and 212-300 micron size effect [49].

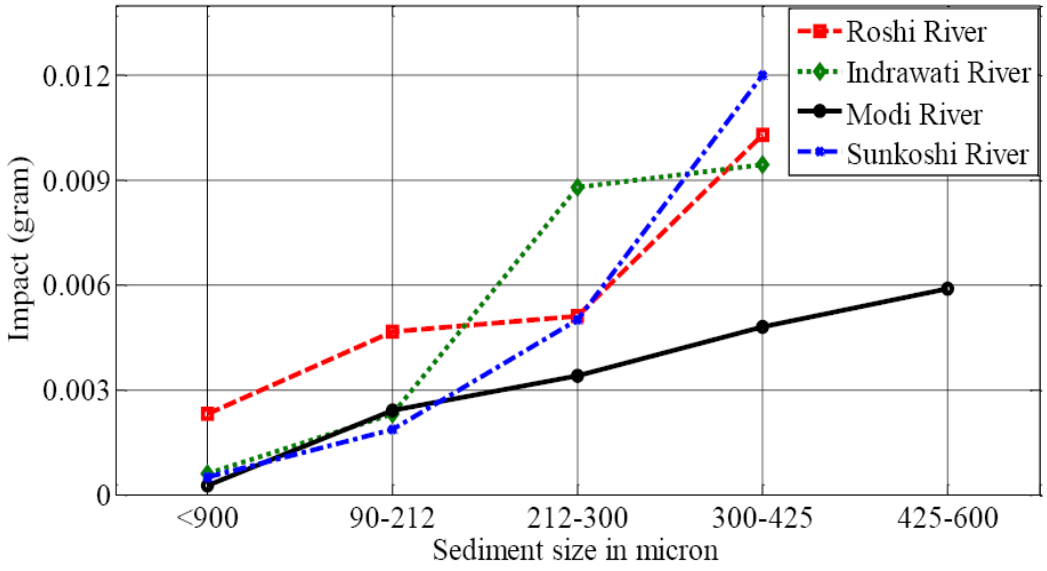

Figure 2.17: Size impact by sediment of four different rivers [49].

Figure 2.17 shows the impact of different size of sediment of Indrawati River on same turbine material. The chart shows little distinction in sediment impact but the trend line is somewhat following same pattern. Sediment size smaller than 90 micron have very less effect tracing only 0.000622 gram of weight loss, whereas 90-212 size sediment have 0.0023 gram of effect which is approximately equal to that of Roshi river sediment impact by size smaller than 90 but 212-300and 300-425 micron sediment size range has about twice much more impact than 90-212 micron size. From each of these graphs, conclusion can be drawn that sediment (from both the rivers) that falls on 300-425 sieve size range has significant impact which accounts four to five times greater than that caused by the smaller size range.

Sediments were collected from five different locations on upstream side of Sunkoshi river. Figure 2.17 shows the average impact of different sediment size on turbine material. It shows that the impact of sediment size in turbine material is gradually increasing in an order of 2. The sediment of size lesser than 90 micron has 0.00054 gram of impact whereas 90-212 micron has 0.0018, 212-300 micron has 0.0049 gram and 300-425 has 0.01188 gram of impact. The impact increment is quite similar to

exponential graph. The size impact by sediment on Modi river is depicted by figure 2.17. The impact is straight line type with equal slope. The impact of sediment size of this river on turbine material is increasing by increment of 0.001 gram of impact. The impact by size range 425-600 micrometer is also considered to follow the same pattern. Sediment size smaller than 90 has 0.00033, 90-212 has 0.0024 gram of impact, 212-300 micron has 0.00344 gram of impact, 300-425 micrometer has 0.0048 gram of impact and 425-600 has 0.0059 gram of impact. The impact is following some pattern from all four rivers size impact. This result concludes that the pattern of sediment size impact depends upon the river sediment which shows increment of effect either by multiple or by some intercepts.

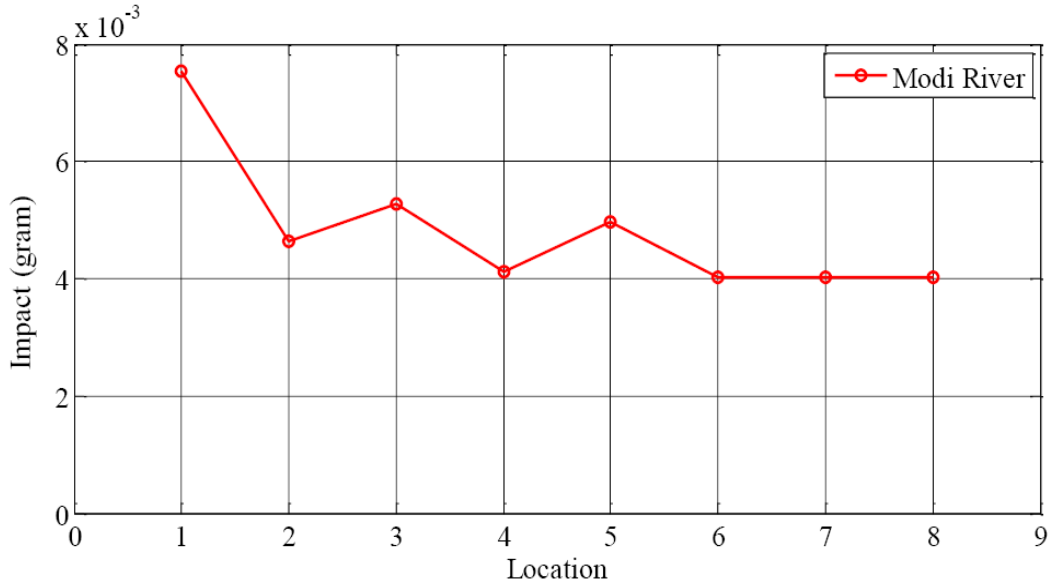

Figure 2.18: Erosion pattern due to sediment of Modiriver [49].

Figure 2.18 shows the actual erosion pattern due to sediment content in Modi River. It was found that the maximum material loss of 0.007 gram is seen in spot 1 and minimum loss of 0.004 is seen in spot number 7 [49]. This shows that the rate of erosion varies according to location, i.e. from upstream to downstream, and it follows the pattern that impact is high in upstream while low in downstream. As the particle flow with water from upstream to downstream, they collided with each other and pointed horns are broken down and the particles are changed into spherical shape.

2.6.2.2 Impact of shape

It is very difficult to define shape of the sediment and its exact impact; however, digital image processing technique has been applied to describe it. Matrox Imaging Library and MatLab software were used to define and count the sediment shape no and its effect. The effect of 21 different shapes on turbine material are clearly shown by figure 2.19 below. The shapes of sediment are indicated by its index no from 1 to 21 and are in horizontal axis with the corresponding impact in vertical one.

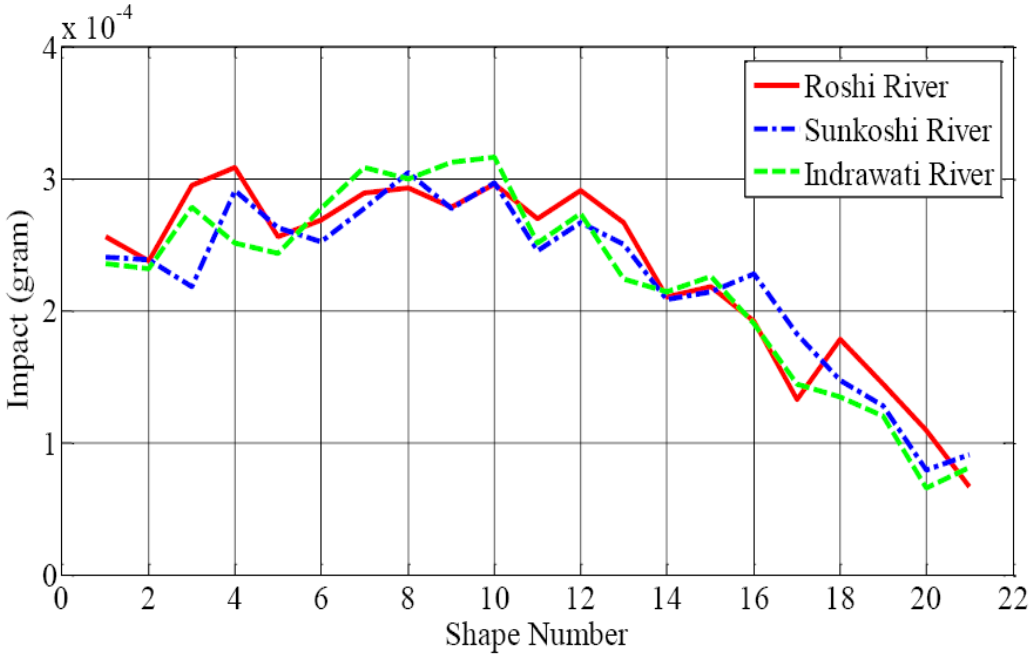

Figure 2.19: Sediment shape effect of three different rivers [49].

The figure 2.19 depicts the shape effect of sediment in Roshi river, which shows the fluctuating nature of line and the shapes are defined in an order rounded, angular, square to irregular shapes with high and low sphericity. The chart clearly depicts that the highest eroding property of shape no 4 while least by shape no 21 which refers to rounded with low sphericity and triangular or most irregular respectively. Similarly it also shows that the impact by shape no of Indrawati river which also has somewhat similar pattern. Unlike Roshiriver, shape number 8 of Indrawati river has highest eroding property and shape number 20 has least one. This study only involves the shape effect depending on the particles count.

Further, the figure 2.19 also shows the impact of sediment shape no on of Sunkoshi river on runner material. It depicts the similar trend as in case of Roshi and Indrawati River shape impact. Shape number 7 referring to rounded angular with high sphericity have highest eroding nature with impact of 0.00031 gram followed by shape number 9 referring to low angular with high sphericity has an impact of 0.00299 gram. Shape number 20 contributes to about 0.00008 gram impact and has least eroding property. All these three figures have similar kind of pattern, so it can be concluded that the shape number impact follows similar trend.

2.7 Progress of hydraulic design of Francis runner for sediment handling

Kathmandu University in close cooperation with NTNU has started a unique project to optimize the design of Francis runners for sediment handling that showed the possibilities of reducing sediment erosion significantly.

Each sites have unique turbine design which takes much time and effort to produce the suitable design for specific conditions. This makes design optimization task even for erosive environment even a challenging one. For the optimization process, it is necessary to evaluate relation of the turbine design parameters on sediment erosion so as to identify those parameters that can be attuned to reduce the erosion. Recent advancements in computing tools and software have added advantage to these studies.

A new program Khoj has been developed to create and optimize the runner design in preliminary stage. It is also featured to compare erosion in runner blades for different design cases. The final design can be exported to CFD and CAD tools for further analysis. Parametric study was carried out with Khoj in order to evaluate the relative effect of each design parameter on sediment erosion. The results from Khoj were compared to that obtained from CFD analysis to estimate effects of the design variables on hydraulic performance. Several optimized designs were developed and

analyzed to fulfill the desired condition of erosion and efficiency.

During the process of developing Khoj software, Gjosater [10] introduced five different shape of β distribution of blades to study erosion effects and is shown in the Figure 2.20. Then, erosion factor was calculated by the Khoj software and shape 1 was found to be less erosive than other types. However, Eltvik [57] found shape 4 was best among all five different shapes.

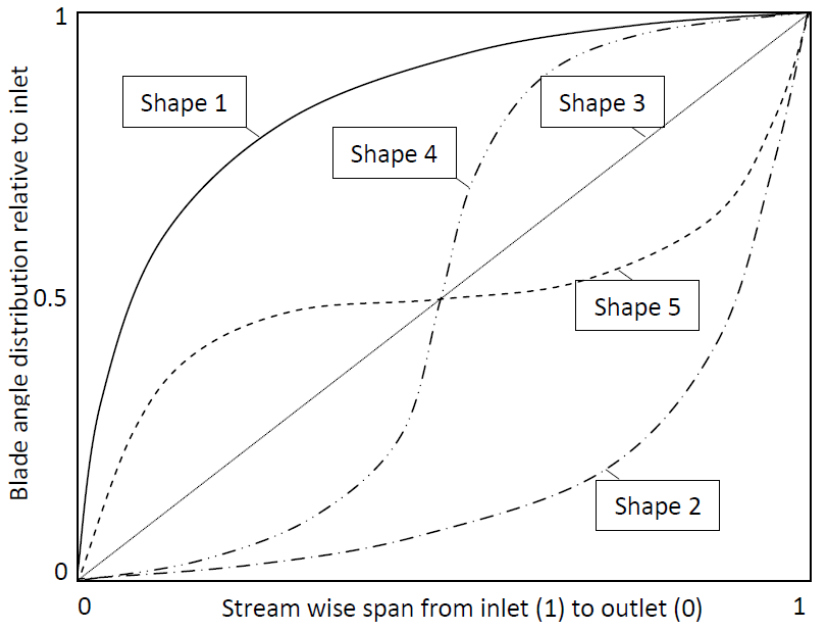

Figure 2.20: Different shapes of the blade distribution for the parameter study [10].

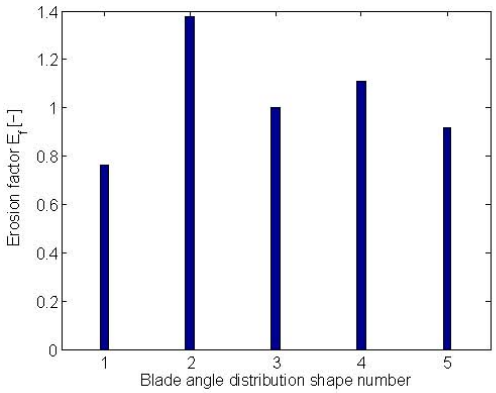

Shape	*Erosion factor*
1	0.76
2	1.38
3	1.00
4	1.11
5	0.92

Figure 2.21: Erosion of five shapes of the blade angle distribution [10].

2.8 Properties of five shapes of blade in terms of energy extraction

The energy extraction through the different set of the runner blade is presented in the Table 2.4. In the shape one, energy is extracted low at in let of the runner and high at out let of the runner. But, in the shape number two blade, energy extraction is opposite to that of the shape one. For the shape three blade energy extraction is liner throughout the blade and it is the simplest kind of structure compared to that of other four type blade shape. Shape four and five blade, extract energy is opposite to one another and the process also talks two folds within each half of the blade.

Table 2.4: Blade shape and its energy extraction type [57].

S.N.	Shape	Energy extraction type	
		Inlet	Outlet
1.	Shape 1	Low	High
2.	Shape 2	High	Low
3.	Shape 3	Linear	Linear
4.	Shape 4	First half span of blade: Low, High	Second half span of blade: High, Low
5.	Shape 5	First half span of blade: High, Low	Second half span of blade: Low, High

2.8.1 Reference Design

Jhimruk Hydroelectric Center (JHC) in Nepal is considered as the reference case for this study. The reference design for this power plant was based on net head of 201.5 m and net discharge of 2.35 m^3/s. It consists of three units of Francis turbine with splitter blade type and each unit of capacity 4.5 MW.

2.8.2 Design Optimization Range

The hydraulic design parameters are varied within a defined range and its effects on erosion factor is evaluated. Table 2.5 lists the range of variation of the design

parameters considered for this study.

Table 2.5: Hydraulic design parameters [8].

S.N.	Parameters	Symbol	Unit	Value for Reference design	Range of optimization
1	Outlet diameter	D2	m	0.54	0.4 - 0.75
2	Number of pole pairs in generator	ZP	-	3	3 - 12
3	Reduced peripheral velocity at inlet	U1	-	0.74	0.65 - 1
4	Acceleration of flow through runner	Acc	%	35	0-50
4	Height of runner	b	m	0.16	0.05-0.4
5	Blade angle distribution	β	^{o}	linear	4 different nonlinear

Evaluating effects of sediment erosions in optimized designs, the following two terms are defined as the indicators and the means of comparison of relative erosion in the Francis turbine runner.

Erosion Tendency (E_t)

It is the quantification of tendency of a specific design of runner to be eroded in similar sediment conditions. Erosion tendency is defined as in equation 2.15 [10]:

$$E_t = \frac{\sum_{i=1}^{n} W_i^3 \times A_i}{\sum_{i=1}^{n} A_i} \qquad [m^3/s^3] \tag{2.15}$$

Where n is the number of segment area (A_i) in the runner blade surface. W_i is the relative velocity of flow in each segment area. The segment area is the area between the intersection of $E_t = \frac{\sum W_i^3 \times A_i}{\sum A_i}$ and stream lines and stream points in the runner blade surface.

Erosion Factor (E_f)

It is ratio of erosion tendency of each new design with respect to the reference design. Erosion factor is defined as in equation 2.16 [10]:

$$E_f = \frac{(E_t)_{New\ Design}}{(E_t)_{Reference\ Design}} \qquad [-] \tag{2.16}$$

The erosion factor estimates a quantitative difference in sediment erosion of runner with the change in hydraulic design alone. In this study this factor is used as a means to compare the relative erosion in the optimized designs of runner with respect to the reference design.

2.8.3 Optimization in Design

Design optimization is the science of producing the best possible design within the stated domain.It has three different states, namely variables, objective functions and constraints. Variables are those that affects the system when it varies within its domain. In this case, variable may be the components of velocities. Symbolically, P1 and P2 are used for radial and tangential velocity respectively. Another important state is objective function which has to be maximized or minimized. Generally, we try to maximize the efficiency (η) and minimize the erosion rate density (P9). Thirdly, we have constraints which are the restrictions on our design. They are the requirements of the design. Mathematically, it is denoted by Const (P7). Here, P7 is revolution per second.

Mathematically, single optimization can be expressed as [70, 71]

$$(P1)_U \geq P1(x) \geq (P1)_L \tag{2.17}$$

$$(P2)_U \geq P2(x) \geq (P2)_{(L)} \tag{2.18}$$

$$Max(\eta), \{Min(P9)(P1)\} \tag{2.19}$$

Where, $x \in S$ and S is the design space.

2.8.4 Multidisciplinary design optimization [MDO]

MDO has couple of other systems. MDO may compose of fluid and structural optimization. In this case, structural and fluid design optimization is simultaneously process during the simulation. Within this MDO, my research focus on optimization of design process while keeping lower erosion tendency [70, 72] i.e. min J(x)

$$s.t.g(x) \leq 0, \tag{2.20}$$

$$h(x) \leq 0 \tag{2.21}$$

$$\text{Where} \quad J(x) = [J_1(x).....J_n(x)]^T \tag{2.22}$$

$$x = [x_1...x_2...x_n]^T \tag{2.23}$$

$$g = [g_1(x).....g_n(x)]^T \tag{2.24}$$

$$h = [h_1(x).....h_n(x)]^T \tag{2.25}$$

Where, $J(x) =$ Objective function to be minimized

$g(x) =$ Inequlity constraints

$h(x) =$ equality constraints

x : Design variables

Design of experiments is a series of scientific experiments planned to measure the optimal response of the output variable by varying input variables at various levels. It is the initial step building a Response Surface over the design space.
The objectives of conducting design of experiments are:

(i) Determine which variable largely influences the erosion.

(ii) Determine the optimal levels of parameters so that it will produce optimum output.

(iii) Determine the optimal levels of parameters so that variability in erosion tendency is small.

The next step in the design of experiment is the selection of appropriate experimental design. There are four types of design of experiment methods are commonly practices by the researchers. They are: two-level full factorial design, central composite design (CCD), Box- Behnken Design (BBD) and three-level full factorial design [70, 71, 73, 74, 75, 76, 76, 77]. These designs vary in both the number of experiments and quality of information that can be extracted from each applied methods.

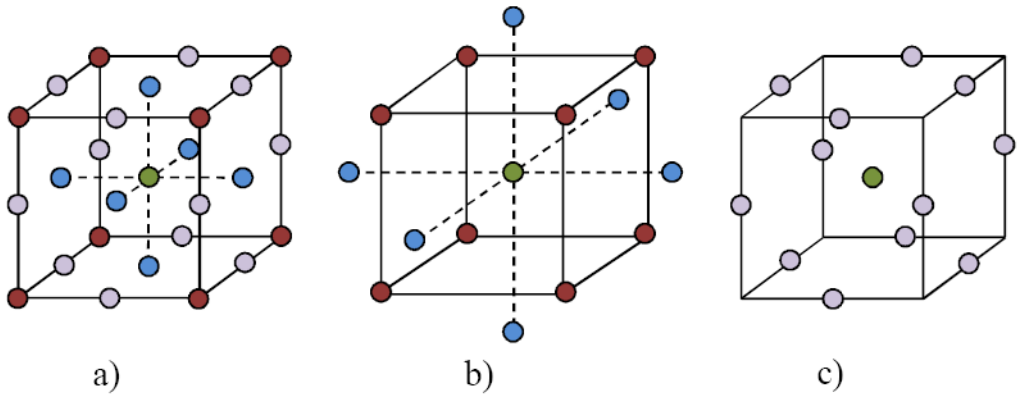

Figure 2.22: Experimental designs in three variables, starting with (a) full factorial design (b) central composite design, and (c) Box-Behnken design [71].

i. Two- level full factorial design:

   The 2^3 full factorial design requires 8 experiments and central point runs. This model is only applicable if the dependence is linear and is disregarded in optimization procedures. It includes the calculation of linear dependence of individual factors; however, the potential assessment of quadratic influence is not possible.

ii. Central composite design (CCD):

   CCD is another type of technique in which a two-level full factorial experiment is added with a center point and two additional points for each factor. This approach estimates 10 coefficients after performing 15 experiments (14+ central points). This indicates that certain degrees of freedom are left which is quite useful to create reliable models whenever the experimental error arises. The mathematical modeling technique used in this design is polynomial regression

which can be expressed as [73]:

$$y = b_o + b_1x_1 + b_2x_2 + b_3x_3 + b_{12}x_1x_2 + b_{13}x_1x_3 + b_{23}x_2x_3 + b_{11}x_1^2 + b_{22}x_2^2 + b_{33}x_3^2 \quad (2.26)$$

Where y is the response term, b_i linear term, b_{ij}interaction terms and b_{ii} quadratic terms.

iii. Box- Behnken Design (BBD):
BBD exists only for 3-7 factors [74]. In case of 3 factors, this design requires 12 experiments and central point runs. For same number of factors, it has similar number of runs and provides same mathematical model as compared to that of CCD [73, 74]. Such approaches is suitable for the situation when corners are not feasible as these designs have no any corners.

iv. Three-level full factorial design:
The 3^3 full factorial design requires 27 experiments and central point runs. This design consists of all the experimental points that are included in CCD and BBD. This increase in experiments leads to the increase of analysis duration and makes it cost-prohibitive approaches as compared to other. Hence, CCD has an edge over this method although it provides extensive information for accurate estimation of factor and interaction effects [73, 74].

2.9 Research gap

All of these hydraulic design of Francis turbine studies gave priority to BEP or the particle classifications, but there is a huge variation in the operating load and flow 45 conditions. To maintain the constant speed of the turbine at different operations, the guide vane angle is adjusted. This adjustment changes the flow behavior, which eventually changes the nature and quantity of erosion in turbines. This study presents a numerical technique to investigate the performances of designs of Francis turbine runner at several operating conditions and its effects on efficiency, power and reduction in erosion when optimized in terms of velocity components.

Chapter 3: METHODOLOGY

3.1 Preliminary design

In this new innovative design initially data in terms of the head, flow, outlet diameter, reduced inlet peripheral velocity, pair of poles in generator and inlet height are implemented into the "Khoj" and "La-Higuera" Softwares. "Khoj" software revel the data in terms of guide curves, blade curves, erosion factor, velocity components, characteristic parameters, turbine dimensions and corresponding domains for the CFD analysis etc. [9, 66]. On the basis of data prevailed by the educational software (Khoj and La- Higuera), turbine blade, hub and shroud data were imported to 3D commercial software to create 3D model.

3.2 Methodologies involved in selecting runner model

Figure 3.1 below shows the methodology used in selection of the runner model for performance test at lab. First of all, the basic turbine data obtained from the hydraulic design of Francis Turbine has been taken from a literature [65]. For the performance analysis of a prototype, the similitude conditions had been employed between the model and prototype. Further, the strength analysis of runner model was done using ANSYS to ensure the strength requirements of the turbine components that could operate at laboratory test conditions.

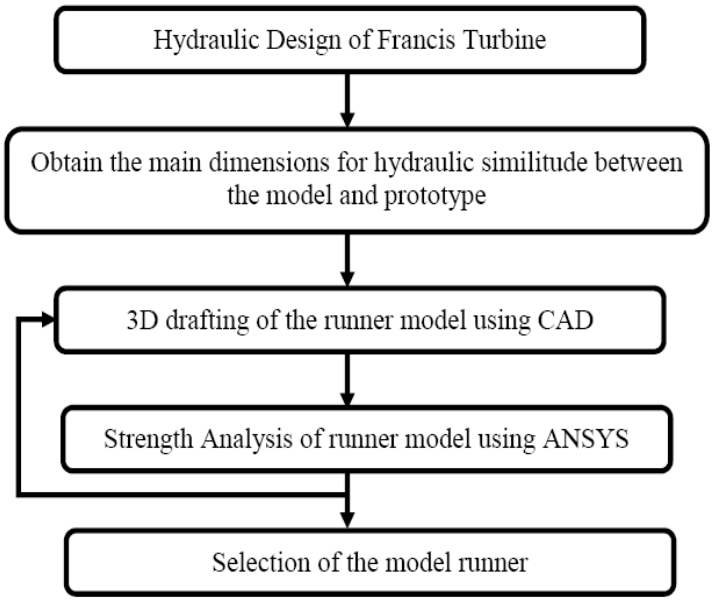

Figure 3.1: Methodology.

3.2.1 Hydraulic Similitude

The laboratory test facility, range of study of the model, and requirements for a model test and operating regimes of hydraulic turbines mentioned in International Electro-technical Commission (IEC 60193, 1992, IEC 1116 1992.,) has been used for obtaining the hydraulic similitude conditions between the model and prototype. The turbine data for the prototype is shown in Table 3.1.

Table 3.1: Turbine Data of Prototype.

S.N	Parameter	Unit	Value
Turbine Dimensions			
1.	Outlet Diameter	m	0.544
2.	Inlet Diameter	m	0.865
3.	Inlet Height	m	0.092
4.	Number of Blades	-	17
Characteristic Parameters			
5.	Rotational Speed	N	1000
6.	Speed Number	Ω	0.321982
7.	Submergence Required	Hs	-0.490201

The hydraulic turbines can be defined as closed conduit models as the flow of water within them occurs within a closed boundary. The main action i.e. dynamic transfer of energy between a rotating runner and the moving fluid, should be considered while designing a model. In an assumed closed-conduit model, the forces of gravity are balanced. Unlike, the surface tension which is not involved, the viscous and inertia forces are found during the steady flow of water, and elastic forces act during unsteady flow. The characteristics of energy transfer are quite similar in model and prototype under the conditions stated below.

i At geometrically similar condition, the ratio of fluid velocity and peripheral velocity of the model should be equal to that of prototype with which the kinematic similarity is achieved.

ii In theoretical principle, a complete similarity is achieved when the Reynolds number equals in both the model and the prototype in addition to kinematic similarity. However, the scaling effect between them causes the variation in Reynolds number.

These two conditions are satisfied if the specific speed that describes the operating conditions with respect to rotational speed, net head and discharge, is equal for both the model and prototype (USBR, 1980). Speed number which defines the operating conditions similar to the specific speed has been used in this paper for obtaining the similitude conditions. The equations 3.1–3.3 of dimensionless numbers describing these conditions mentioned below [78].

$$\text{Speed Number}(\Omega) = \omega\sqrt{Q} \tag{3.1}$$

$$\text{Speed Factor}(n_{ed}) = \frac{nD}{\sqrt{E}} \tag{3.2}$$

$$\text{Flow Factor}(Q_{ed}) = \frac{Q}{D^2\sqrt{E}} \tag{3.3}$$

The laboratory test facility available at Turbine Testing Lab, Kathmandu University was considered while choosing an appropriate size of model turbine. The testing facility is tabulated in Table 3.2.

Table 3.2: Laboratory Limitations.

S.N.	Parameter		Unit	Value
1.	Head (H)	Open System	M	30
2.		Closed System	M	150
3.	Discharge (Q)		m^3/s	0.5
4.	Torque (T)		Nm	2000

The selection of domain for the model turbine was then done using the approximate Turbine Operating Regime for Francis Turbine guided by IEC 60193, 1992 document and head, discharge and torque lies within the laboratory limitations.

Table 3.3: Range of Selection of Model.

S.N.	Parameter	Unit	Range of Value
1.	Head (H)	M	20 - 45
2.	Discharge (Q)	m3/s	0.12 0.4
3.	Power (P)	kW	50 - 100

The minimum conditions to select a model of the Francis turbine are shown in Table 3.4 (IEC 1116, 1992). These values gave good confirmation of hydraulic similarity between the model and prototype which ensures the test results with sufficient measurement accuracy.

Table 3.4: Minimum Values for model size of Francis Turbine.

S.N.	Parameters	Unit	Value
1.	Reynolds Number	-	4×10^6
2.	Specific Hydraulic Energy	J/Kg	100
3.	Diameter	m	0.25

The scaling effect due to a Reynolds number is taken into consideration only on the runner efficiency and impellor power since the available data for scaling discharge and specific hydraulic energy shows inconsistent trends [79].

3.2.2 Mechanical Design

In order to prevent the possible damage due to deflection caused by the loading during the operation of turbine, they are provided with gap between the rotating and non-rotating components. In addition to this, the stress is also induced in both these components. So, analysis of turbine behavior is essential at real working environment. A 3D drafting of the turbine was done using the hydraulic similitude results. The thickness of the turbine components was assumed based upon the existing system. The 3D CAD model was then exported to ANSYS to study the mechanical strength at laboratory constraints. This process was repeated until desired strength with deflection and stresses induced within the acceptable limits was obtained.For selected reference design, the similitude conditions for obtaining a hydraulically similar model turbine has been calculated and tabulated in Table 3.5.

Table 3.5: Calculated Similitude Conditions.

S.N.	Parameters	Unit	Value
1.	Speed Number(Ω)	-	0.321982
2.	Speed Factor (Ned)	-	12.240
3.	Flow Factor (Qed)	-	0.178

As the selection of model size is an iterative process, the calculated similitude conditions was used repeatedly to obtain the minimum operating conditions for the model of the turbine. The selected operating conditions and size of the model is tabulated in table 3.6.

Table 3.6: Selected Operating Conditions and Model Size.

S.N.	Parameters	Unit	Value
1.	Head (H)	m	42.520
2.	Discharge (Q)	m3/s	0.227
3.	Outlet Diameter (D2)	m	0.250
4.	Inlet Diameter (D1)	m	0.397
5.	Inlet Height (B_1)	m	0.042

All the aspect ratio between the model and prototype was maintained for all other parts during 3D design processes.

3.2.3 Sector model

Sector model was prepared in 3D Commercial software. Model was divided into seventeen equal parts ensuring the cyclic symmetry which has to be accommodated by design modular in ANSYS for the fluid structure interaction simulation (FSI) [9]. Each sector is of 21.18^0 was maintained. 3D design software and ANSYS CFX, limit of readable value up to 7 digits after decimal is set. Figure 3.2 shows the reference design model and optimized design model prepared for the FSI simulation.

For the CFD analysis, similar boundary conditions were used for both model and prototype to ensure both will act in same environment as predicted by geometric and dynamic similarity. In this case, mass flow at inlet and static pressure at the outlet were set as boundary conditions for the both analysis [9]

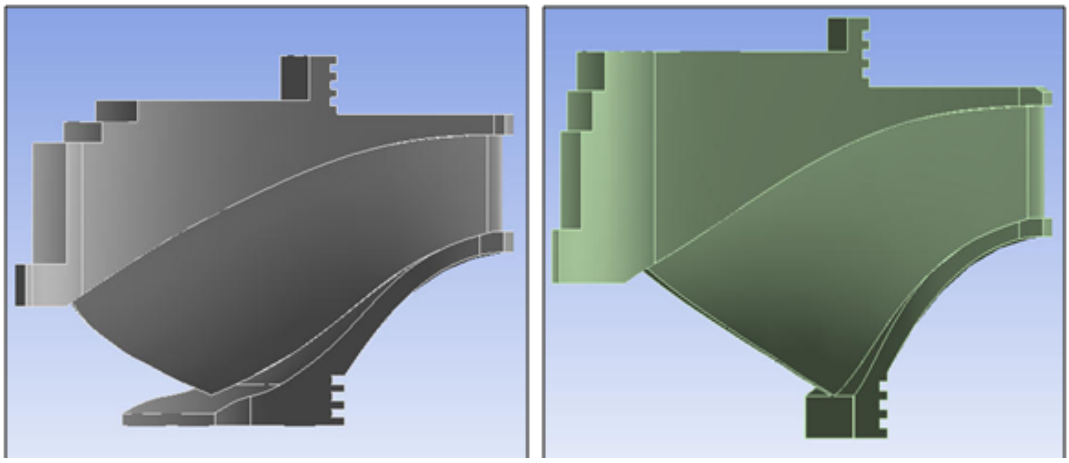

Figure 3.2: A part model of reference design (left) and optimized design (right).

3.3 Computational fluid dynamics

The simulations were performed for 100 combinations of Guide Vane (GV) opening angles and the runner blade profiles. The estimation of erosion on stay vanes, guide vanes and runner blades were based on Lagrangian calculation of particle paths in

a viscous flow. The original turbine contains 17 runner blades, 24 guide vanes and 24 stay vanes. However, considering the cyclic symmetricity of the region, a single blade passage, containing one stay vane, one guide vane and one runner blade was modeled in ANSYS CFX in order to reduce the computational time and the resources required. During the study, k-epsilon and SST turbulence models based on RANS (Reynolds Averaged Navier-Stokes) equations were used in all the cases, as it offers a good combination of accuracy and robustness[57, 80]. The algebraic equations were solved iteratively with second order accurate approach.

3.3.1 Governing equations

In the ANSYS CFX fluid phase was modeled with the NS equations whereas the particle phase with particle kinematics. This particle phase was later on coupled with fluid phase with the help of source term. In this case, two general governing equation available for the continuous phase simulation are represented by equations 3.4 and 3.5 [80, 81, 82].

$$\frac{\delta \rho}{\delta t} + \nabla.(\rho U) = 0 \tag{3.4}$$

$$\frac{\delta (\rho U)}{\delta t} + \nabla.(\rho U \times U) = -\nabla p + \nabla.\tau + S_M \tag{3.5}$$

Where, S_M is Energy source and the stress tensor, τ, is related to the strain rate by

$$\tau = \mu(\nabla U + (\nabla U)^2 - \frac{2}{3}(\delta \nabla.U) \tag{3.6}$$

3.3.2 Spatial discretization

Initial Model analysis was discretized by selecting the course mesh. Program controlled Triangular surface mesh was generated by program controlled and axis of rotation was set to cylindrical. Soft behavior of material was chosen [9] [83]. Later case of Fluid dynamics analysis in rotating machinery was performed by creating high-quality hexahedral meshes in each of the fluid domains with the help of Turbo-grid an in-built tool inside ANSYS. To incorporate the near wall refinements in the blades, the factor ratio for this analysis was chosen to be 1.15 [57]. The y+ value of

$\sim$30 was maintained around runner blade for all simulations as increase in the value of factor ratio causes convergence problem [10, 57, 62].

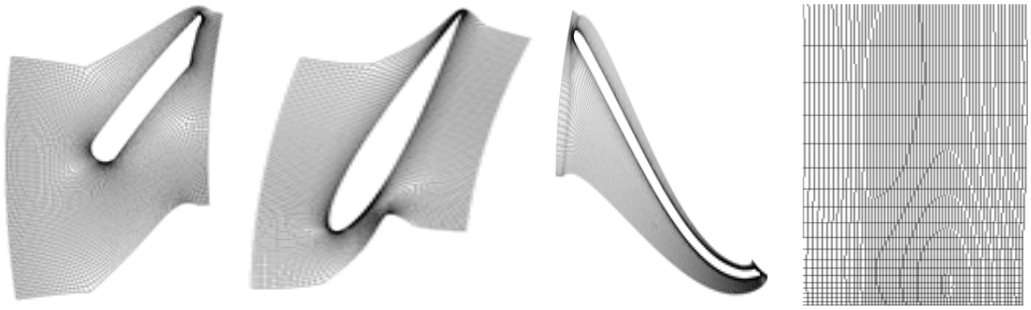

(a) Stay vane (b) Guide Vane (c) Runner blade (d) a portion of draft tube

Figure 3.3: Mesh used in the study for different domains.

In this prototype, mesh for domain R1 (blade), S1 (guide vane), S2 (stay vane), and S3 (short draft tube) are tabulated in Table 3.7

Table 3.7: Statistics condition for prototype.

Domain	Nodes	Elements
R1	795060	747296
S1	259191	242640
S2	265639	247440
S3	84420	78408
All Domains	1404310	1315784

Calculation of discretization error by Grid convergence index (GCI) method

For the numerical stability and to minimize error, grid convergence index method was adopted. The discretization error was performed on the basis of the GCI method suggested by Roache and Celiket. al. [83, 84]. This method calculates the grid size on the basis of equation (3.7). The grid refinement factor in equation (3.9) was maintained to above 1.3. The sequential procedure for this method is given from steps 1 to step 5.

1. Grid size h was calculated by the equation (3.7)

$$h = \left[\frac{1}{N} \sum_{i=1}^{N} (\nabla V)_i \right]^{\frac{1}{3}} \tag{3.7}$$

$$h = \left(\frac{\text{Total volume}}{\text{Total number of element}} \right)^{\frac{1}{3}} \tag{3.8}$$

Where $(\nabla V)_i$ is the volume and N is the total number of cells use in this computations.

2. Grid refinement factor was calculated by the equation (3.9)

$$r = \frac{h_{course}}{h_{fine}} > 1.3 \tag{3.9}$$

3. Order of h was maintained as $h_1 < h_2 < h_3$ and $r_{21} = \frac{h_2}{h_1}$ and $r_{32} = \frac{h_3}{h_2}$ than order of p was calculated by equation (3.10)

$$p = \frac{1}{ln(r)_{21}} |ln| \frac{\epsilon_{32}}{\epsilon_{21}}| + q(p)| \tag{3.10}$$

Where $q(p) = ln\left(\frac{r_p^{21} - s}{r_{32}^p - s}\right)$

$$s = 1.sign\left(\frac{\epsilon_{32}}{\epsilon_{21}}\right) \tag{3.11}$$

where $\epsilon_{32} = \Phi_3 - \Phi_2$ and $\epsilon_{21} = \Phi_2 - \Phi_1$

4. Calculation of the extrapolated values was done from the equation (3.12)

$$\Phi_{ext}^{21} = (r_{21}^p \Phi_1 - \Phi_2)/(r_{21}^p - 1) \tag{3.12}$$

Similarly, calculation of Φ_{ext}^{32} value was done.

5. Calculate and report the following error estimates along with the apparent order p:

Approximate relative error

$$e_{\alpha}^{21} = \left| \frac{\Phi_2 - \Phi_1}{\Phi_1} \right| \tag{3.13}$$

6. The fine grid convergence index:

$$GCI_{Fine}^{21} = \frac{1.24 e_{\alpha}^{21}}{r_{21}^{p} - 1} \tag{3.14}$$

Three different grid size fine (N1), medium (N2) and course (N3) were used to carry out the calculation of discretization error. The simulation was performed in each grid size and head, efficiency and power are recorded as presented in Table 3.8.

Table 3.8: Calculation of discretization error.

N1 ,N2, N3	2855979, 640584, 164000		
r_{21}	1.66305013624535		
r_{32}	1.59888191510596		
Items	**Head**	**Efficiency**	**Shaft power**
Φ_1 (fine mesh)	208.349	97.0978	4740580
Φ_1 (medium mesh)	210.823	96.2814	4801420
Φ_1(coarse mesh)	215.186	95.3322	4890270
$\Phi_{ext}^{2}1$	204.6178	98.3291	4648822
GCI fine 21	2.24%	1.59%	2.42%
GCI medium 32	4.32%	2.06%	3.86%

The interested quantity (Φ_{ext}^{21}), head, efficiency and power was calculated using the equation (3.12) by inserting the values from equations (3.10) and (3.11). The GCI index for fine mesh for head, efficiency and shaft power was obtained as 2.24 %, 1.59 % and 2.42 % respectively. Both GCI fine 21 and GCI medium 32 was found to be within acceptable range.

3.3.3 Particle Tracking

The particle displacement was calculated using Euler integration of the particle velocity over times δt, and is used for the equation (3.15) [80, 81, 82].

$$X_p^n = X_P^o + U_p^o \delta t \tag{3.15}$$

In the above expression, superscripts 0 and n refer to old and new value of particle velocity(U_p^o). At end of each time step particle velocity is calculated by particle momentum equation (3.16) as

$$m_p \frac{du_p}{dt} = F_{all} \tag{3.16}$$

F_{all} is representation of sum of all the forces acting on the particle, is presented in the table 3.9.

Table 3.9: Forces acting on particle [80, 81, 82].

F_D (Drag force acting on the particle)	$$F_D = \frac{1}{2} C_D \rho_F a_f \lvert U_F - U_p \rvert \quad (3.17)$$ where, C_D=Drag Coefficient $$C_D = max\left(\frac{24}{R_e}(1 + 0.15R_e^{0.687}) \times 0.44\right) \quad (3.18)$$ Schiller-Naumman Correlation A_f=Effective particle cross section
F_B= Buoyancy force due to gravity	$$F_B = \frac{\pi}{6}\frac{d^3}{p}(\rho_D - \rho_F) \times g \quad (3.19)$$
F_R= Rotational Force	$$F_r = m_p(-2 \times \Omega \times U_p - \Omega \times \Omega r_p) \quad (3.20)$$
F_{VM}=Virtual or added mass force	$$F_{VM} = \frac{C_{VM}}{2} m_F \left(\frac{dU_F}{dt} - \frac{dU_p}{dt}\right) \quad (3.21)$$
F_p=Pressure gradient force	$$F_p = m_p \frac{\rho_f}{\rho_p}(U_f \nabla U_f - R_F) \quad (3.22)$$

Two way coupling is necessary if there is turbulent dispersion when solid particle is injected into fluid domain. In this case, particle source term is included in fluid momentum equations. The generic particle source is given by;

$$\frac{dS_p}{dt} = C_s\Phi_p + R_S \tag{3.23}$$

Where, $C_s\Phi_p$ are the contributions from the particles that are linear in the solution variable and R_s contains all other contributors [80].

3.4 Single objective optimization

For the optimization using ANSYS CFX facilities, basic design data of Jhimruk Power plant is taken as a reference design. Optimized hydraulic design parameters presented in table 3.10. In this optimization process, optimized values of radial component of velocity (P1), corresponding head (P3), shaft power (P4) and Efficiency (P5) are determined by keeping value for RPS (P7), flow rate (P6) and cylindrical component (P2) as a constant.

Table 3.10: Optimized values for P1-vel R and head-H.

S.N.	P1	P3	P4	P5	P6	P7
1	0.24	183.794	4084080	94.696	2.35706	104.72
2	0.20	218.972	4882860	93.4553	2.35706	104.72
3	0.28	160.439	3486090	93.0557	2.35706	104.72
4	0.22	199.2	4454800	94.5628	2.35706	104.72
5	0.26	171.097	3761720	94.0276	2.35706	104.72

For the given condition of the Jhimrukpower plant, optimized values of row 4 from table 3.10 were selected and processed for the further CFD analysis for five different shapes of turbine blades. In the Table 3.10, simulated value of the fourth row, shows the highest power but it is discarded for the further simulation or selection since the available head is only 201 m.

The CFD simulation was perform on blade shape R1 to R4 with 15 mm leading edge thickness to 8 mm trailing edge thickness. For the R5 blade shape has 10 mm leading edge blade thickness to 6 mm trailing edge thickness was chosen.

Lagrangian particle tracking method was applied to evaluate the CFD results. Comparative study was done for the evaluation of pressure distribution, velocity gradient, and velocity at trailing edge. The figures 3.4 – 3.8 present the CFD analysis on runner blades.

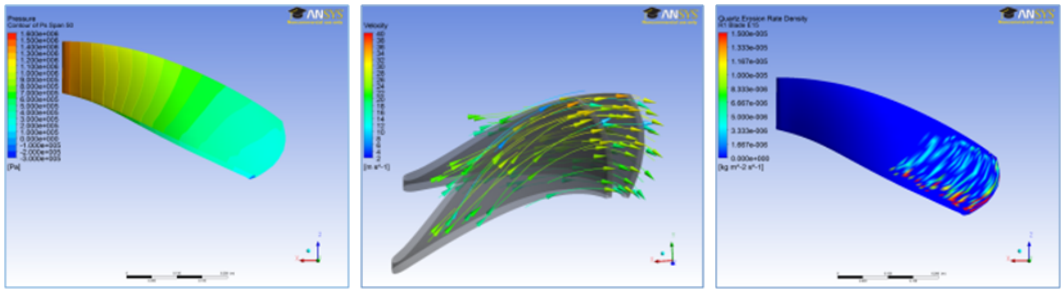

(a) (b) (c)

Figure 3.4: Pressure and velocity streamlines distribution and effect of sand erosion on R1 blade [85].

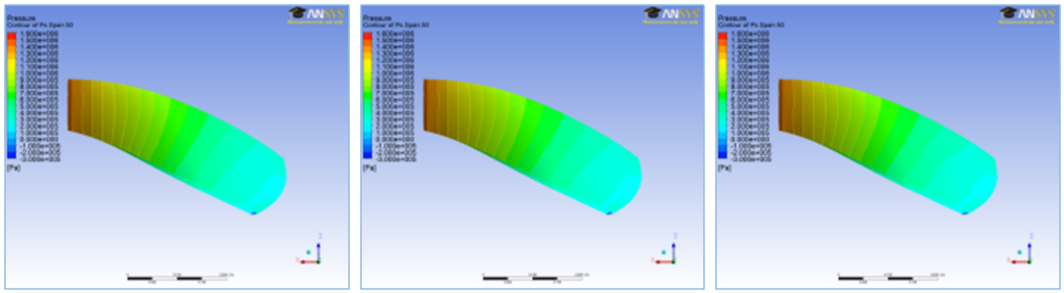

(a) (b) (c)

Figure 3.5: Pressure and velocity streamlines distribution and effect of sand erosion on R2 blade [85].

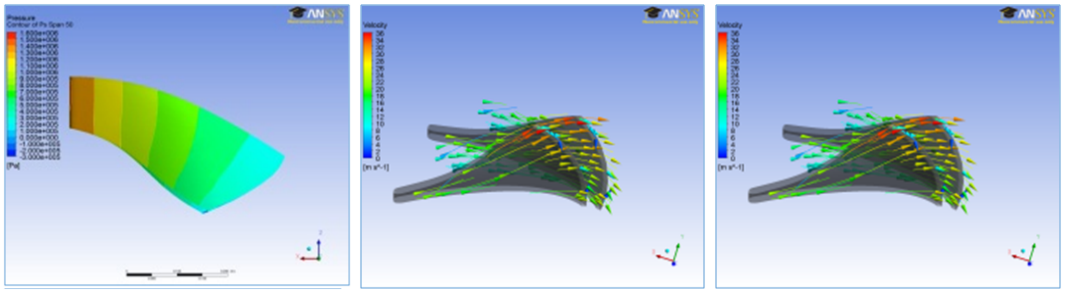

(a) (b) (c)

Figure 3.6: Pressure and velocity streamlines distribution and effect of sand erosion on R3 blade [85].

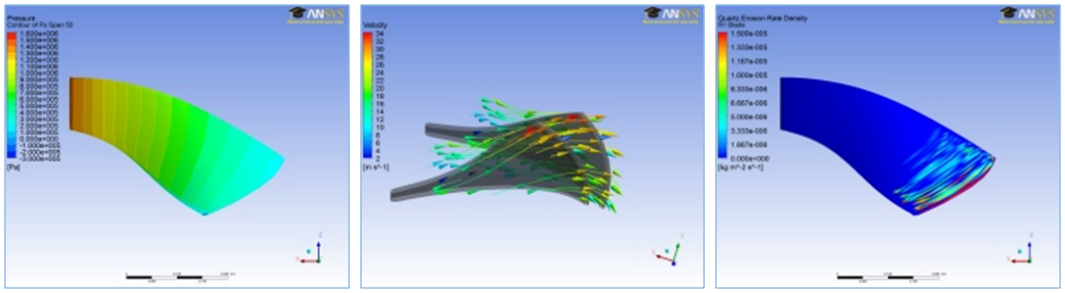

(a) (b) (c)

Figure 3.7: Pressure and velocity streamlines distribution and effect of sand erosion on R4 blade [85].

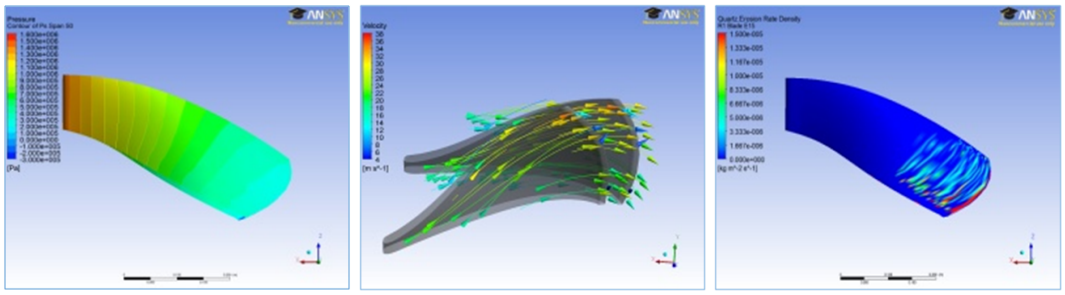

(a) (b) (c)

Figure 3.8: Pressure and velocity streamlines distribution and effect of sand erosion on R5 blade [85].

On the basis of optimized data obtained from CFD analysis, two optimized trade-off charts are drawn. Figure 3.1 is crated from efficiency (P5), head (P3), shaft power (P4), and velocity components (P1) and Figure 3.10 is created from efficiency (P5), flow rate (P6), shaft power (P4), and velocity components (P1). These optimized

trade-off charts helps to minimize simulation and reduce time for design process.

The trade of charts made of by designs of experiments can be used as nomogram for selecting the optimized values of corresponding efficiency and shaft power by knowing the radial velocity component and flow. For example, if given condition radial velocity components and flow than by drawing the straight line on the curve P1 and P4, will get shaft power and similar by the straight line on P1 and P5 will give corresponding efficiency.

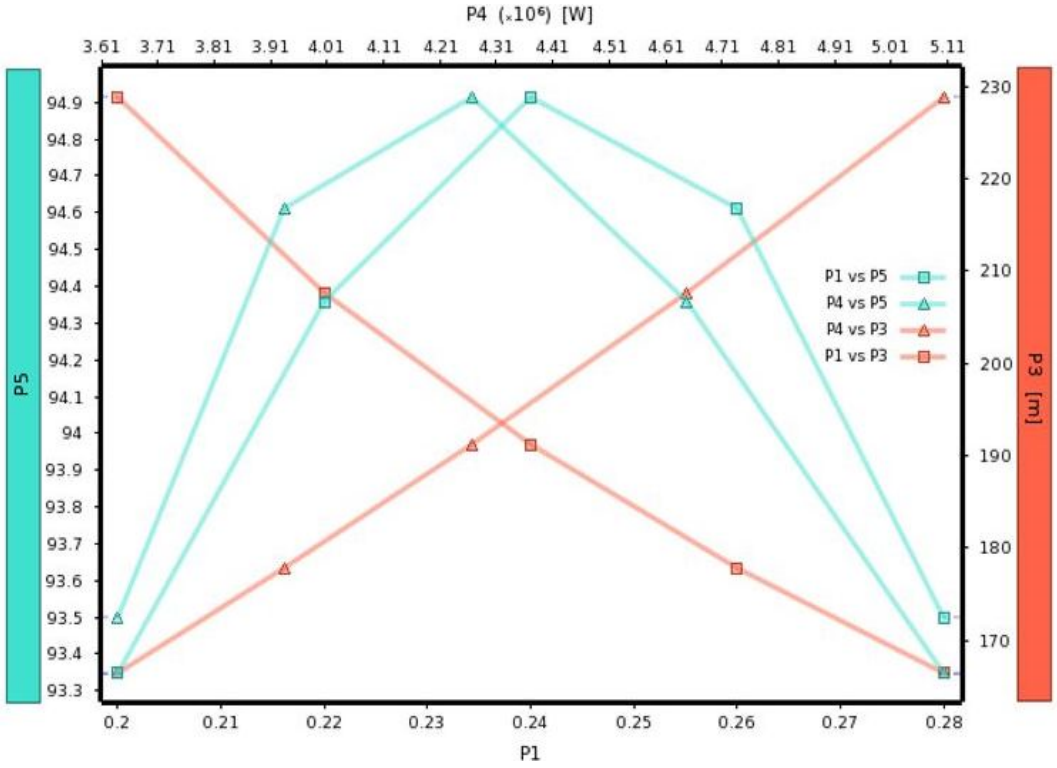

Figure 3.9: Optimized Trade off among efficiency, head, Shaft power and Velocity component.

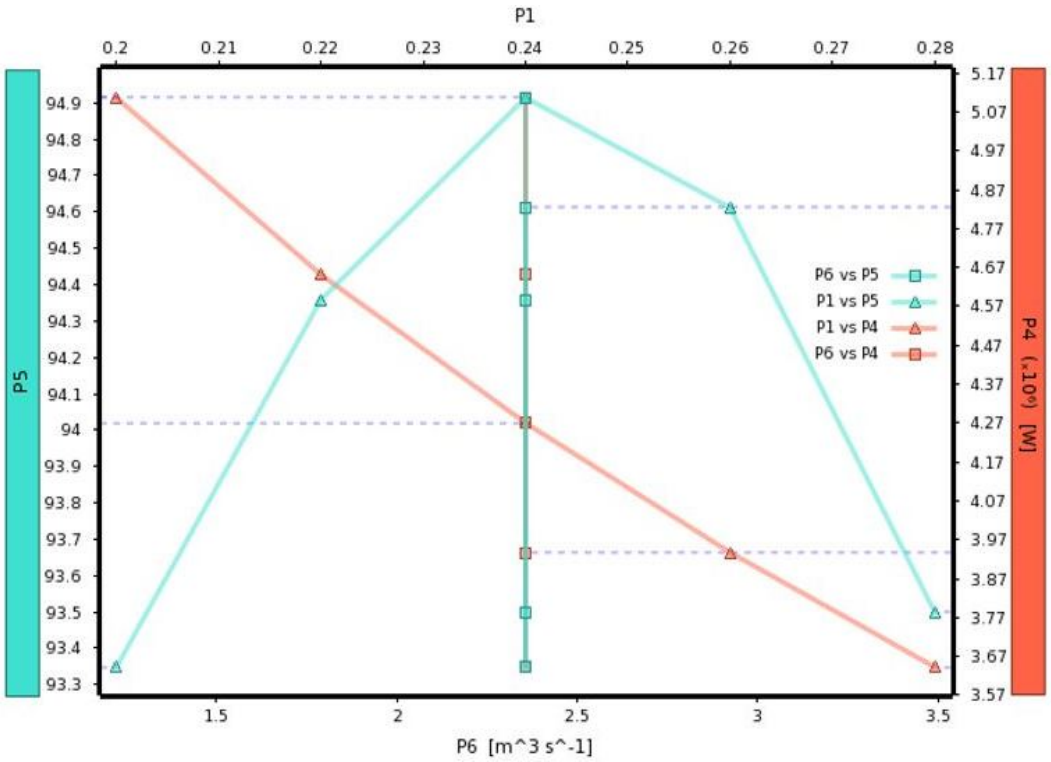

Figure 3.10: Optimized Trade off among efficiency, Flow, Shaft Power and Velocity component.

3.5 Structural analysis

For the structural analysis of finite element method (FEM) was adopted. FEM is a numerical method that is used to solve initial value and boundary value problems. Such method is widely applied in aerospace, hydro machinery, thermal engineering, chemical engineering, Nano technology etc. [9, 86].

In FEM, area of interest (also called as domain) is virtually broken down into small pieces called elements. The point of connection of elements is called node where governing differential equation boundary conditions are specified. In this process, fine elements are generally desirable which ensures the better approximation of the solution [9]. The structural analysis were performed assuming structural steel as a construction material. The properties of structural steel are listed in the table 3.11: During the structural analysis for hub and shroud, variable pressure was applied as boundary condition by literatures [9, 87]. These boundary conditions can also be applied for top and bottom cover [87].

Table 3.11: Properties of structural steel.

Young's Modulus (Pa)	Poisson's Ratio	Bulk Modulus (Pa)	Shear Modulus (Pa)
2.0×10^{11}	0.3	1.6667×10^{11}	7.6923×10^{10}

3.6 One and two way fluid structure interaction simulation(FSI)

Fluid Structure Interaction (FSI) analysis is a coupled solution of Computational fluid Dynamics (CFD) and Structural analysis [86] . There are two ways to couple between them unidirectional and bidirectional. The former coupling also called as one way coupling exchanges forces from CFD grid points into structural analysis and displacement on structural grid point into CFD grid point [9, 64]. This method is inappropriate if there is relatively large deformation of the structure. In bi-directional coupling CFD analysis and structural analysis exchanges the response variable value between them and hence also called two way of coupling[9, 64, 86].

3.6.1 FSI Procedure

Following steps were adopted during FSI simulation:

i. For the FSI analysis (performed by maintaining one way coupling), geometries were firstly imported from the 3D commercial software. Then, an optimized CFD result from ANSYS is brought into connection with the ANSYS Static Structural Analysis.

ii. Meshing was done by body sizing and match control. Triangular surface meshing was done by Program Controlled. Axis of rotation was set to cylindrical and soft behavior of material was chosen.

iii. Three dimensional solid model created in 3D commercial software was divided into seventeen equal parts and one of the sections was taken in the design modular. Then, boundary conditions were defined by variable load pressure and fixed support.

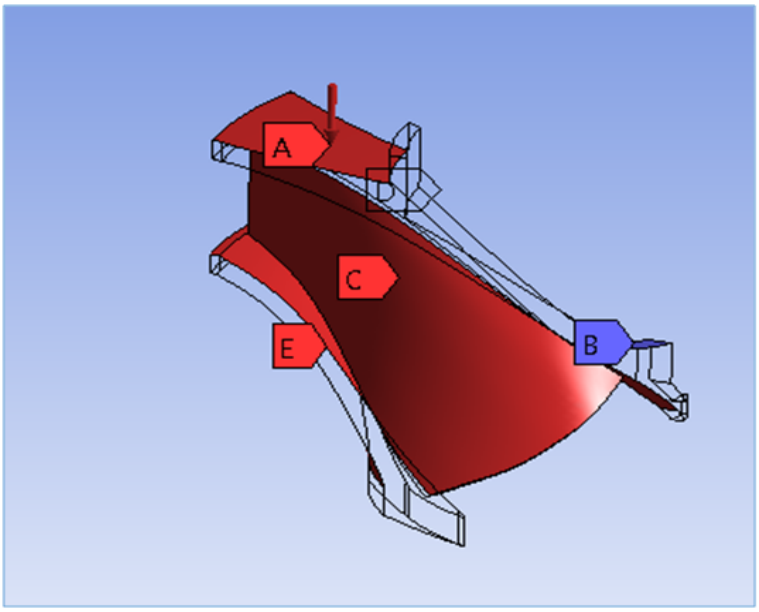

Figure 3.11: Boundary condition location.

In figure 3.11, alphabet A represents variable load pressure, B is the fixed support, C, D, and E represent imported pressure 1, 2, and 3 respectively.

iv. Since the model is divided into the seventeen parts, APDL cyclic command was used to view the whole runner.

v. In solution steps, Von mises stress, total deformation and factor of safety runner assembly were observed.

The Von Mises stress is an equivalent stress at which yielding is predicted in a ductile material [88]. Mathematically, it can be defined as shown in equation (3.24)

$$\sigma' = \frac{1}{\sqrt{2}}\sqrt{[(\sigma_1 - \sigma_2)^2 + (\sigma_2 - \sigma_3)^2 + (\sigma_3 - \sigma_1)^2]} \tag{3.24}$$

Where, σ_1, σ_2 and σ_3 are three principle stresses.

3.6.2 Limitations of FSI analysis

The experiments were carried out with following limitations:

i. Optimization was performed for only one set of blade profile.

ii. FSI analysis was performed only on Francis turbine runner assembly.

iii. During the FSI analysis, Unidirectional Coupling was chosen, considering there was no large deformation on runner.

3.6.2.1 Boundary condition for FSI analysis

For the FSI analysis, fixed support was provided in the place where a shaft was connected. Variable pressure was applied on the upper part of hub and bottom part of the shroud whereas imported pressure resulted from the CFD analysis was applied to the blade and inner part of hub and shroud as shown in figure 3.11 [9, 89].

3.7 Multidisciplinary optimization with two way FSI simulation

In this method, two variables P1 and P2, associated with the components of velocity, were set within the range specified during the comparative study of five different types of shape. Efficiency was set to 95% or more than 95 % as an inequality constraint, 105 RPS was set as an equality constraint. The other parameter were set as follows [70, 75]:

$$\text{Maximum}(P4) \quad \text{and minimum}(P5) \tag{3.25}$$

$$\text{constant}(P7) \tag{3.26}$$

$$(P1)_U \geq P1(x) \geq (P1)_L \tag{3.27}$$

$$(P2)_U \geq P2(x) \geq (P2)_L \tag{3.28}$$

$$\text{minimum} \quad (P9)\{P1(x), P2(x)\} \tag{3.29}$$

Where, $x \in S$ and S is design space.

In the multidisciplinary optimization, fluid domain get design variables as input values. Once the CFD simulation is completed, the structural analysis gets initial values from the CFD analysis. The dynamics of exchange of data will generated the output

values once achieved the boundary conditions and limits are meet. Output values from the structural analysis gives the objective vector as an output. The objectives for the multidisciplinary optimization and objective vector is connected with the coupling as an approximation method and sensitivity analysis. The objectives are also connected with the input variables with coupling as design exploration. In this system, input variables, CFD analysis, structural analysis and design objectives are serially connected by couplings. In this sequence, multidisciplinary simulation, the values are pass on the sequentially from fluid domain to structural domain and vice versa. Each values has to check the equality and inequality constrains before producing the output. Once all the criteria has been fulfilled than optimized values in terms of erosion rate density and safety factor are recorded as an output.

3.8 Francis runner design procedure for sand laden water

For the design of optimized Francis runner, first preliminary design data were obtained from Khoj or La-Higeura; both programs are MATLAB based, developed at NTNU waterpower laboratory through Renewable Nepal Project. CFD analysis was performed using these design data. The limit of head, power, efficiency, and erosion tendency was analyzed. When it was found to be within limit, single objective optimization was performed. This optimization process was used to find out the maximum and minimum erosion tendency and its relation with the velocity components. At the same time, one way FSI was performed to check the runner blade strength and its factor of safety. Once the factor safety found to be limit than two way FSI with Multidisciplinary optimization was performed. Through this steps limits of P3, P4, P5, P9 and FOS was checked. The limiting values obtained from this step was considered the final optimized value for the Francis runner. The flow chart of this procedure is illustrated by the Figure 3.12.

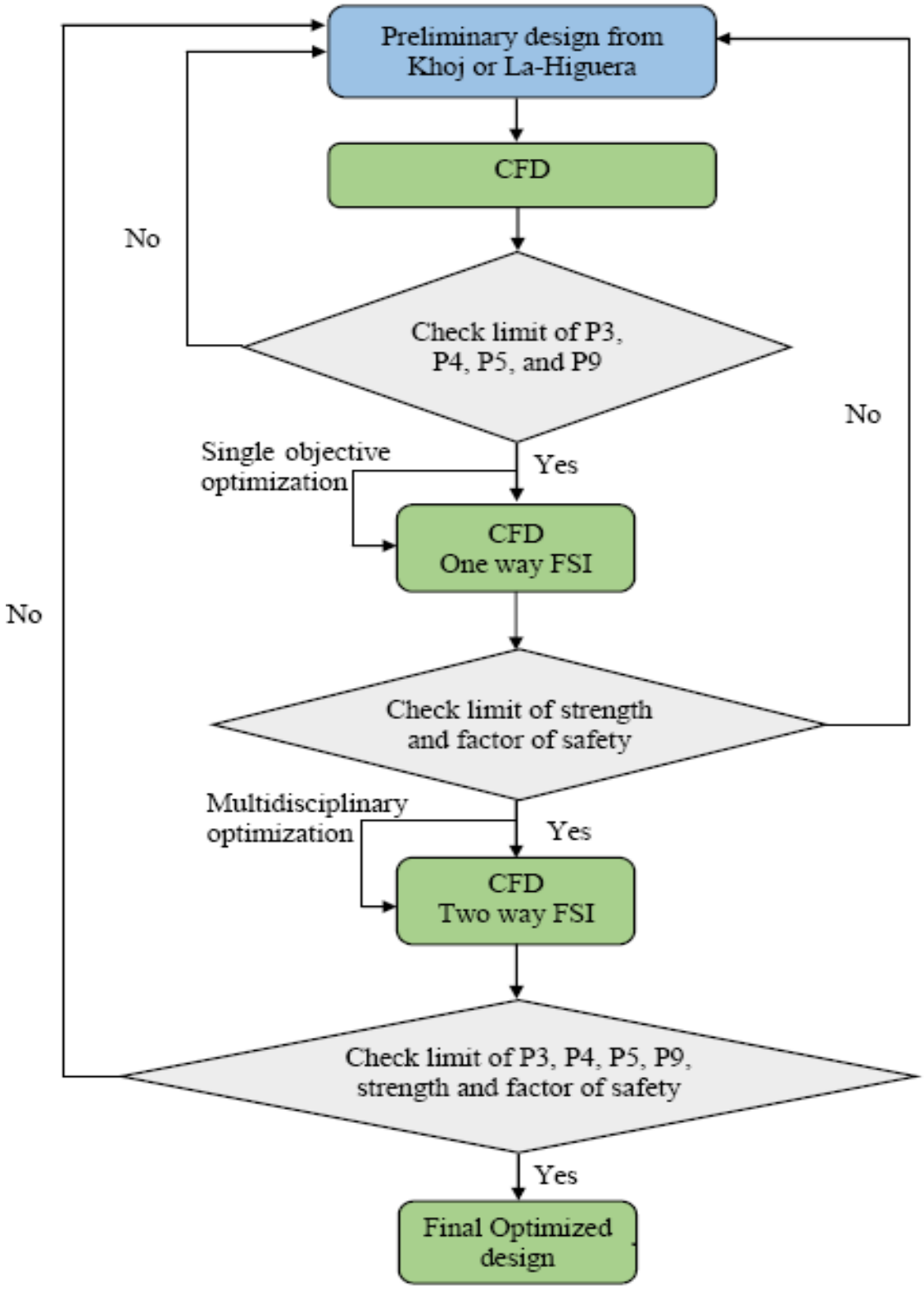

Figure 3.12: Flow chart of Francis turbine design for sand laden water.

Chapter 4: RESULT AND DISCUSSION

In this chapter, the best result obtained from the CFD simulation was compared with the field measurement data. Multidisciplinary design optimization was then carried out on best results and its relation among the parameters which influences the erosion in Francis turbine were thoroughly discussed.

4.1 Result of design optimization

Khoj design program was used to evaluate the consequences of variation in each design parameter and results were compared with that obtained from CFD analysis. During this study, erosion factor was of primary interest although several other design parameters were also observed [8]. It was concluded from the study that the runner outlet diameter, peripheral velocity at inlet, and blade angle distribution are greatly affected by the sediment erosion of Francis runner.

It was found that greater the number of pole pairs, smaller will be erosion effect which motivates to decrease the rotational speed of the turbine drastically [8]. Though this approaches tend to increase the size of both the turbine and the generator, thereby amplifying the investment costs as well, higher hydraulic efficiency for this design compared to the reference one negate the effect of cost.

Result shows that efficiency can also be increased by varying blade angle distribution, and consequently also the energy distribution, so that significant reduction of erosion is possible without changing the dimensions or the rotational speed of the turbine. The combination of these two effects tends to reduce the erosion by 50 percent as compared to the reference design. CFD analysis was also performed for this design which showed good efficiency and acceptable flow conditions in the turbine material.

CFD simulation was performed to optimize the reference design which prevailed to draw trade-off chart among different parameters that signify reduction in simula-

tion and cost of the design. Trade-off chart among different variables was used to show the relation between variables. The chart determined the trade-off points for a particular blade within a specified range without performing additional simulation.

The pressure distribution and velocity at trailing were observed for the five different samples of blades. Among them, FSI analysis was done on selected R2 Blade as it has uniform pressure distribution along the blade as well as relatively lower velocity among all other blades that signifies the less erosion impact with compare to reference runner. The FEM analysis performed on guide vane, upper and lower cover showed that the material stress is well within the safe limits for calculated loads. Unidirectional coupled FSI analysis prevailed that total deformation of runner assembly was 0.00016931 m which is safe for structural steel. And number of nodes and elements were found 262,815 and 173,035 respectively for this analysis. The element size was 5×10^{-3} m [89].

In addition to CFD analysis, model testing was also followed in order to optimize the design as the test is a suitable procedure to predict the performance behavior of the turbine at reduced time and cost. A hydraulically similar model was selected using the dimensionless parameters like speed number, speed factor and flow factor which describes the operating conditions of the Francis turbine in terms of the head, discharge and speed. During this testing phase, it was found impractical to satisfy the equality equation for Reynolds number between model and prototype since it required either a larger size model runner or higher angular velocity [90]. The effects due to Reynolds number could be overcome in prediction of performance behavior by considering the relative roughness or surface conditions between the model and prototype.

The CFD analysis showed that the total head of model runners was found to be 46 m and 42.5 m respectively for the reference runner and optimized runner. The predicted head was slightly increased than the numerically calculated head for the reference runner. For the optimized blade, CFD simulation determined head was

good agreement with the calculated head. FSI analysis performed on these models showed that the maximum deflection was found to be 0.33 mm and 0.32 mm respectively which is safe for the structural steel [90]

Optimization was focused on effect of velocity component. This study prevailed that for the optimized turbine to operate with smoothly decreasing or increasing efficiency, the stay vane should be placed in such a way that flow entering the guide vane should ensure velocity component of 8 to 9m/s [85]. This ensured the turbine efficiency to be 94 percent for the guide vane opening position of 12 degree, provided that all other flow component remained constant. This approach also showed acceptable result with other guide vane opening of 14, 13 and 11 degree [85].

4.2 Comparison of simulated results

The simulation was performed using both k-ϵ and SST turbulence model. The results obtained from these were first validated with the site measurement values. The absolute velocities obtained at inlet and outlet of stay vane and guide vane and relative velocities at runner inlet and outlet were compared and graph was drawn as shown in Figure 4.2–4.4 [91].

The graph shows the velocities at corresponding power which were quite less than the experimental values of power output. This means that for an experimental testing, the velocity of water should be higher than the simulated data for same power generation. This is due to the position of the sensor placed during the measurement and wear and tear of the turbine runner, guide vane and stay vane. The runner and guide vane condition along with the location of the sensors are presented in Figure 4.1 [16]. However, the experimental value of power output with respect to the absolute velocity at SV outlet is higher than simulated value of k-ϵ and SST. the other values are calculated by based on measured flow rate and cross-sectional areas.

(a) Locations of sensors. (b) Runner condition during experiment. (c) Guide vane eroded condition.

Figure 4.1: [91]

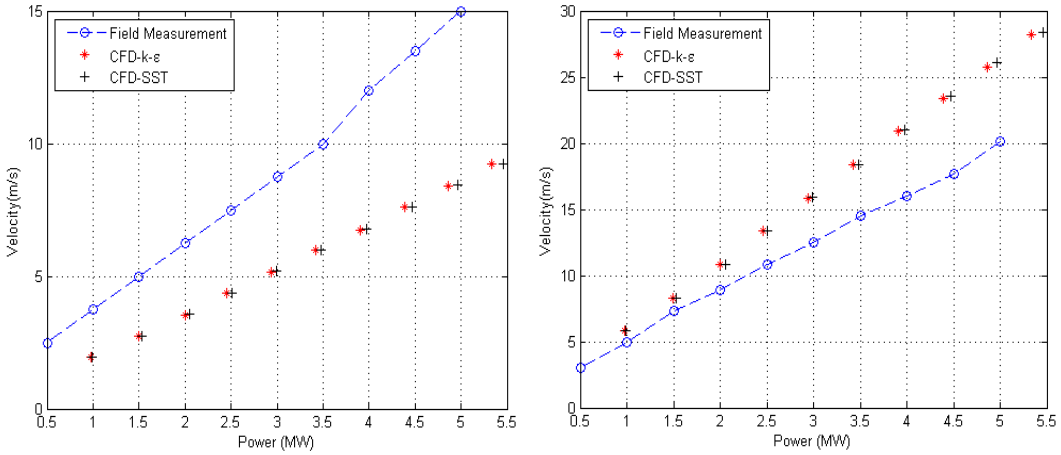

Figure 4.2: Absolute velocity at SV inlet (left) and SV outlet (right) [91].

In an ideal condition, power output increases with increase in water velocity; however, the CFD results and measurement values showed that the trend is deviated from one another while increasing the velocity. While calculating absolute velocity at GV outlet, field measurement and CFD analysis (both turbulence model) shows similar decreasing trend for power output at 2.5 MW to 3.5 MW. But for other cases, the results are substantially different from one another. The results are substantially different from one another.

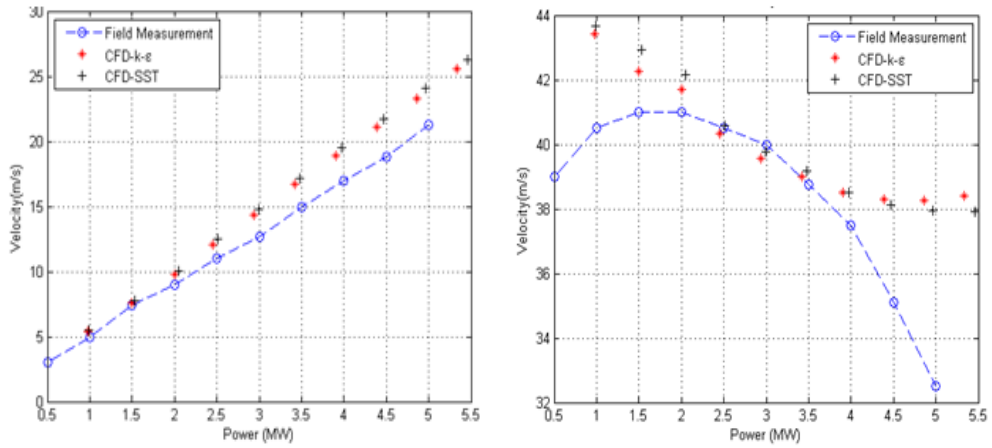

Figure 4.3: Absolute velocity at GV inlet (left) and GV outlet (right) [91].

Similarly, on comparing the relative velocities at inlet and outlet, both experimental and CFD results showed similar increasing trend of velocities while increasing the power output, as shown in figure 4.4. However, this trend was slightly deviated from the trend line of relative velocity at runner outlet. The relative velocity of outlet showed the similar trend for power output between 2 MW and 5 MW. Generally, Jhimruk power plants do not operate at power output less than 2 MW.

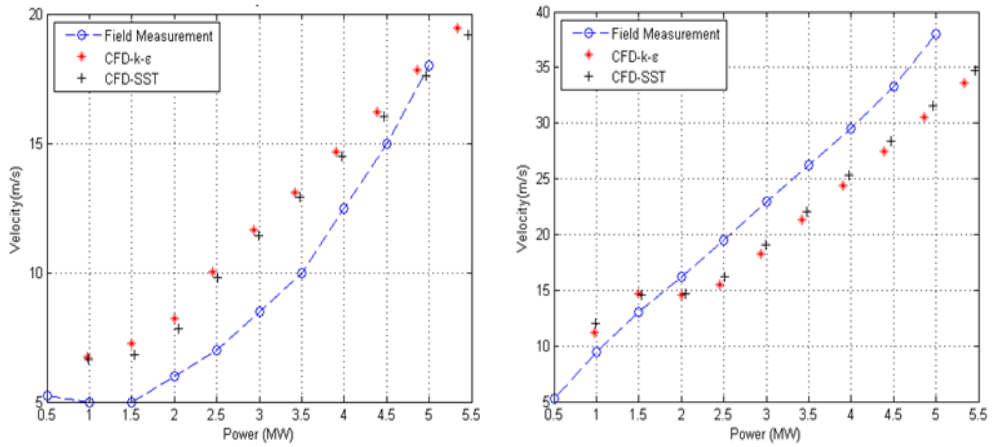

Figure 4.4: Relative Velocity at Runner Inlet (left) and Runner Outlet (right) [91].

Specific condition of sand i.e. spherical shape with same diameter, concentration and flow rate was used to perform simulation analysis on eroded turbine. The eroded turbine in the plant was observed and compared with simulated results for extreme cases and compared with the actual condition. Figure 4.5 (a), (b) and (c) shows the erosion on the runner at BEP, full flow and part flow conditions respectively.

It showed that erosion majorly takes place at the outlet of the blades for full flow and designed conditions. Turbines in run-off-river type projects such as Jhimruk are mostly vulnerable to full flow conditions. This occurs due to following two reasons:

i. The flow has high velocity, which directly influences the erosion and

ii. The flow carries plenty of sand particles during monsoon season, when excess water is available whereas in dry season, the water is cleaner, and is less susceptible to erosion.

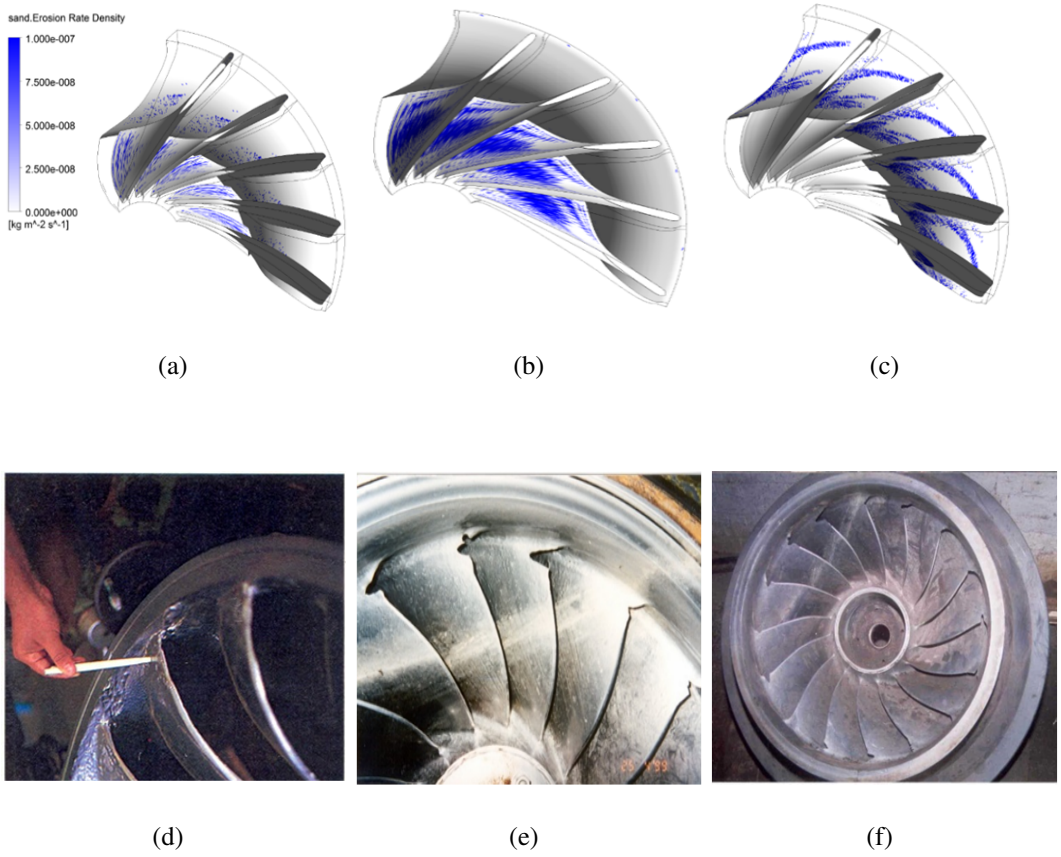

Figure 4.5: Erosion on the runner at a) BEP b) Full flow condition c) Part flow condition d) Accumulated effect on the actual runner [91].

4.5 (d) shows the erosion on the actual runner. These observations showed that the runner is heavily eroded on the outlet of the blades. 4.5 (c) shows that erosion is mostly concentration at mid-stream position of blades for part flow conditions.

4.2.1 Comparison of Efficiency

Figure 4.6 shows the graph of efficiency Vs Guide Vane (GV) opening for five different shape of runner. Here, the flow conditions are represented by GV opening angles with reference to BEP. In Table 4.1, 0^o GV opening angle represents 72% opening. Similarly, 6^o opening angle represents 100% opening and -12^o represents 18% opening. The best efficiency for all the shapes is obtained between 45–55% of guide vane opening as the runner gets optimum flow during this condition [91]. As a result, performance too increases and hence this condition is used as the design condition for all shapes of runner. When GVs are at closing position i.e. at part load condition, the efficiency reduces as the turbine is exposed to limited flow only. The best runner efficiency (i.e. 97.71%) was obtained in Shape-1 and Shape-3 for 55% GV opening. The deviation of efficiency from its optimum value is observed more at lower and higher GV openings. During full opening condition, Shape-1 and Shape-3 showed optimum performance, whereas at full closing, the turbines had lowest efficiencies. On contrary to this, Shape-2 and Shape-4 showed maximum efficiency at full closing conditions, whereas the efficiencies tended to decrease significantly at greater GV openings. On comparison, the Shape-5, with every single other shape in part and full load condition, has the flattest curve, demonstrating acceptable performances for both part load and full load conditions. Though, the difference is not quite significant for two turbulence models, in overall, the efficiency predicted by SST model is larger as compared to that by k-ϵ model.

Table 4.1: Guide vane opening in % corresponding to flow conditions.

Flow kg/s	132.8	121.2	109.5	97.9	86.2	74.6	62.9	51.2	39.6	27.9
GV open%	100	91	81	72	63	54	45	36	27	18
Angle	6^o	4^o	2^o	0^o	-2^o	-4^o	-6^o	-8^o	-10^o	-12^o

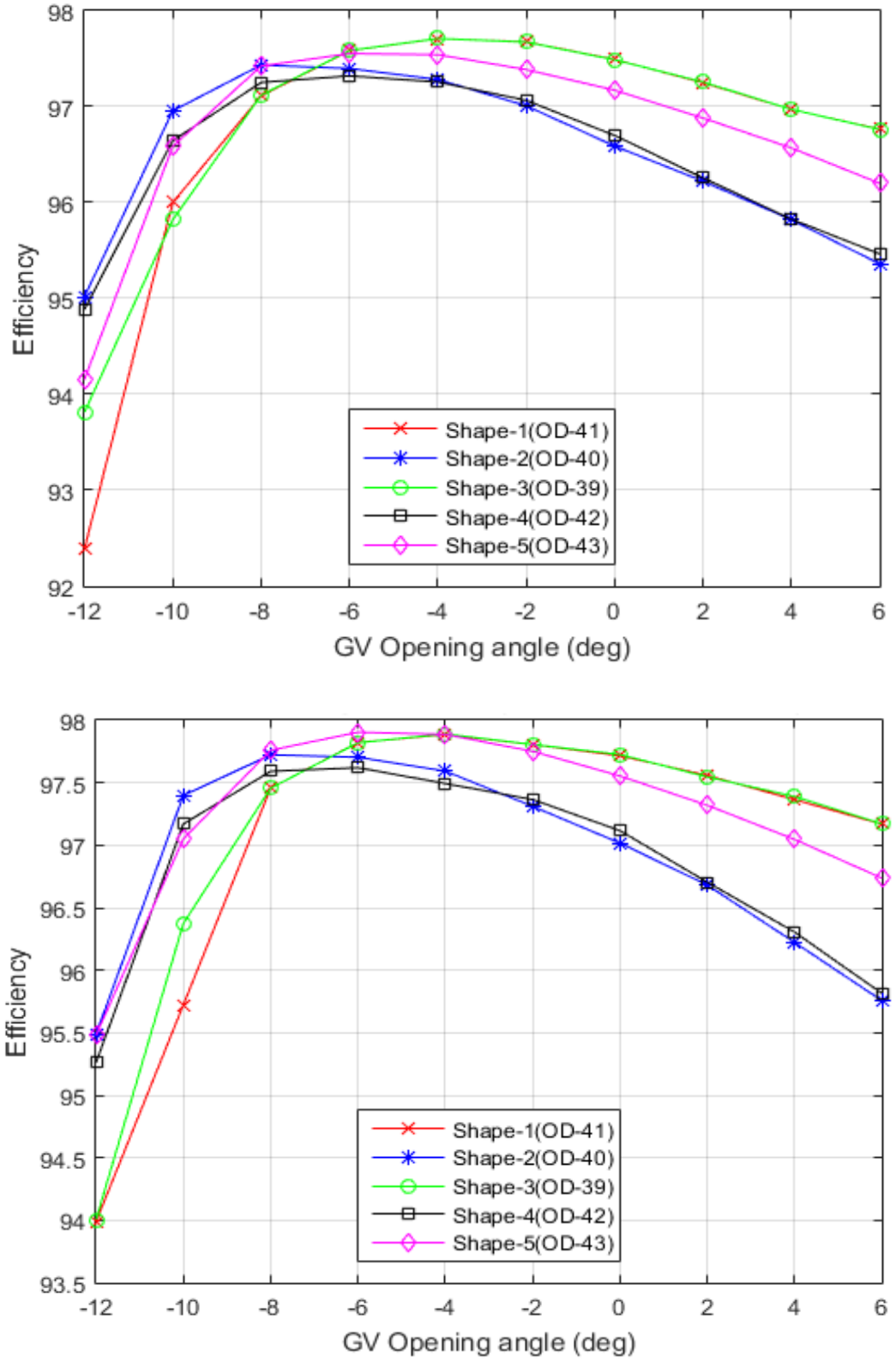

Figure 4.6: Efficiency corresponding to runner blade design and operating conditions with k-ϵ and SST Turbulence model [91].

4.2.2 Comparison of Erosion

Figure 4.7 and 4.8 showed the erosion observed in runner blade shapes and GV for all the designs and turbulence models. Normally, the trend of the curves of GV opening angles and the erosion for all the shapes is irregular but the graph showed that minimum runner blade erosion occurs at best efficiency points. In this condition, particles carried by flow regime is less likely to strike the wall of runner blades. When the guide vane is at the closing positions, flow is in more turbulent condition and the glided particle with flow experience the high centrifugal force which in terns more particles strike towards the wall of the runner blade. For both the turbulence model, Shape-1 and Shape-3 had the maximum erosion at all the GV openings whereas rest of the blades showed a similar trend at best efficiencies point and fully loaded conditions. The erosion was found to be maximum for Shape-2 and Shape-4 and minimum for Shape-5 at full closing position as depicted in the figure 4.7 [91].

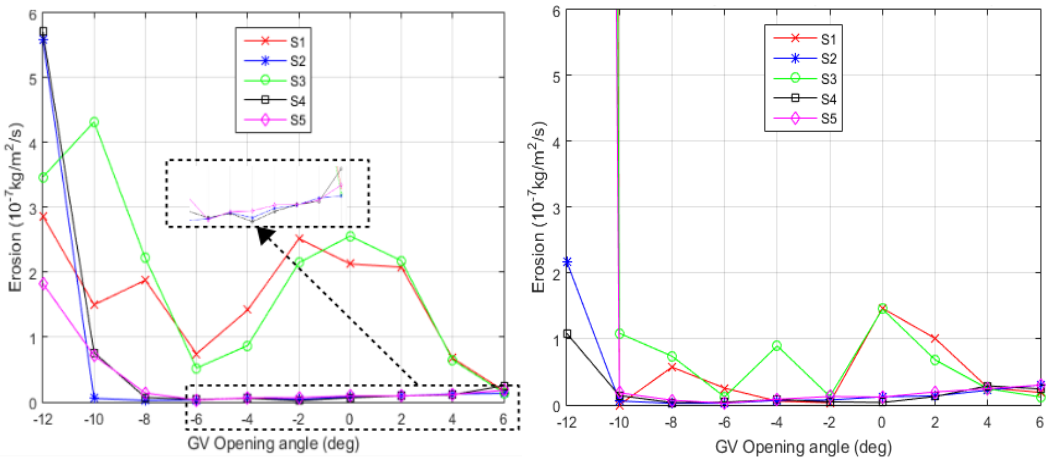

Figure 4.7: Erosion on runner blade corresponding to runner blade design and operating conditions using two turbulence models [91].

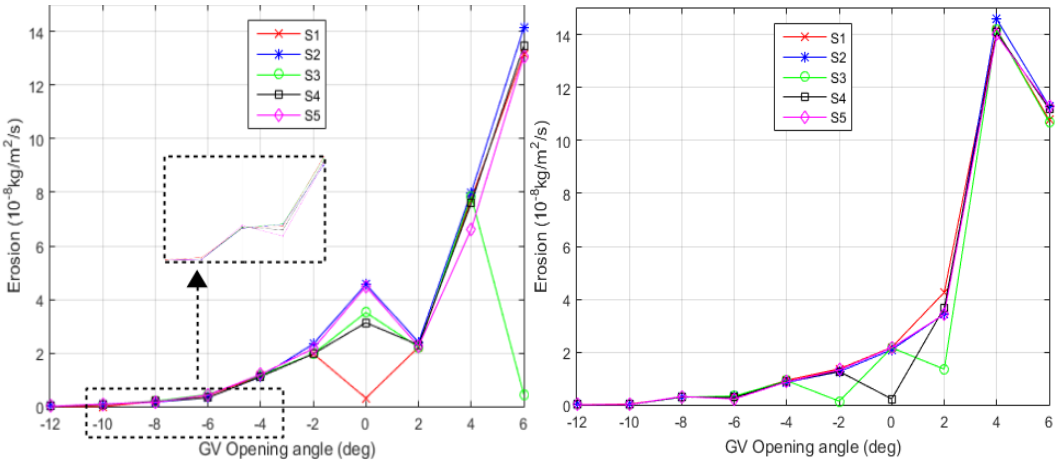

Figure 4.8: Erosion on guide vane corresponding to runner blade design and operating conditions [91].

Figure 4.8 depicts the erosion on guide vane corresponding to runner blade design and operating conditions. The curve of GV erosion rate versus GV opening showed an opposite trend as the erosion was found to be maximum for fully opening position. This occurs due to the velocity difference, as velocity is higher during the full flow condition than the part flow condition and erosion rate has direct relation to the velocity. Also, when the flow is in design conditions, particle glided in flow first strike on the leading edge of turbine. In this condition, flow is dispersed around leading edge, which forces the particle away from the leading edge zone of pressure side and suction side. The particle tracking demonstrated the path of the particle during guide vane in closing and near BEP positions as presented in Figure 4.9. During partial closing position of GV, flow is not streamline along the pressure side and suction side of GV. This causes the flow through guide vane to have more turbulence and hence particle carried by flow experiences more kinetic energy. During full opening condition, Shape-3 and Shape-4 showed less erosion in between 14.37^0 to 18.37^0. However, no significant deviation occurred due to the runner blade shapes on guide vane erosion. Shape-5 demonstrated the overall optimum performance while considering the erosion rate and the efficiency curve among all five different shapes of the runner.

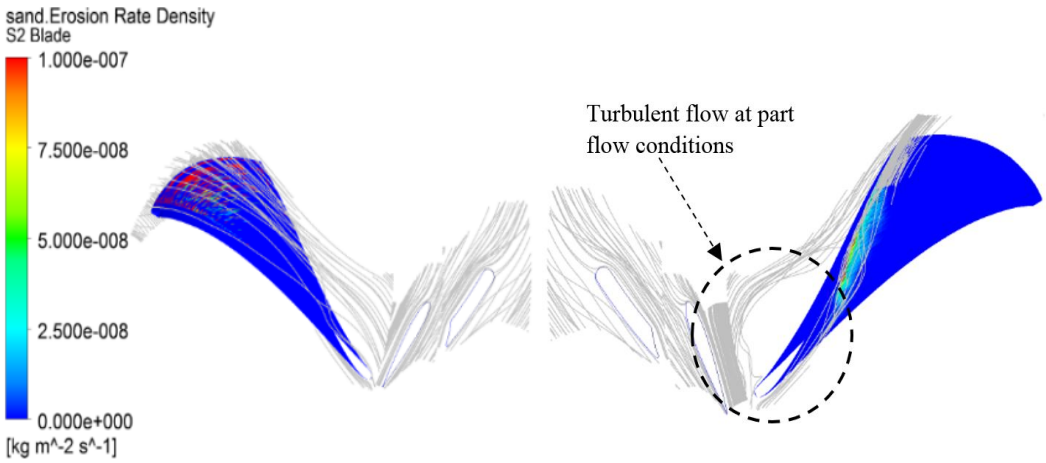

(a) (b)

Figure 4.9: Particle travelled path when guide vane is (a) near BEP and (b) closed position [91].

When the turbine is operated in the part load condition, there will be arises the swirl flow between the outlet of the guide and inlet of the runner blade [92]. In this condition, particles experience the centrifugal force(FC) and drag force(FD).The drag force on the particle is due to the relative velocity of particles in radial direction towards the center of the runner and the centrifugal force is cause by the velocity of particle in tangential direction (away from the center of runner) [56]. If the larger particle which has more centrifugal force (F_C) than the drag force (F_D), particle will be circulating inside the swirl with striking the wall. The particle remains there, unless and until the particle either has change the flow velocity due to the load demand or particle is breakdown so that later develop centrifugal force more than drag force . In this case particle driven out along with the flow of water. The particle drag force and centripetal force is given by the equation [92].

$$F_C = \rho_p \cdot \frac{\pi d^3}{6} \cdot r \cdot \omega^2 = \rho_p \cdot \frac{\pi d^3}{6} \cdot \frac{C_u^2}{r} \tag{4.1}$$

$$F_D = \frac{1}{2} \cdot C_D \cdot \rho C_m^2 \cdot A_p \tag{4.2}$$

The ciritcal diameter of particle which may experience the swirl can be calculated

as:

$$d_c = \frac{3}{4} \cdot C_D \cdot \left(\frac{\rho}{\rho_p}\right) \cdot \left(\frac{C_m}{C_u}\right)^2 \cdot r \tag{4.3}$$

Three possible conditions of the particles [92]:

- Particle remains say at the swirl orbit of radius r if $F_C = F_D$.
- Particle will strike outer wall if $F_C > F_D$.
- Particle will flow along with water towards outlet of the runner if $F_C < F_D$.

4.2.3 Comparative study of relative velocity at inlet and outlet of the runner

As the erosion rate has direct relation with the velocity, so, less relative velocity at the outlet of the runner is desirable. This relative velocity on combination with stream function at outlet makes the erosion of runner at outlet even worse. Figure 4.10 depicts the comparative study of relative velocity at inlet and outlet of the runner for the five different shapes of runner blades. This showed that shape 1 and shape 3 of the runner blades give the similar trend of low relative velocity at outlet but high relative velocity at inlet of the runner. This clarifies that outlet is less prone to erosion as compared to the inlet of the runner. Furthermore, it is shown that shape 1 or 3 have higher erosion rate at the leading edge of the runner blade whereas these geometries are more suitable to reduce the sand erosion at trailing edge of the runner than other shapes. On comparison among 5 shapes of different blades,shape 5 encountered least erosion rate but slightly higher relative velocities whereas shape 1 and 3 and lesser relative velocities as compared to that of shape 2 and 4 [91].

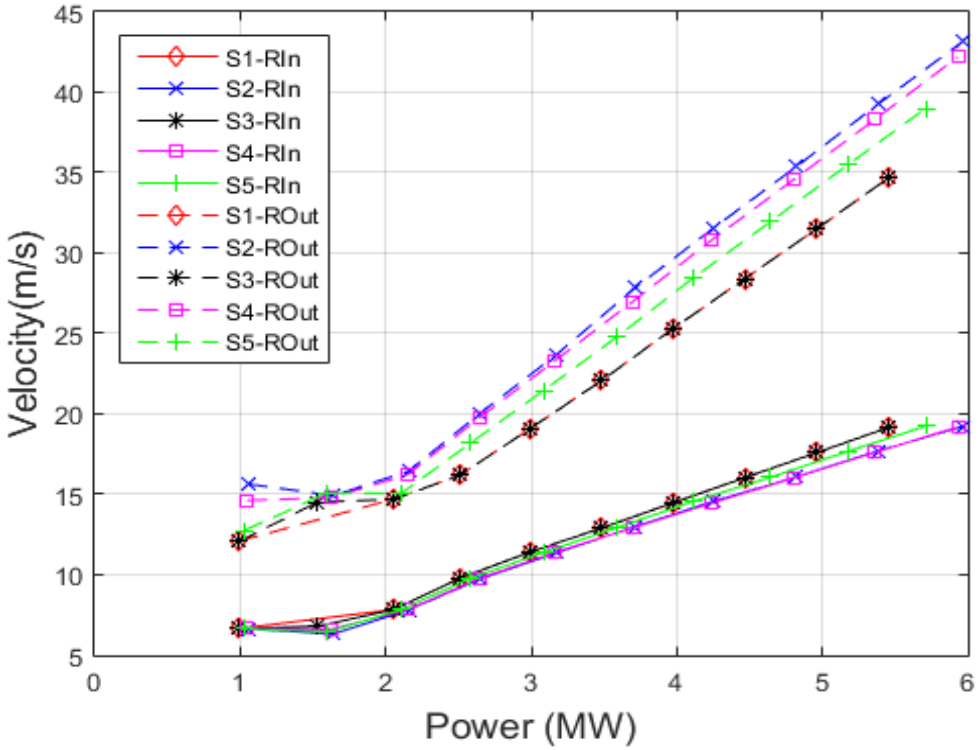

Figure 4.10: Relative velocity at inlet and outlet of runner[91].

4.2.4 Structural Analysis

The structural analysis were performed taking structural steel as a construction material. The properties of structural steel are listed in the Table 3.11: The analysis was carried out to obtain the equivalent stress distribution, total deformation in runner assembly and Von Mises stress distribution in blade assembly. Figure 4.11 shows the maximum equivalent stress of 1.712e+8 Pa in the inner portion of the hub and minimum stress of 5712.5 Pa throughout the flange zone of the hub. Similarly, on observing the total deformation in runner assembly maximum deformation of 0.000169 m was obtained at outer portion of the blade and zero deformation was obtained at its inner portion as shown in Figure 4.12. Figure 4.13 shows the Von Mises Stress distribution in the blade assembly with maximum value of 4.627e+7 Pa and minimum value of 3.711e+5 Pa.

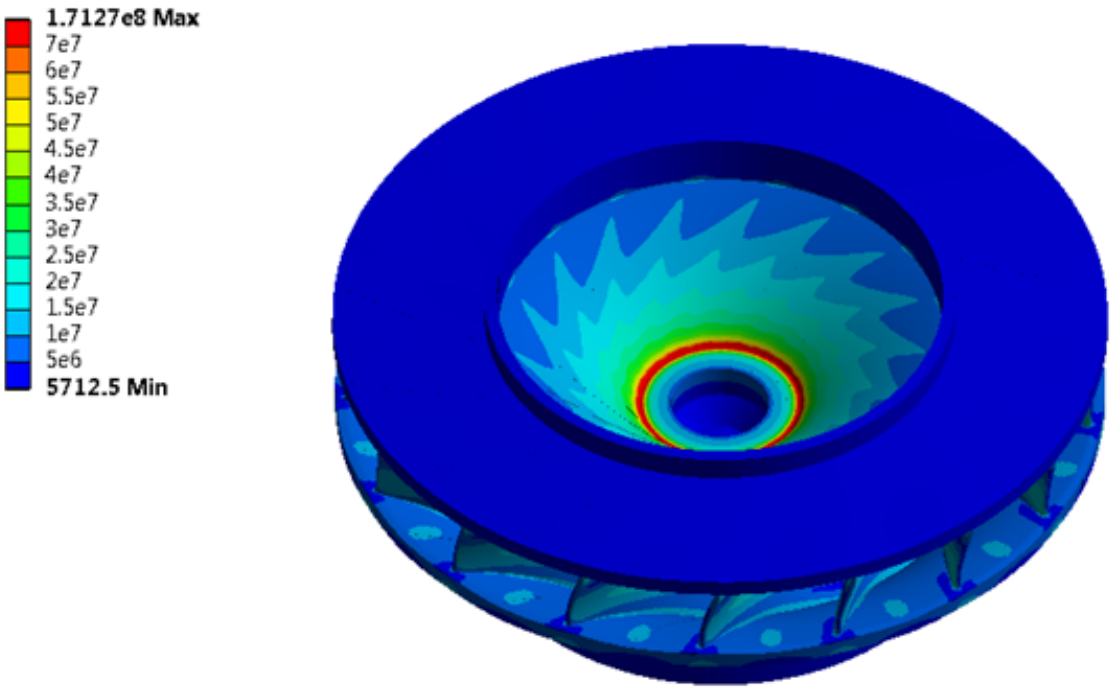

Figure 4.11: Equivalent stress distribution on runner assembly.

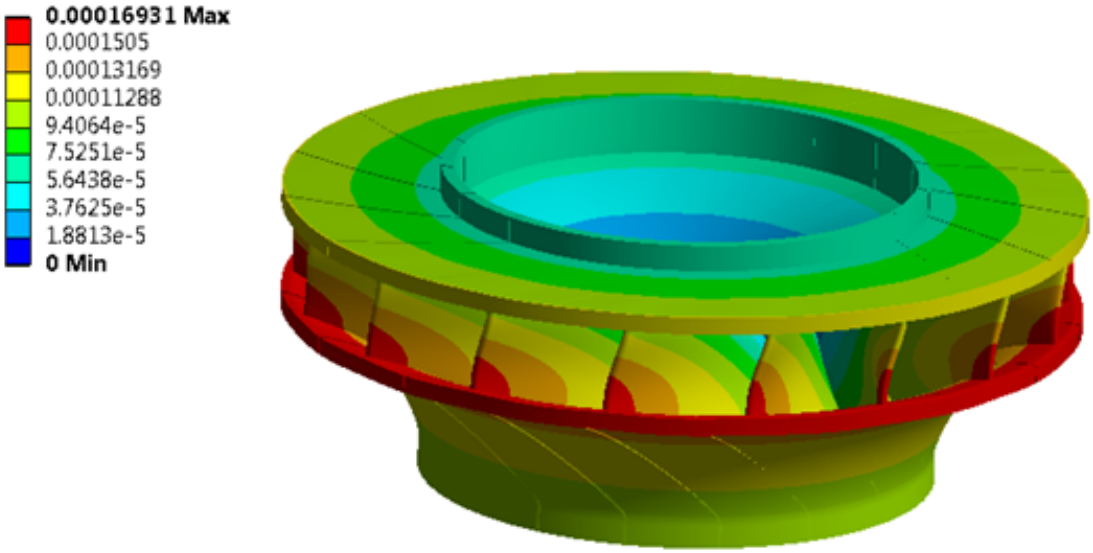

Figure 4.12: Total deformation on runner assembly.

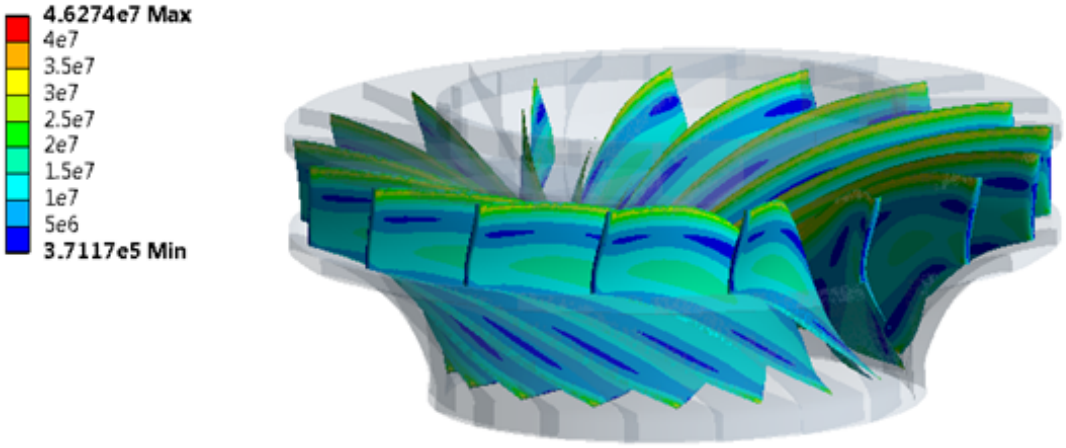

Figure 4.13: Equivalent (Von Miss) Stress Distribution on blade assembly.

4.2.4.1 Design of Experiments

For the multidisciplinary design optimization, the design of experiments were carried out to obtain best possible information from the limited design data by placing design points within the design space. For this, outline of all parameters are tabulated in Table 4.2. Different approaches like two-level factorials, three-level factorials, CCD, and BBD were considered. After the investigation of advantages and drawbacks of each methods, CCD was selected based on number of experiments required to obtain the quality data. It is a popular method for Response Surface Modeling due to the expanse of design space covered and higher order information obtained [70, 71, 73, 74, 75, 76, 77].

Table 4.2: Parameters

ID	P1	P2	P3	P4	P5	P6	P7	P9
Parameter Name	Radial velocity	Tangential velocity	Head	Shaft Power	Total effi-ciency	Disc harge	RPS	Sand Ero-sion

4.2.4.2 Matrix of Experiments

i. Parameter Parallel Chart:

From the design of experiment, out of 1,003 points, three best points were chosen and their combination and compatibility with other variables were mapped

in such a way that the variables have to be within the stated domain and constraints. In the Figure 4.14, three best candidate points of each radial and tangential velocity components were taken from the design of experiments and its possible combinations with other parameters such as head, efficiency, and erosion are shown.

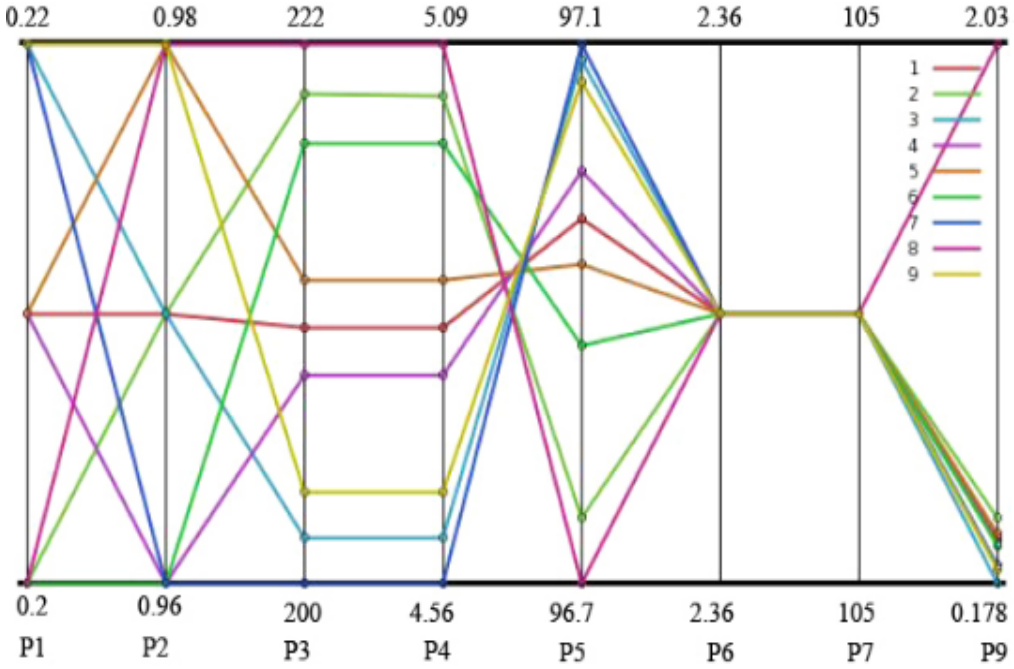

Figure 4.14: Parameters Parallel Chart.

Each vertical line represents member of the optimization candidate. Initial two vertical line that represents the meridian and tangential component. Each component will have three combinations of data. In this design of experiments flow rate and revolution per (rps) second are set to be equality constrains. Head, efficiency, power and erosion rate density was calculated by using components of velocity and other parameters.

When the combination with 0.21 radial component of velocity and 0.96 tangential component of velocity gives the higher erosion rate density and it is represented by line number 4. The erosion rate density represented by line number 4 is 2.03 $kgm^{-2}S^{-1}$. Whereas the combination with 0.22 $kgm^{-2}S^{-1}$ radial component of velocity and 0.97 tangential velocity component gives the least

erosion with $0.178 kgm^{-2}S^{-1}$ and it is represented by legend number line 3. The second best possible combination in terms of least erosion rate density is legend number line 9. In this case, the combination takes the value 0.22 for radial component of velocity and 0.98 for the tangential component of velocity.

ii. Response Surface:

It is a meta-model built from Design of Experiments for an efficient exploration of the design space [93]. It shows how functional value keeps relation with the variables. Goodness of fit provides charts and metrics to understand how each output parameter is approximated by the response surface. In the given experiment, a graph is plotted between predicted points from response surface and observed from the design points. The graph shows that the parameters P3, P4, P5, P7 and P9 are not deviated much and follows the straight line path.

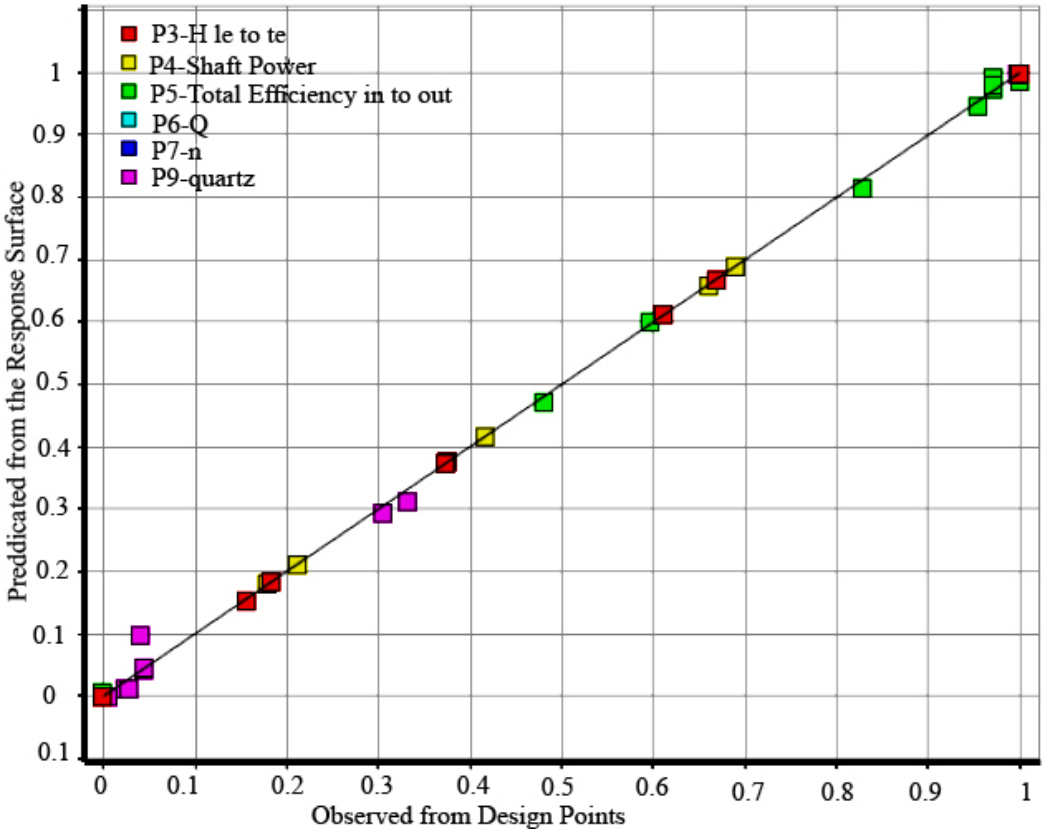

Figure 4.15: Predicted versus observed- normalized values showing goodness of fit.

iii. Correlation matrix:

Correlation matrix shows the correlation of a parameter with other parameters.

Figure 4.16 shows the general relation among different parameters while Table 4.3 shows the exact correlation between them. In the given Table 4.3, the positive sign shows that two variables are related in such a way that one variable increases (or decreases) as other increases (or decreases) whereas negative sign shows that one variable increase as other decreases and vice versa.

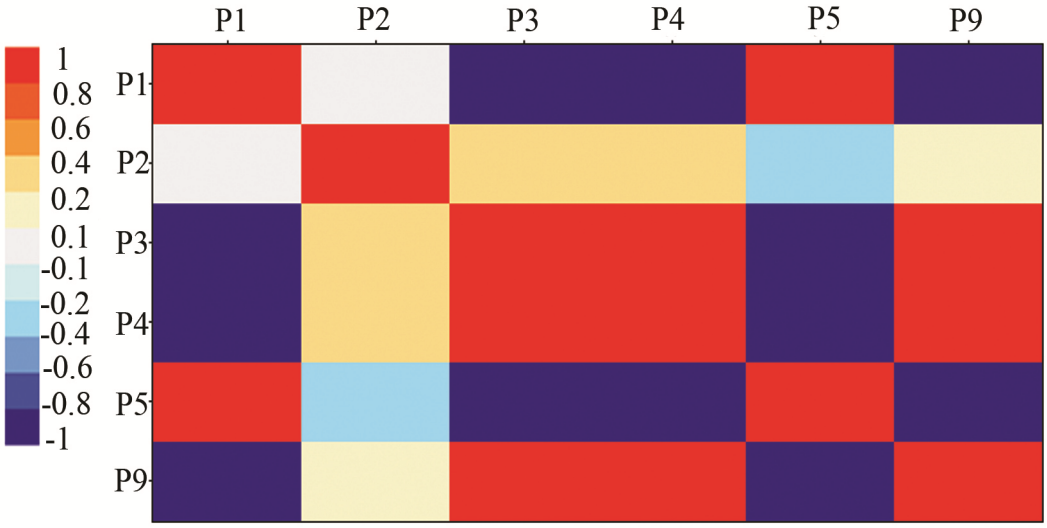

Figure 4.16: Correlation matrix.

Table 4.3: Correlation matrix co-efficient.

Parameters	P1	P2	P3	P4	P5	P9
P1	1	-0.08802	-0.95227	-0.97292	0.962065	-0.87438
P2	-0.08802	1	0.301897	0.29066	-0.3237	0.137383
P3	-0.95227	0.301897	1	0.976567	-0.98233	0.850756
P4	-0.97292	0.29066	0.976567	1	-0.99491	0.873806
P5	0.962065	-0.3237	-0.98233	-0.99491	1	-0.86267
P9	-0.87438	0.137383	0.850756	0.873806	-0.86267	1

In the tabulated result, radial velocity (P1) is found to have negative correlation with P2, P3, P4, and P9 whereas it has positive relation with P5. Meanwhile, tangential velocity (P2) is found to have negative correlation with P1, P5 whereas it has positive dependence with P2, P3, and P4. Each parameters has correlation of one with itself.

iv. Sensitivity Analysis:

The optimization depends upon the Response Surface evaluations. From the mass of several sample points, 3 best candidate points are chosen and its relation with other parameters are established.

As per the sensitivity curve shown in Figure 4.17, radial velocity keeps positive correlation with parameter P5 whereas negative correlation with other parameters like P3, P4, P6, P7, and P9. Similarly, tangential velocity shows slightly positive correlation with P3, P4, and P9 whereas slightly negative correlation with P5. Meanwhile, it has no correlation with P6 and P7.

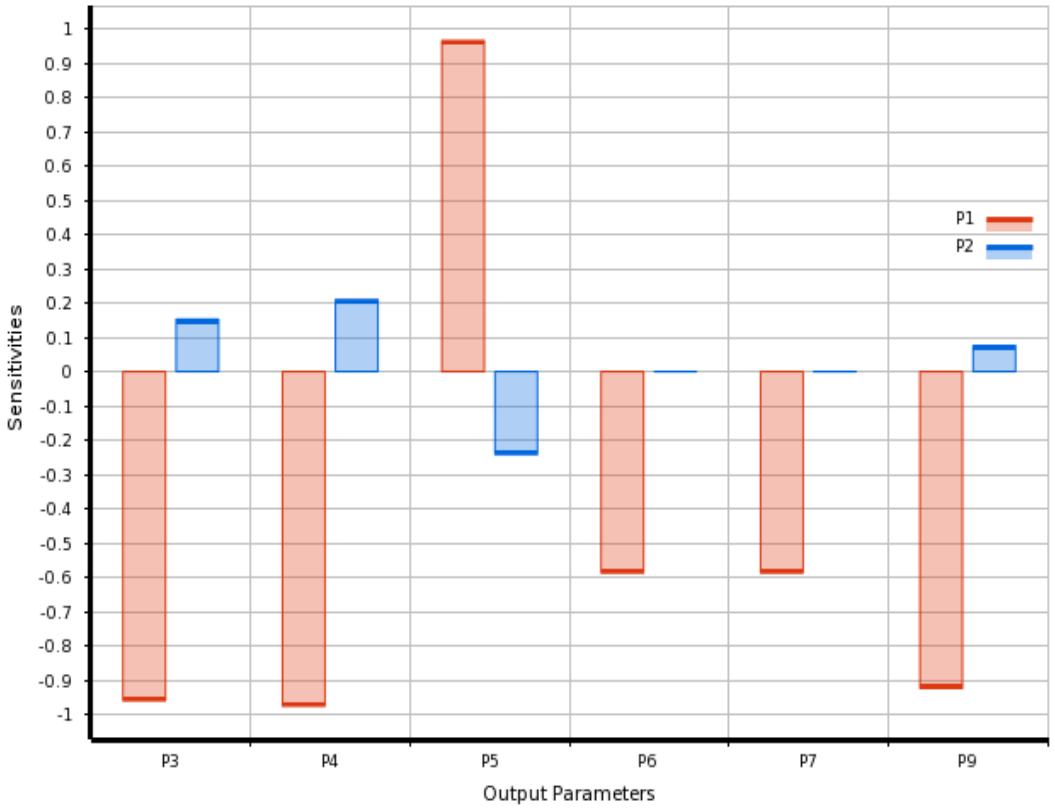

Figure 4.17: Sensitivity Bar.

Figure 4.18 shows the one way FSI performed with single objective optimization. In this case, only radial components of velocity (P1) is kept as function of erosion rate density. The Von Mises Stress distribution was observed through this optimization and factor of safety was found to be 3.75 considering the material as structural steel.

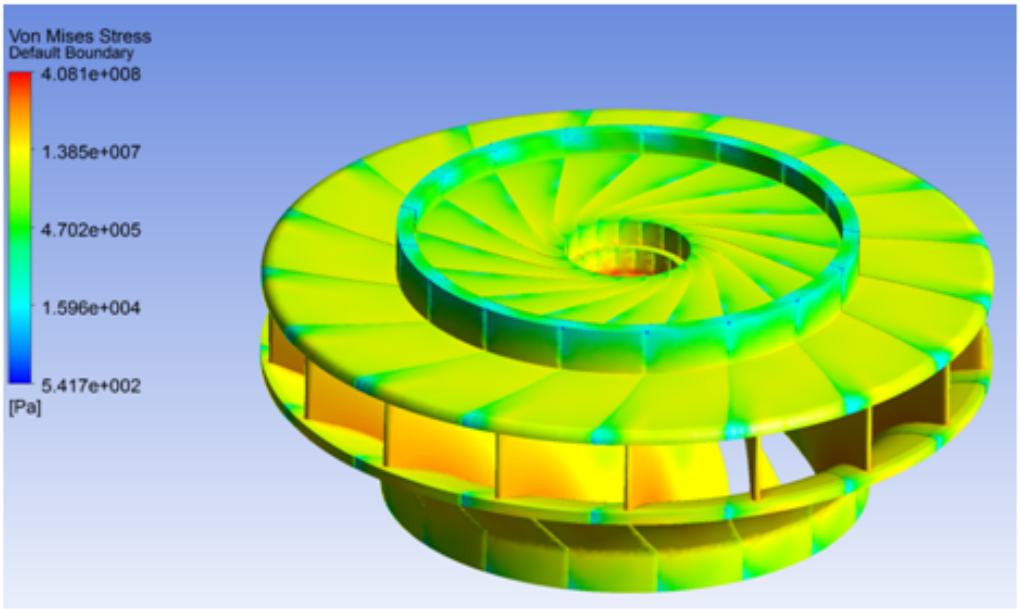

Figure 4.18: One way FSI simulation combined with single objective optimization.

As single objective optimization combined with one way FSI cant capture all the required flow physics, multidisciplinary optimization was carried out to overcome these limitations. Figure 4.19 shows two way FSI conducted alone in Francis runner turbine which decreases the factor of safety drastically to 2.23 while increases the Von Mises Stress. While conducting two way FSI along with goal driven optimization, the stress was further increased whereas the safety factor was reduced slightly to 2.01. This is shown by Figure 4.20.

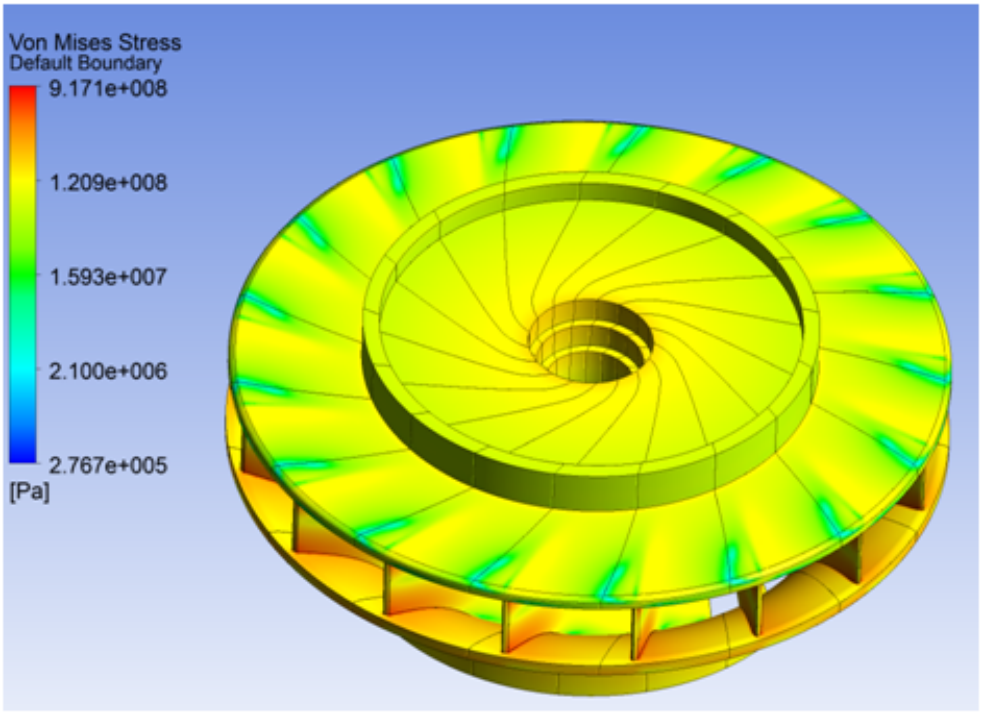

Figure 4.19: Two way FSI simulation.

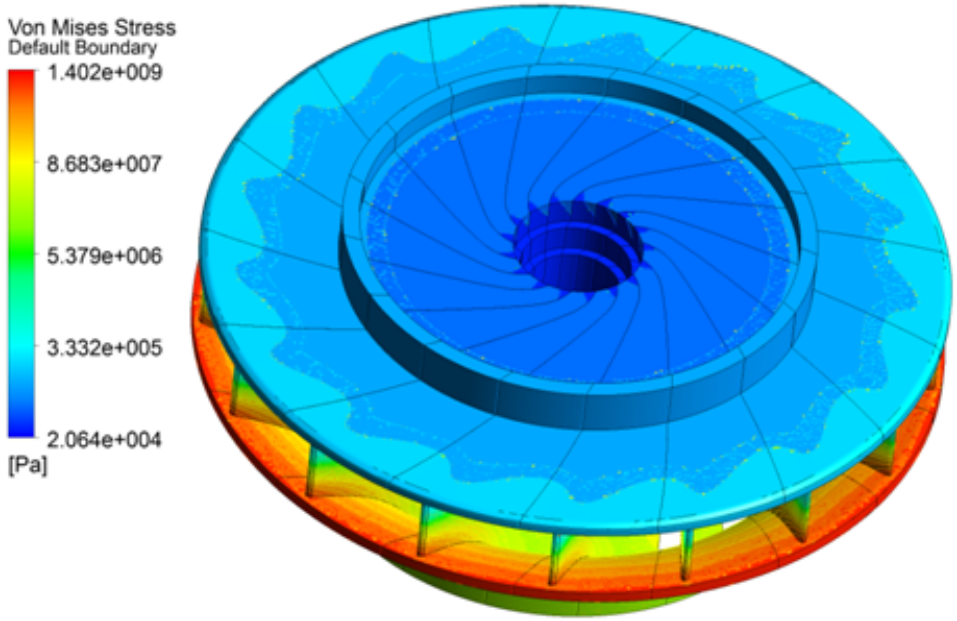

Figure 4.20: Two way FSI simulation combined with multidisciplinary optimization.

4.2.5 Relation of velocity components with other parameters

The radial and tangential velocity components, relation with the erosion rate density, head, efficiency, and shaft power are observed to be the quadratic in nature. The general quadratic relation of velocity components in terms of radial (P1) and tangential velocity (P2) was found to as given by equations Equation (4.4) and Equation (4.5)

$$y_{Radial} = \xi_1 P_1^2 + \xi_2 P_1 + \xi_3 \tag{4.4}$$

$$y_{Tangential} = \xi_1 P_2^2 + \xi_2 P_2 + \xi_3 \tag{4.5}$$

Where, different values for the coefficients (ξ_1, ξ_2) constant terms(ξ_3)and its root mean least square values (R) for the erosion rate density, head efficiency and shaft power are presented on the conclusion section of this thesis.

Chapter 5: CONCLUSIONS AND RECOMMENDATIONS

5.1 Conclusions

In this research, design and analysis have been carried out by varying the blade loading, angle distribution and angle of absolute velocity to flow in the runner. The comparison analysis was done to find the potential effects of erosion on the performances of five designs of Francis turbine runner blades for ten different operating conditions. This means flow domain was divided into ten sub division. Taking into account the erosion rate at different operating conditions, relative velocities for power generated and distribution of efficiencies, shape five showed the optimized performance compared to all other design types. In the shape five design, the least erosion tendency due to the geometrical property of the blade, the sediment contents in the fluid flow directed towards the middle of the runner without moving towards the edges. This result is expected to be very much helpful during design and operation of Francis turbine for industrial application.

Geometrically, the study of Francis runner blade design process shows that instead of choosing linear distribution, angle should be chosen in such a way that energy distribution throughout the blade has to be distributed in two folds. In the first half, energy extractions occur with high and low energy distribution from inlet to mid span and then from mid span to the outlet of the runner in the latter half. Shape 5 was found to have the best performance considering the lowest erosion tendency. When compared other shape runners with runner fitted the blade shape five as least erosion tendency, shape 1, 2, 3 and 4 found to have more erosion amount in terms of percentage as 56.8%, 206%, 89.6% and 212% respectively.

Through the Multidisciplinary optimization result, safety factor of the blade thickness for the shape five runner blade was perceived to be 2.01. This is the least value obtained while compared to the safety factor obtained through one way and two way FSI only. The relation between the components of velocities with the erosion rate

density, head and efficiency is found to be quadratic in nature. The coefficient of velocities, relation with erosion rate density observed to be negative correlation and its coefficients, constant and least square value for the radial component are -9e-7, 2e-6, 2e-6, 0.8339 and for the tangential components values are -8e-5, 0.0002, -7e-5 and 0.6798 respectively. Similar trend of negative correlation was also observed with the efficiency and its coefficients, constant and the least square values for the radial component are -277.31, 87.462, 90.065 and 0.92 and for the tangential components, these values are found to be -5262.5, 10343, -4985.3 and 0.8557 respectively.

But the Velocity components, relation with head and shaft power is found to be positive correlation. The coefficients of velocities relation with head, coefficient, constant term and the least square values for radial component are found as 2752.8, 1354.6, 374.01, 0.9588 and its values for the tangential components are 4967, -95488, 46102, 0.5624 respectively. Similar trend of positive correlation was also observed with shaft power and its coefficients, constant terms and the least square values for the radial components are 3e7, 2e6, 3e6, 0.9761 and these values for the tangential components are 4 10e7,-1e8,1e8 and 0.9503 respectively.

5.2 Recommendations

The laboratory test for the performance of shape 5 has not been done yet. It will be very useful if the testing is done in future and compare with this result in order to enhance the design specification against sand erosion.

The multidisciplinary optimization was performed only considering the components of velocity as variables and head, shaft power, efficiency as equality and inequality constraints to optimize the less erosion tendency and maximize the efficiency and shaft power. It does not change any configurations of design points of blade. If it was performed by surrogating the system with Khoj or La-Higeura, it would have produced the best runner with less erosion tendency without compromising the efficiency.

When the turbine operating under the part load conditions, swirl circulation was observed in between the blades of runner at the leading edge. This swirl circulation mostly depends on particle size and Reynold's number of the flow field. To avoid circulation of particles in between the runner blades, during the turbine operation, calculation procedure has to develop, show that operating procedure can be recommended for the particular site.

Erosion on Francis runner depends on parameters such as velocity, concentration, implement angle, erosion density, etc. To incorporate the own erosion model, in house code has to develop so that more control on parameters that associated with the erosion can be controlled easily during simulation.

Topology optimization with multidisciplinary optimization, can produce less weight, more efficient and less erosion tendency runner but it demands more sophisticated computer. It is also recommend to carry out such simulation for the better shape size and less erosion tendency runner.

Bibliography

[1] H.M. Shrestha. "Cadastre Of Potential Water Power Resources of Less Studied High Mountainous Regions (In the example of Nepal". *Moscow Power Institute, USSR*, 1966.

[2] WECS. "Energy Sector Synopsis Report". Water and Energy Commission Secretariat, Kathmandu, Nepal, 2010.

[3] WECS. "Water Resources Of Nepal In The Contex Of Climate Change".

[4] S. Gautam. "CA Election Of Nepal: Are parties energy sector promises feasible?". Energy for Nepal, November 13, 2013.

[5] B. Thapa, R. Shrestha, P. Dhakal, and B. S. Thapa. "Problems Of Nepalese Hydropower Projects Due To Suspended Sediments". *Journal Of Aquatic Ecosystem Health & Management*, pp. 251–257, 2005.

[6] B. Thapa. "Sand Erosion Of Hydrolic Machinary". Doctoral Thesis at NTNU, 2004.

[7] J. J. Rund. "Sediment Handling Proglems Jhimruk Hydroelectric Center Nepal". NTNU, Norway, 2004.

[8] B. S. Thapa, K. P. Shrestha, B. Thapa, and O.G. Dahlhaug. "Experiences Of R & D Of Hydraulic Turbines At Kathmandu University". In *First Asia-Pacific Forum On Renewable Energy*, Busan, Korea, 2011.

[9] J. B. Paulsen. "FSI-Analysis Of A Francis Turbine". Master's thesis, NTNU, 2012.

[10] K. Gjosater. "Hydrolic Design of Francis Turbine Exposed To Sediment Erosion". Master's Thesis at NTNU, 2012.

[11] S. Basnyat. "Average Sediment Concentration In Jhimruk river". *BPC*, 1998.

[12] V. Galay, H. Schreier, and R. Bestbier. "Himalayan Sediments: Issues And Guidelines". *CD publication*, Water and Energy Commission Secretariat (WECS), Kathmandu, 2002.

[13] B. Thapa, P. Upadhyay, O. G. Dahlhaug, M. Timsina, and R. Basnet. "HVOF Coatings For Erosion Resistance Of Hydraulic Turbines: Experience of Kaligandaki-A Hydropower Plant". *Water Resources And Renewable Energy Development in Asia, Danang*, Central Vietnam, 2008.

[14] O. G. Dahlhaug and B. Thapa. "Sand Erosion In Francis Turbine: A Case Study From Jhimruk Power Plant". *IHAR symposium On Hydraulic Machinery And Systems*, Stockholm, 2004.

[15] "TTL, Feasilbility Study For Francis Turbine Manufacturing And Testing Facility in Nepal", Turbine Testing Lab (MED, KU), Dhulikhel, Kavre. 2012.

[16] O. G. Dahlhaug. "Lecture Notes On Design Of High Head Francis Turbine". NTNU, Nowray, 2012.

[17] K. Wellinger and H. S. Uetz. "Sliding, Scouring and Blasting Wear Under The Influence Of Granular Solids". *VDI-Forschungsheft*, Vol. 21B, 1955.

[18] W.A. Stauffer. "The Abrasion Of Hydraulic Plant By Sandy Water". *Schweitzer Archiv fur Angew. Wiss. Technik*, Vol. 24, pp. 3-30, 1958.

[19] E. Bak. "Construction Materials And Testing Tesults Of The Wear Of Pumps For Transporting Solid Media". *Biuletyn Glownego Instytuta Gornictwa*, Vol. 12, 1966, B.H.R.A. traslation available.

[20] S. P. Kozirev. "Hydroabrasive Wear Of Metals Under Cavitation". Mashinostroenie, Translation by University of Michigan, 1964.

[21] J. E. Goodwin, W. Sage, and G. P. Tilly. "Study Of Erosion By Solid Particles". *Proceedings Of The Institution Of Mechanical Engrs*, 1969-70.

[22] R. C. Worster and D. F. Denny. "Hydraulic Transport Of Solid Material In Pipes". *Proceedings Of The Institution Of Mechanical Engrs*, 1955.

[23] F. F. Antunes and N. R. Youlden. "Centrifugal Pump Wear and Wear Analysis". Factory and Plant, 1996.

[24] G. F. Truscott. “A Literature Survey On Abrasive Wear In Hydraulic Machinery”. *Wear*, Vol. 20, 1972.

[25] T. Bovet. “Contribution To The Study Of The Phenomenon Of Abrasive Erosion In The Realm Of Hydraulic Turbines”. *Bull. Tech. Suisse Romande*, pp. 37–49, 1958.

[26] A. Bezinge and F. Schafer. ”Storage Pumps And Glacial Waters”. *Bull. Tech. Suisse Romande*, B.H.R.A. translation T 1019, 1969, pp. 282–290.

[27] S. Ferry, G. Willm, and J. Thouvenin. “The Effect Of Wear On The Efficiency Of Hydraulic Turbines”. *Proc. 5th Hydraul. Conf. Hydraul. Turbines And Pumps*, I, 1958.

[28] P. Bergeron and J. Dollfus. “The Influence Of The Nature Of The Pumped Mixture And Hydraulic Characteriscs On The Design And Installation Of Liquid/Solid Mixture Pumps”. *Proc. 5th Conerence On Hydraulics Turbines et Pompes Hydrauliques*, 1958.

[29] V. Vasiliev. “On Evaluation Of Wear Of Centrifugal Pump Parts In Hydroabrasive Mixtures”. *Proc. 1st Conference On Hydraulics Transport Of Solids In Pipes*, 1970.

[30] A. F. Shchelkanov. ”The Influence Of Hardness And Micro-structure On The Abrasion And Cavitation Resistance Of Steel”. *Energomashinostroenie*, Vol. 11, no. 1, pp. 32–36, 1965.

[31] M. K. Padhy and R. P. Saini. “A Review On Silt Erosion In Hydro Turbines”. *Renewable And Sustainable Energy Reviews*, pp. 1974–1987, 2008.

[32] A. Kjolle. “Hydropower In Norway Mecanical Equipment” . NTNU, Trondheim, December, 2001.

[33] J. H. Neilson and A. Gilchrist. “Erosion By A Stream Of Solid Particles”. *Wear*, Vol. 11, pp. 111–122, 1968.

[34] A. G. Bain and S. T. Bonnington. “The Hydraulic Transport Of Solids By Pipeline.”. *1st ed. Oxford: Pergamon Press*, pp. 131–136, 1970.

[35] B. K. Gandhi, Singh S. N, and V. Seshadri. “Study Of The Parametric Dependence Of Erosion Wear For The Parallel Flow Of Solid–Liquid Mixtures”. *Tribology International*, Vol. 32, pp. 275–282, 1999.

[36] T. Takagi, T. Okamura, and J. Sato. “Hydraulic Performance Of A Francis-Turbine For Sediment-Laden Flow. *Hitachi Review*, no. 2, 1988.

[37] M. Krause and H. Grein. “Abrasion Research And Prevention”. *Hydropower Dams*, Vol. 4, pp. 17–20, 1996.

[38] B. Naidu. “Addressing The Problems Of Silt Erosion At Hydro Plants”. *Hydropower Dams*, Vol. 3, pp. 72–77, 1997.

[39] B.N. Asthana. “Determination Of Optimal Sediment Size To Be Excluded For Run-of-river Project–a Case Study”. *Seminar On: Silting Problems In Hydro Power Stations. WRDTC, Roorkee, India*, May, 1997.

[40] C. Schneider and T. Kchele. “Recent Research Results On Predicting And Preventing Silt Erosion”. *Silting Problems In Hydro Power Plants: Proceedings Of The First International Conference, New Delhi, India,*, 1999.

[41] J. G. A. Bitter. “A Study Of Erosion Phenomena Part 1 and 2”. *Wear*, Vol. 6, pp. 5–21 and 169–190, 1963.

[42] G. W. Stachowiak and A. W. Batchelor. “Turbine: Abrasive, Erosion and Fatigue. *Engineering Tribology, Third Edition, Elsevier*, pp. 535–537, 2005.

[43] A. V. Levy, N. Jee, and P. Yau. “Erosion Of Steels In Coal-Solvent Slurries”. *Wear*, Vol. 117, pp. 115–127, 1987.

[44] A.V. Levy and G. Hickey. “Liquid-Solid Particle Slurry Erosion Of Steels”. *Wear*, Vol. 117, pp. 129–146, 1987.

[45] H. Hojo, K. Tsuda, and T. Yabu. “Erosion Damage Of Polymeric Material By Slurry”. *Wear*, Vol. 112, pp. 17–28, 1986.

[46] H. Brekke. “PhD lecture notes at NTNU”. 1984.

[47] A. A. Hamed, W. Tabakoff, R. B. Rivir, K. Das, and P. Arora. "Turbine Blade Surface Deterioration By Erosion". 2003.

[48] A. K. Chauhan, D. B. Goel, and S. Prakash. "Erosion Behaviour Of Hydro Turbine Steels". *Bulletin Of Materials Science*, Vol. 31, no. 2, pp. 115–120, April 2008.

[49] L. Poudel, B. Thapa, B. P. Shrestha, B. S. Thapa, K.P. Shrestha, and N. K. Shrestha. "Computational And Experimental Study Of Effects Of Sediment Shape On Erosion Of Hydraulic Turbines". *IOP Conference Series: Earth and Environmental Science*, Vol. 15, pp. 032054, 2012.

[50] B. P. Shrestha and S.K. Suman. "Shape Feature Extraction And Pattern Recognition Of Sand Particles And Their Impact". *Proc. SPIE Int. Soc. Opt. Eng*, pp. 59960, 59960X, 2005.

[51] S. Hassani, J. E. Klemberg-Sapieha, M. Bielawski, W. Beres, L Martinu, and M. Balazinski. "Design Of Hard Coating Architecture For The Optimization Of Erosion Resistance". *Wear*, Vol. 265, pp. 879–887, 2008.

[52] B. Thapa, B. S. Thapa, O. G. Dahlhaug, and K. P. Shrestha. "Accelerated Testing For Resistance To Sand Erosion In Hydraulic Turbines". *International Journal Of Hydropower And Dams. Chiang Mai, Thailand*, March 26-27, 2012.

[53] P. Chaudhary. "Study Of Combined Effect Of Sand Erosion And Cavitation In Hydraulic Turbines". Master Thesis at Kathmandu University, Nepal, 2008.

[54] V. Y. Karelin, V. Denisov, and Y. Wu. "Fundamental Of Hydroerosive Erosion Theory". *Hydraulic Erosion And Corrosion Check*, London, Imperial Collage Press, 2002, pp. 1–52.

[55] H. Brekke, Y. Wu., and B. Y. Cai. "Design Of Hydraulic Machinery Working In Sand Laden Water". *Series On Hydraulic Machinery-Vol 2, Abrasive Erosion & Corrosion Of Hydraulic Machinery*, pp. 155-186, Imperial Collage Press, 57 shelton Street, 2002.

[56] H. P. Neopane. “Sediment Erosion In Hydro Turbines.”, Doctoral Thesis at NTNU, 2010.

[57] M. Eltvik. “Sediment Erosion In Francis Turbines.”, Doctoral Thesis at NTNU, 2013.

[58] H. Brekke. “Hydraulic Turbines Design, Erection and Operation.”, Norway: NTNU. 2001.

[59] K. P. Shrestha, B. Thapa, O. G. Dahlhaug, H. P. Neupane, N. Gurung, and A. Kayastha. “Optimized Design Of Francis Turbine Runner For Sand Laden Water.”. *Hydro Nepal*, pp. 36-43, 2013.

[60] M. Rogner. “Design Of A High Head Francis Turbine That Are Exposed For Sand Erosion.”. NTNU, Norway, 2008.

[61] H. Meland. “A New Design Of A Francis Turbine In Order To Reduce Sediment Erosion”, NTNU, Norway, 2010.

[62] S. Chitrakar. “FSI Analysis Of Francis Turbines Exposed To Sediment Erosion”, Master Thesis at KTH, 2013.

[63] P. Drtina and M. Sallaberger. “Hydraulic TurbinesBasic Principles And State-of-the-art Computational Fluid Dynamics Applications”. *Proceedings Of The Institution Of Mechanical Engineers*, Vol. 213, 1999.

[64] A. Sun. “Numerical Simulation Of FluidStructure Interaction For Blade Abased On CFX and Workbench”. In *2nd International Conference On Control, Instrumentation And Automation (ICCA)*, 2011.

[65] B. S. Thapa, K. Gjosater, M. Eltvik, O. G. Dahlhaug, and B. Thapa. “Effects Of Turbine Design Parameters On Sediment Erosion Of Francis Runner”. In *Developments In Renewable Energy Technology (ICDRET)*, Dhaka, Bangladesh, 2012.

[66] B. S. Thapa, M.and Eltvik K. Gjoster, and O. G. Dahlhaug. “Design Optimization Of Francis Turbine For Sediment Handling. In *Proc. In The Int. Conf. On*

Water Resources And Renewable Energy Development In Asia, Thailand, 26-27 March, 2012.

[67] H. Brekke. "The Influences On The Design Manufacture, Testing And Operation". General Doctoral Lecture NTH, NTNU, Trondheim, 1984.

[68] P. E. Dahlhaug, O. G .and Skare, V. Mossing, and A. Gutierrez. "Sediment Resistive Francis Runner At Cahua Power Plant". *International Journal Of Hydropower And Dams*, Vol. 2, pp. 109–112, 2010.

[69] H. P. Neopane, O. G. Dahlhaug, and B. Thapa. "Alternative Design Of A Francis Turbine For Sand Laden Water". In *International Conference On Hydropower-Hydro Sri Lanka 07, Sri Lanka*, 2007.

[70] I. Yong Kim. "Computational Multidisciplinary Design Optimization". *Department Of Mechanical And Materials Engineering, Queen's University*, 1 November 2005.

[71] A.-B. Ryberg, R. D. Backryd, and L. Nilsson. "Metamodel-Based Multidisciplinary Design Optimization For Automotive Applications". Division of Solid Mechanics, Linkoping University, Linkoping, September, 2012.

[72] O. d. Weck and K. Willcox. "Multidisciplinary System Design Optimization (MSDO)". Massachusetts Institute of Technology, Lecture Note, 4th February, 2004.

[73] T. Rakic, I. Kasagic-Vujanovic, M. Jovanovic, B. Jancic-Stojanovic, and D. Ivanovic. "Comparison Of Full Factorial Design, Central Composite Design, And Box-Behnken Design In Chromatographic Method Development For The Determination Of Fluconazole and Its Impurities". pp. 37-41, Mortimer Street, London WIT3JH, UK, May 2, 2014.

[74] M. Ramu, V. P. Raja, P. R. Thyla, and M. Gunaseelan. "Design Optimization Of Complex Structures Using Metamodels". *Jordan Journal of Mechanical and Industrial Engineering*, vol. 4, no. 5, pp. 653–664, November 2010.

[75] R. B. d. F. e. Albuquerque and W. d. Oliveria. "Conceptual Design Optimization Of Francis Turbines". *21st Brazilian Congress Of Mechanical Engineering*, Natal, RN, Brazil, 24-28 October 2011.

[76] G. G. Wang and S. Shan. "Review Of Metamodeling Techniques For Product Design With Computation-Intensive Processes". Department of Mechanical and Manufacturing Engineering, The University of Manitoba, Winnipeg, MB, R3T5V6.

[77] K. Leiviska. "Introduction To Experiment Design". Control Engineering Laboratory, University of OuluControl Engineering Laboratory, University of Oulu, 2013.

[78] "Electromechanical Equipment Guide For Small Hydroelectric Installations". *International Electro-Technical Commission, IEC*, Vol. 1116, 1992.

[79] I. E. Commission. "Hydraulic Turbines, Storage Pumps And Pump-TurbinesModel Acceptance Tests". IEC, 3, rue de Varembe Geneva, Switzerland, 1999.

[80] A. Inc. ANSYS CFX Solver Theory Guide, Release 14, ANSYS. 2011.

[81] S. Nicolici, I. Prisecaru, and D. Dupleac. "Two-phase Flow CFD Modeling For Evaluation of Particulate Erosion". *U.P.B. Scientific Bulletin, Series D*, Vol. 75, no. 1, ISSN 1454–2358, 2013.

[82] J. M. Gimenez, D. Ramajoa, and N. M. Nigroa. "Particle Transport In Laminar/Turbulent Flows". *Mecnica Computacional*, Vol XXXI, Salta Argentina, November 13-16, 2012.

[83] P. J. Roache. "Perspective: A Method For Uniform Reporting Of Grid Refinement Studies". *Journal Of Fluids Engineering*, Vol. 116, no. 405, September 1994.

[84] I. B. Celik. "Procedure For Estimation And Reporting Of Uncertainty Due To Discretization In CFD Applications". *Journal Of Fluids Engineering Of The ASME*, Vol. 130, JUly 2008.

[85] K. P. Shrestha, B. Thapa, and O. G. Dahlhaug. "Effect Of Velocity Component On Efficiency Of Optimized Design Francis Runner". *Renewable Energy For Sustainable Development In Asia And Asia Pacific Region.*

[86] "ANSYS Help Verion 14". 2012.

[87] H. Brekke. "Konstruksjon av pumper og turbine"". Waterpower laboratory, NTNU, December, 2008.

[88] I. P. ANSYS. "ANSYS Mechanical Structural Nonlinearities". ANSYS, Inc., 2010.

[89] K. P. Shrestha, B. Thapa, O. G. Dahlhaug, H. P. Neopane, and B. S. Thapa. "Innovative Design Of Francis Turbine For Sediment Laden Water". In *TIM International Conference*, 2012.

[90] K. P. Shrestha, A. Panthee, B. Thapa, O. G. Dahlhaug, H. P. Neopane, B. S. Thapa, and L. Poudel. "Design Of Model Francis Turbine Runner For Performance Test Against Sand Erosion". *Proceedings of 2013 IAHR World Congress*, 2013.

[91] K. P. Shrestha, S. Chitrakar, B. Thapa, and O. G. Dahlhaug. "Performance Comparison Of Optimized Designs Of Francis Turbines Exposed To Sediment Erosion In Various Operating Conditions".

[92] B. Thapa and H. Brekke. "Effect Of Sand Particle Size And Surface Curvature In Erosion Of Hydro Turbine". *IAHR Symposium On Hydrolic Machinary And Systems.*, Stockholm, 2014.

[93] I. Ansys. "ANSYS user guide". ANSYS, USA, 2015.

APPENDIX

1. Performance Comparison of Optimized Designs of Francis Turbines Exposed to Sediment Erosion in Various Operating Conditions. (Reviewing)

2. Optimized Design of Francis Turbine Runner for Sand Laden Water.
(www.nepjol.info/index.php/HN/article/download/10038/8183)

3. Computational and experimental study of effects of sediment shape on erosion of hydraulic turbines.
(http://iopscience.iop.org/1755-1315/15/3/032054/)

4. Effect of Velocity Component on Efficiency of Optimized Design Francis Runner.
(http://icmr.crru.ac.th/article-detail.php?id=12)

5. Design of Model Francis Turbine Runner for Performance Test Against Sand Erosion. (Proceedings of 2013 IAHR World Congress.)